

การขนส่งอนุภาคและสปีนของระบบที่มีคู่ควบสปินกับวงโคจรแบบรัชบาใน
แบบจำลองแลททิซและแบบจำลองต่อเนื่อง

นายเอก จันทะยอด

วิทยานิพนธ์นี้เป็นส่วนหนึ่งของการศึกษาตามหลักสูตรปริญญาวิทยาศาสตรดุษฎีบัณฑิต
สาขาวิชาฟิสิกส์
มหาวิทยาลัยเทคโนโลยีสุรนารี
ปีการศึกษา 2554

**PARTICLE AND SPIN TRANSPORT OF
RASHBA SPIN-ORBIT COUPLING SYSTEM
IN A LATTICE AND A CONTINUOUS
MODEL**

Aek Jantayod

A Thesis Submitted in Partial Fulfillment of the Requirements for the

Degree of Doctor of Philosophy in Physics

Suranaree University of Technology

Academic Year 2011

**PARTICLE AND SPIN TRANSPORT OF RASHBA
SPIN-ORBIT COUPLING SYSTEM IN A LATTICE
AND A CONTINUOUS MODEL**

Suranaree University of Technology has approved this thesis submitted in partial fulfillment of the requirements for the Degree of Doctor of Philosophy.

Thesis Examining Committee

(Asst. Prof. Dr. Chinorat Kobdaj)

Chairperson

(Assoc. Prof. Dr. Puangratana Pairor)

Member (Thesis Advisor)

(Assoc. Prof. Dr. Yongyut Laosiritaworn)

Member

(Assoc. Prof. Dr. Santi Maensiri)

Member

(Dr. Michael F. Smith)

Member

(Dr. Worawat Meevasana)

Member

(Prof. Dr. Sukit Limpijumnong)

Vice Rector for Academic Affairs

(Assoc. Prof. Dr. Prapun Manyum)

Dean of Institute of Science

เอก จันตะยอด : การขนส่งอนุภาคและสปินของระบบที่มีคู่ควมสปินกับวงโคจรแบบ
รัชบาในแบบจำลองแลททิซและแบบจำลองต่อเนื่อง (PARTICLE AND SPIN
TRANSPORT OF RASHBA SPIN-ORBIT COUPLING SYSTEM IN A LATTICE
AND A CONTINUOUS MODEL) อาจารย์ที่ปรึกษา : รองศาสตราจารย์ ดร.พวงรัตน์
ไพเราะ, 84 หน้า.

วิทยานิพนธ์นี้ศึกษาเชิงทฤษฎีเกี่ยวกับการขนส่งอนุภาคและสปินในระบบผสมสองมิติที่ประกอบด้วยโลหะและระบบที่มีคู่ควมสปินกับวงโคจรแบบรัชบา โดยจำลองลักษณะการเคลื่อนที่ของอนุภาคและสปินด้วยแบบจำลองแลททิซ เพื่อศึกษาผลของสภาพนำไฟฟ้าที่อุณหภูมิศูนย์เคลวินแล้วเปรียบเทียบกับการศึกษาในระบบดังกล่าวด้วยการจำลองลักษณะการเคลื่อนที่ของอนุภาคและสปินด้วยแบบจำลองต่อเนื่อง นอกจากนี้ได้ใช้การจำลองอนุภาคแบบแลททิซพิจารณาหาสปินโพลาไรเซชันของสภาพนำไฟฟ้าของระบบ

สำหรับการจำลองอนุภาคแบบต่อเนื่อง ผลของค่าสภาพนำไฟฟ้าถูกพิจารณาเป็นฟังก์ชันของแรงดันไฟฟ้า พบว่าแรงดันไฟฟ้าระหว่างจุดเริ่มต้นถึงจุดการเปลี่ยนของเส้นสเปกตรัมรวมของสภาพนำไฟฟ้าของระบบมีค่าเท่ากับขนาดของพลังงานของระบบรัชบา นอกจากนี้อิทธิพลของความหนาแน่นของอิเล็กตรอนและความแรงของระบบรัชบาได้ถูกพิจารณาต่อค่าสภาพนำไฟฟ้าที่ระดับพลังงานเฟอร์มิ พบว่า ค่าสภาพนำไฟฟ้าเพิ่มขึ้นเมื่อจำนวนความหนาแน่นของอิเล็กตรอนเพิ่มขึ้น และเกิดจุดเปลี่ยนแปลงของสภาพนำไฟฟ้าเมื่อความหนาแน่นของอิเล็กตรอนเท่ากับจุดตัดกันของแถบพลังงานของระบบรัชบา ในขณะที่สภาพนำไฟฟ้าลดลงเมื่อความแรงของการคู่ควมสปินกับวงโคจรของระบบรัชบาเพิ่มขึ้นจนถึงค่าวิกฤต หลังจากค่าวิกฤต ค่าสภาพการนำไฟฟ้าจะมีขนาดเพิ่มขึ้นตามความแรงของการคู่ควมสปินกับวงโคจรของระบบรัชบา

สำหรับการจำลองอนุภาคแบบแลททิซ เงื่อนไขที่เหมาะสมที่รอยต่อได้ถูกพิจารณาขึ้นเพื่อคำนวณหาสภาพนำไฟฟ้าของระบบซึ่งเป็นฟังก์ชันของแรงดันไฟฟ้า ซึ่งแบบจำลองนี้สามารถคำนวณหาสภาพนำไฟฟ้าได้ทั้งอิเล็กตรอนและโฮล พบว่าเมื่อรอยต่อไม่โปร่งใส (รอยต่อที่สามารถปรับเปลี่ยนทิศทางของสปินได้ และไม่สามารถปรับเปลี่ยนทิศทางของสปินได้) ผลต่างของแรงดันไฟฟ้าตั้งแต่จุดเริ่มต้นและจุดเปลี่ยนของเส้นสเปกตรัมของสภาพนำไฟฟ้าของอิเล็กตรอนและโฮล มีค่าเท่ากับขนาดของพลังงานระบบรัชบาเช่นเดียวกับการจำลองอิเล็กตรอนแบบต่อเนื่อง ส่วนค่าสปินโพลาไรเซชันของสภาพนำไฟฟ้าจะมีค่าสูงสุดเมื่อแรงดันไฟฟ้าเท่ากับจุดตัดกันทั้งสองจุดของแถบพลังงานทั้งสองของระบบรัชบา และพบว่าอิทธิพลของรอยต่อที่สามารถปรับเปลี่ยน

ทิศทางของสปริงได้สามารถเปลี่ยนแปลงค่าสปริง โพลาริเซชันของสภาพนำไฟฟ้าจากค่าลบเป็นค่าบวก



สาขาวิชาฟิสิกส์
ปีการศึกษา 2554

ลายมือชื่อนักศึกษา _____
ลายมือชื่ออาจารย์ที่ปรึกษา _____

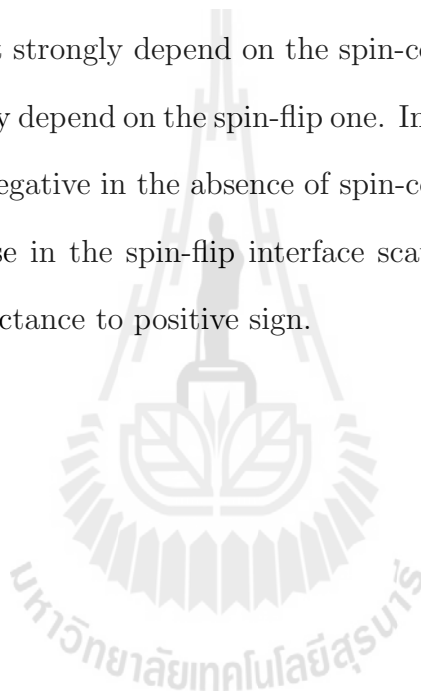
AEK JANTAYOD : PARTICLE AND SPIN TRANSPORT OF
RASHBA SPIN-ORBIT COUPLING SYSTEM IN A LATTICE AND A
CONTINUOUS MODEL. THESIS ADVISOR : ASSOC.
PUANGRATANA PAIROR, Ph.D. 84 PP.

RASHBA SPIN-ORBIT COUPLING/SPIN-POLARIZATION/TUNNELING
CONDUCTANCE/LATTICE MODEL

This thesis is a theoretical study of the particle and spin transport in a heterostructure that consists of a normal metal and a two-dimensional electron gas with Rashba spin-orbit coupling system. A lattice model is used in comparison with a continuous model, to investigate conductance spectra of the system, In addition, the spin polarization of conductance also consider with with a lattice model.

In a continuous model with the assumption that the two-dimensional electron gas band is empty, the tunneling conductance was calculated as a function of applied voltage and showed the containment of two distinguished features, the energy spacing between which is equal to the Rashba spin-orbit coupling energy. The impact of the electron density in the conduction band and the Rashba coupling strength on the conductance at Fermi level was also investigated. The conductance is increased with the carrier density. However, it is decreased with the strength of the Rashba spin-orbit coupling strength, until the strength reaches to a critical value, after which the conductance is increased with the strength. It also found that there is a kink in the relationship between the conductance and the carrier density. This kink occurs when the carrier density of the Rashba system is at the level of the crossing point.

In the lattice model, appropriate matching conditions at the interface was developed in order to calculate the particle current across the junction. This model can provide the conductance value for both electron and hole Fermi surfaces. Similar results to the continuous model were found in the conductance spectrum of the system. As for spin polarization of conductance in the absence of spin-flip scattering potential, the maximum magnitude occurs at the voltages equivalent to the two crossing points in the Rashba energy band. The spin polarization of conductance does not strongly depend on the spin-conserving interface scattering potential, but strongly depend on the spin-flip one. In the voltage region, where the spin polarization is negative in the absence of spin-conserving interface scattering potential, the increase in the spin-flip interface scattering potential can flip the polarization of conductance to positive sign.



School of Physics

Student's Signature _____

Academic Year 2011

Advisor's Signature _____

ACKNOWLEDGEMENTS

There are many people I would like to thank for their help and encouragement for the completion of this thesis. First of all, I would like to thank Assoc. Prof. Dr. Puangratana Pairor for her guidance throughout my graduate years at SUT.

Special thanks also go to all my friends: Tan, Bass, and P'Mas for sharing both fun and stressful experiences. I also would like to thank P'Ed, P'Jod, P'Pick and P'Dull, who always gave me help and advice about physics and programming.

Deepest gratitude also goes to the members of the thesis committee, Assoc. Prof. Dr. Santi Maensiri, Assoc. Prof. Dr. Yongyut Laosiritaworn, Asst. Prof. Dr. Chinorat Kobdaj, Dr. Michael F. Smith, and Dr. Worawat Meevasana for their valuable comments that helped improve this thesis.

This work has been financially supported by the Research, Development and Engineering (RD&E) Fund through National Nanotechnology Center (NANO-OTEC), National Science and Technology Development Agency (NSTDA), Thailand.

Last but not least, I wish to express my gratitude to my beloved families: mom, dad, my elder sister and her husband, for their understanding patience and endless support.

Aek Jantayod

CONTENTS

	Page
ABSTRACT IN THAI	I
ABSTRACT IN ENGLISH	III
ACKNOWLEDGEMENTS	V
CONTENTS	VI
LIST OF FIGURES	VIII
LIST OF ABBREVIATION	XV
LIST OF SYMBOLS	XVI
CHAPTER	
I INTRODUCTION	1
1.1 Motivation	1
1.2 Outline of Thesis	6
II ELECTRON DESCRIPTION OF RASHBA SPIN-ORBIT	
COUPLING SYSTEM IN TWO MODELS	8
2.1 Free Electron Model	8
2.1.1 Density of States (DOS)	10
2.1.2 Carrier Density at Zero Temperature	11
2.2 Lattice Model	13
2.2.1 Density of States (DOS)	16
2.2.2 Carrier Density at Zero Temperature	18
III A METAL/RASHBA SYSTEM JUNCTION IN A CONTIN-	
UOUS MODEL	19

CONTENTS (Continued)

	Page
3.1 Model and Assumptions	19
3.2 Results and Discussion	26
3.3 Conclusions	34
 IV A METAL/RASHBA SYSTEM JUNCTION IN A LATTICE	
MODEL	35
4.1 Model and Assumptions	35
4.2 Boundary Conditions	40
4.3 Electric Current Density and Conductance Formula	44
4.4 Results and Discussions	46
4.4.1 Transmission Probability	46
4.4.2 Differential Conductance	50
4.4.3 Spin Polarization of Conductance	58
4.5 Conclusions	60
V CONCLUSIONS	67
REFERENCES	70
 APPENDICES	
APPENDIX A HAMILTONIAN AND EIGENENERGY OF THE RSOC SYSTEM IN A CONTINUOUS MODEL	78
APPENDIX B HAMILTONIAN AND EIGENENERGY OF THE RSOC SYSTEM IN A LATTICE MODEL	80
CURRICULUM VITAE	84

LIST OF FIGURES

Figure		Page
1.1	Examples of Rashba spin-orbit coupling systems. (a) Surface alloys such as Bi/Ag(111) and Pb/Ag(111). Light and dark circles represent each of the two atomic species. (b) Two-dimensional electron gas in quantum well in InGaAs/InAlAs interfaces.	2
2.1	Schematic illustration of the energy-momentum dispersion of Rashba system (a). The energy contours in the momentum space, (b) above the crossing point, (c) below the crossing point. The arrows represent the direction of electron spin at the corresponding momentum on the contours.	10
2.2	(a) Plots of $-$ branch (solid curves), $+$ branch (dashed curve), and total (thick-solid curve) density of states in unit of $m^*/\pi\hbar^2$ (b) and the total electron density in unit of k_0^2/π	12
2.3	Schematic illustration of the square lattice of the 2DEG with RSOC, $t_R(t_{\sigma\sigma'(\sigma'\sigma')\rightarrow\sigma'\sigma'(\sigma\sigma)})$ and $t_{so}(t_{\sigma\sigma'(\sigma'\sigma)\rightarrow\sigma'\sigma(\sigma\sigma')})$ are the normal hopping energy and the ROSC strength.	14
2.4	The energy-momentum dispersion of RSOC in a lattice model, when $k_y = 0$. $E_{so}^{bot,top} \equiv \frac{t_{so}^2 a}{t_R}$, $E_{R1}(k_y)$, and $E_{R2}(k_y)$ are defined in the text.	14

LIST OF FIGURES (Continued)

Figure		Page
2.5	Plots of the energy contour of Rashba system, (a) the energy slightly above the 1 st crossing point, (b) the energy slightly below the 2 nd crossing point. The solid line and dotted line are for the minus and plus branch, respectively.	15
2.6	Density of states of Rashba system is in a unit of $\mathcal{A}/8\pi^2t_R$, where \mathcal{A} is the area of the system.	16
2.7	Density of states of 2DEG without RSOC is in a unit of $\mathcal{A}/8\pi^2t_N$	17
2.8	The plot of carrier density of particle of the 2DEG with RSOC system in a lattice model.	18
3.1	Example of a metal/Rashba system junction in a 2-dimensional system.	19
3.2	The sketches of the energy spectra of the metal (on the left) and the Rashba system (on the right). E_F , U_0 , and $E_\lambda = \hbar^2k_0^2/2m^*$ are the Fermi energy, the Rashba offset energy and the Rashba energy, respectively.	22
3.3	Differential conductance spectra G as a function of applied voltage for different Z_0 in case of $Z_F = 0$	27
3.4	Differential conductance spectra G as a function of applied voltage for different Z_F in case of $Z_0 = 0$	27
3.5	Differential conductance spectra G as a function of applied voltage for different Z_F in case of $Z_0 = 0.5$	28

LIST OF FIGURES (Continued)

Figure		Page
3.6	Plots of normalization of discontinuity of conductance at the crossing point (NDG) of Figure 3.4 (dashed line) and of Figure 3.5 (solid line), depends on the spin-flip scattering Z_F	28
3.7	Plots of conductance spectrum as a function of applied voltage for different values of k_0 . In these plots, we set $Z_0 = 0, Z_F = 0$	29
3.8	Conductance G at different apply voltages as a function of k_0 . We set $Z_0 = 0, Z_F = 0$	30
3.9	Plots of conductance spectrum as a function of applied voltage for different values of m^* . In these plots, we set $Z_0 = 0, Z_F = 0$	30
3.10	Differential conductance at zero voltage G as a function of carrier density of electron for different k_0 in case of $Z_0 = 0$ and $Z_F = 0$. where $n_0 = m^* E_\lambda / \pi \hbar^2$ is the Rasha carrier density.	32
3.11	Plots of critical value of electron carrier density and k_0 in case of $Z_0 = 0$ and $Z_F = 0$	32
3.12	Differential conductance at zero voltage G as a function of strength of Rashba spin-orbit coupling k_0 for different n in case of $Z_0 = 0$ (a), $Z_0 = 0.5$ (b), and $Z_0 = 1.0$ (c). All plots set $Z_F = 0$	33
4.1	Schematic illustration of the square lattice representing the metal/Rashba system junction. This system is the same lattice constant a , and n, m indicate the column and row indices of the lattice, respectively. The energy at on-site ϵ_M is for metal and ϵ_{RS} is for RSOC system.	37

LIST OF FIGURES (Continued)

Figure		Page
4.2	The sketches of the energy dispersion relations of an electron in the metal (left) and the Rashba system (right) for $k_y = 0$. The dashed line represents the same energy. E_{max}, E_{min}, E_{R1} , and E_{R2} are dependent on k_y and are defined in the text.	38
4.3	Energy contours of the metal, where $t'_N = 0.1t_N$	39
4.4	Plots of energy contours of the Rashba system. On the left is for the plus branch and on the right is for the minus branch.	39
4.5	Plots of total transmission probability as a function of energy for different $k_y a$	47
4.6	Plots of transmission probability as a function of energy for $k_y = 0.02/a$	48
4.7	Plots of transmission probability as a function of energy for $k_y = 0.05/a$	48
4.8	Plots of $T^+(E, k_y)$ and $T^-(E, k_y)$ as a function of energy for $k_y = 0.02/a$ near bottom of the Rashba band.	49
4.9	Plots of $T^+(E, k_y)$ and $T^-(E, k_y)$ as a function of energy for $k_y = 0.05/a$ near top of Rashba band.	49
4.10	Sketch of RSOC energy dispersion is split by k_y , the range of energy splitting is $4t_{so} \sin k_y a$	50
4.11	Plots of conductance spectra as a function of energy for $V_0 = 0$ and $V_0 = 0.5t_N$. V_F is zero in these plots.	51

LIST OF FIGURES (Continued)

Figure		Page
4.12	Magnified plots of conductance spectra as a function of energy for several values of V_0 near the bottom, middle, and top of the band. V_F is zero in these plots.	52
4.13	Plots of conductance spectra as a function of energy for several values of V_F and V_0 is taken to be zero.	53
4.14	Plots of conductance spectra as a function of energy for several values of V_F in case of $V_0 = 0.5t_N$	53
4.15	Plots of conductance spectra as a function of energy for several values of V_F in case of $V_0 = 1.0t_N$	54
4.16	Plots of conductance spectra as a function of energy for several values of V_F in case of $V_0 = 2.0t_N$	54
4.17	Differential conductance at applied voltage $eV = -10.125t_{so}$ (top panel) and $eV = -9.5t_{so}$ (bottom panel) plotted as a function of the barrier strength V_0 for different V_F , the maximum conductance is occurred at the value of $V_0 \simeq V_F$	55
4.18	Differential conductance at applied voltage $eV = 0$ (top panel), $eV = 9.5t_{so}$ (middle panel), and $eV = 10.125t_{so}$ (bottom panel) plotted as a function of the barrier strength V_0 for different V_F , the maximum conductance is occurred at the value of $V_0 \simeq V_F$	56
4.19	Plots of the spin-flip V_F and the spin-conserving V_0 scattering values lead to the maximum tunneling conductance. The square is for the apply voltage equivalent to the energy around the 1 st crossing point and the circle is for the energy around the 2 nd crossing point. . . .	57

LIST OF FIGURES (Continued)

Figure		Page
4.20	Differential conductance plotted as a function of t_{so} for different values of applied voltages.	57
4.21	Spin polarization of conductance in the metal side plotted as a function of eV for different values of V_0 in case of $V_F = 0$. The upper panel is for eV equivalent to the energy around the lower crossing point and lower panel is for eV equivalent to the energy around the higher crossing point.	59
4.22	Spin polarization of conductance in the metal side plotted as a function of eV for different values of V_F in case of $V_0 = 0$. (a) is for eV equivalent to the energy around the 1 st crossing point, (b) is for eV equivalent to the energy around half-filled level, and (c) is for eV equivalent to the energy around the 2 nd crossing point. . .	62
4.23	Spin polarization of conductance in the metal side plotted as a function of eV for different values of V_F in case of $V_0 = 0.5t_N$. (a) is for eV equivalent to the energy around the 1 st crossing point, (b) is for eV equivalent to the energy around half-filled level, and (c) is for eV equivalent to the energy around the 2 nd crossing point. . .	63
4.24	Spin polarization of conductance in the metal side plotted as a function of eV for different values of V_F in case of $V_0 = 2.0t_N$. (a) is for eV equivalent to the energy around the 1 st crossing point, (b) is for eV equivalent to the energy around half-filled level, and (c) is for eV equivalent to the energy around the 2 nd crossing point. . .	64

LIST OF FIGURES (Continued)

Figure		Page
4.25	Spin polarization of conductance in the metal side plotted as a function of spin-conserving scattering V_0 for different values of V_F . (a) is for eV equivalent to the energy below the 1 st crossing point, (b) is for eV equivalent to the energy at half-filled level, and (c) is for eV equivalent to the energy above the 2 nd crossing point.	65
4.26	Spin polarization of conductance in the metal side plotted as a function of spin-flip scattering V_F for different values of V_0 . (a) is for eV equivalent to the energy below the 1 st crossing point, (b) is for eV equivalent to the energy at half-filled level, and (c) is for eV equivalent to the energy above the 2 nd crossing point.	66

LIST OF ABBREVIATION

RSOC	Rashba Spin-Orbit Coupling
2DEG	Two-Dimensional Electron Gas
FM	Ferromagnetic
G	Conductance
NM	Normal Metal
QSV	Quantum Spin-Valve
TMR	Tunneling Magnetoresistance
SC	Semiconductor
S	Superconductor
LCAO	Linear Combination of Atomic Orbital (LCAO).
DOS	Density of State
T	Transmission Probability
R	Reflection Probability

LIST OF SYMBOLS

k, q	Wave vector
k_0	Spin-orbit coupling strenght
\hbar	Plank constant
j	Current density
G	Conductance
D	Density of state
n	Electron carrier density
eV	Bias voltage
P	Polarization
Z, V_0	Potential strength at the interface
Z_f, V_F	Spin-flip scattering at the interface
λ	Rashba parameter
m^*	Electron effective mass
E_0	Off-set energy
E_F	Fermi energy
E_{RS}	Eigenvalue of Rashba system
E_λ	Rashba spin-orbit coupling energy
ψ_{RS}	Wave function of Rashba system
H_{RS}	Hamiltonian of Rashba system
H_M	Hamiltonian of metal
t_N	Hopping energy of normal metal
t_R	Hopping energy of Rashba system
t_{so}	Hopping spin-orbit coupling energy

CHAPTER I

INTRODUCTION

1.1 Motivation

Spin transport is a relatively new area in condensed matter physics. It has been extensively explored due to the possibility in using the spin degree of freedom as carrier of information as well as combining the spin-dependent effect for new generation of electronic devices (Barnas et al., 1990; Saibich et al., 1988; Oestreich, 1999; Wolf et al., 2001; Zutíć et al., 2004). The ability to polarize spin system, to control the spin orientation, and to detect the spin are desired to further the development of the application of spintronic devices.

The natural choices of materials that possess the spin polarization are ferromagnetic materials. They have nonzero net magnetic moment, or spontaneous magnetization, in the absence of an external magnetic field. The examples of ferromagnetic metals are Fe, Co, and Ni, whereas those of ferromagnetic semiconductors are GaMnAs, GaMnSb, InMnAs, and InMnSb. The net magnetic moment reflects an imbalanced number of up spins and down spins in these systems. There are many interesting behaviors that can occur in heterostructures containing ferromagnetic materials. For instance, the resistance of alternating layers of ferromagnetic metals and non-magnetic metals depends strongly on the relative magnetization directions of ferromagnetic layers. When the alternating spins are in parallel, the resistance is lower than when they are opposite in direction (Julliere, 1975; Moodera et al., 1995; Maekawa and Gafvert, 1982; Slonczewski, 1989). This phenomenon leads to the Giant magnetoresistance (Barnas et al., 1990; Saibich et al.,

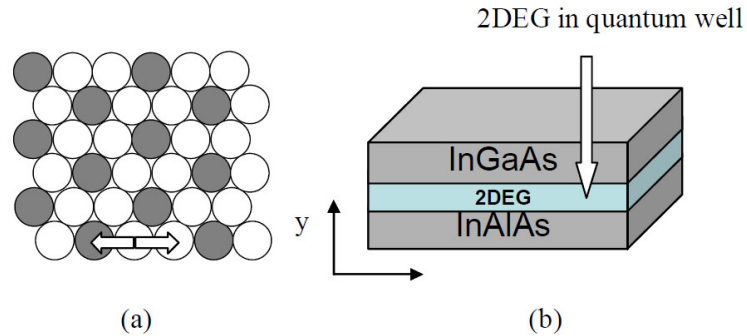


Figure 1.1 Examples of Rashba spin-orbit coupling systems. (a) Surface alloys such as Bi/Ag(111) and Pb/Ag(111). Light and dark circles represent each of the two atomic species. (b) Two-dimensional electron gas in quantum well in InGaAs/InAlAs interfaces.

1988), which is the change in electrical resistance of alternating ferromagnetic layers in response to an applied magnetic field.

A material with Rashba spin-orbit coupling is also of interest for the application of spin transport. This type of spin-orbit coupling arises from the presence of a structure inversion asymmetry (Rashba, 1960a; Rashba, 1960b; Bychhov and Rashba, 1984a), like surface alloys Bi/Ag(111) and Pb/Ag(111) (see Figure 1.1a). A structure inversion asymmetry can also be caused by a confining potential of a quantum well of a two-dimensional electron gas (2DEG) along the perpendicular direction of the 2D plane, such as in the interface planes of AlGaAs/GaAs (Lommer et al., 1988), InGaAs/InP (Schapers et al., 1998) and InGaAs/InAlAs (Nitta et al., 1997) (see Figure 1.1b). For the latter type, the Rashba spin-orbit coupling strength can be modulated by an external electric field (Nitta et al., 1997; Koga et al., 2002; Heida et al., 1998; Engels et al., 1997; Sato et al., 2001; Hu et al., 1999).

In most theoretical studies of transport in a heterostructure of Rashba spin-orbit coupling systems, a continuous model is often used. For instance, Larsen et al. (2002) studied the electrical conductance modulation of a three-layer structure of a two-dimensional electron gas sandwiched by ferromagnetic metals using a free electron approximation and S-matrix method. They found that the conductance can be modulated by either changing the magnetization direction in the ferromagnetic layers, or the Rashba spin-orbit coupling strength. Mireles and Kirczenow (2002) studied quantum spin-valve effect within the Landauer formalism and explored the interplay between spin injection and quantum coherence, which give rise to a quantum spin-valve effect. The signature of this effect is found to be sensitive to temperature. Grundler (2001a, 2001b) studied spin dependent electron transmission at the interface and found that a fundamental effect due to band-structure mismatch provides an intrinsic spin-dependent barrier, giving rise to the magnetoconductance effect. Sun and Xie (2005) investigated electron transport through a two-dimensional semiconductor with a non-uniform Rashba spin orbit interaction and found that a spontaneous spin-polarized current could appear due to the combination of the coherence effect and Rashba spin-orbit interaction in the absence of magnetic field. Cai et al. (2008) showed that the spin-orbit coupling influences a transmission probability of spin-up and spin-down electron and the tunneling magnetoresistance (Julliere, 1975; Moodera et al., 1995; Maekawa and Gafvert, 1982; Slonczewski, 1989). Matsuyama et al. (2002) found that the spin-injection rate across the ferromagnetic material/two-dimensional electron gas interface depends on the carrier density of the electron gas and showed that the spin filtering is enhanced by increasing the strength of elastic scattering potential at the interface. Wu et al. (2003) studied the effect of the Rashba spin-orbit coupling on the traversal time in a ferromagnet/semiconductor (SC)/ferromagnet

heterostructure. They found that the traversal time is decreased with the increase of RSOC strength and showed that as the length of the semiconductor layer increase, the traversal time does not increase linearly but appears a step behavior. Zhang et al. (2006) also calculated the spin-tunneling time in the similar heterostructure as a function of the Rashba spin-orbit coupling strength and the length of semiconductor layer. They found that the tunnel barriers have dominant effects on the electronic properties of the spin-up and spin-down electron. As the length of the layer increase, the spin-tunneling time shows behavior of slight oscillation. They also showed that as the spin-orbit coupling and the tunnel barrier becoming stronger, the spin-tunneling time will increase. Furthermore, the in-plane tunneling spectroscopy of the hybrid structure composed of a metal and the two-dimensional electron gas with Rashba spin-orbit coupling was studied by Srisongmuang et al. (2008). It was found that the Rashba spin-orbit coupling energy can be measured from the conductance spectrum and that an increase in spin-flip scattering probability in some circumstance can enhance the tunneling conductance.

In addition to a continuous model, a tight binding model is also applied to study particle and spin transport in the heterostructures containing two-dimensional electron gas with the Rashba spin-orbit coupling, along with the Green's function method (Pareek and Bruno, 2001; Molenkamp et al., 2000). For instance, Mireles and Kirczenow (2001) studied the effect of the spin-orbit coupling on the spin-transport properties of narrow quantum wire. They showed that the strong coupling can change the spin-polarized electron injected into ballistic narrow wire and induce a dependence of the spin precession of the inject electron. Yang et al. (2009) investigated the proximity effect in the interface between a conventional superconductor and two-dimensional electron gas with the Rashba

spin-orbit coupling. It was found that an injection of a quasiparticle from the superconductor perpendicular to the interface can induce singlet superconductivity correlation in the electron gas region, and the Rashba spin-orbit coupling has a little effect on the Cooper pair penetrating into the electron gas region from the superconducting lead. Wang et al. (2006) studied the nonequilibrium spin accumulation in the interface between two Rashba systems in a quantum wire and found that the spin accumulation concentrates on the two lateral edges of the wire in nonlinear transport regime. Yamamoto et al. (2005) investigated the numerical expression of spin polarization transport in a T-shaped conductor with the Rashba coupling and found that for stronger coupling, the spin-polarized of the current becomes almost perfect.

One of the advantages of the lattice model is that it can reproduce more realistic Fermi surface of each part of the heterostructure than the continuous model; therefore, one can investigate the effect of the band structure in more detail. Furthermore, the potential barrier at the interface can be modeled to have arbitrary strength, ranging from a metallic contact to a tunneling limit. However, most of the above-mentioned studies using the lattice model ignore the influence of the interface quality and assume the interface potential barrier to be infinitely high, i.e. only in a tunneling limit. It has been shown in many studies that the quality of the junction can strongly influence the particle transport in a heterostructure. As can be seen in the junction between a ferromagnet or a metal and superconductor, when the potential interface barrier is low Andreev reflection can occur (Andreev, 1964a; Andreev, 1964b). This phenomenon enhances the charge transport across the junction.

In this thesis, the particle and spin transport in a heterostructure consisting of a metal and a Rashba system are theoretically studied in a lattice model. There

are two main aspects of the investigation: the effect of the band structure of the Rashba system and the quality of the junction. The outline of this thesis is given in the next section.

1.2 Outline of Thesis

This thesis is organized as follows. In Chapter II, some physical properties of a Rashba system are investigated in two models: a continuous model and a lattice model. In the continuous model, the electronic properties of the system of interest is described by a free electron model. In the lattice model, the electronic properties of the system are described by tight-binding approximation. In each model, the energy dispersion relation, the density of states, and the carrier density of the system are investigated.

In Chapter III, the theoretical investigation of particle transport across a metal and a two-dimensional electron gas with the Rashba spin-orbit coupling in a continuous model is given. The interface is modeled by a delta-function like potential with arbitrary strength. The detailed calculation of the conductance as a function of applied voltage of the junction is shown. The results of how the conductance spectrum is affected by the interface potential, the strength of the Rashba spin-orbit coupling and the carrier density of the Rashba system are included.

The development of a lattice model to describe particle and spin transport across a metal/Rashba system junction and the related results are in Chapter IV. The eigenfunction and eigenenergy of the Rashba system, the appropriate matching conditions of the electronic wave functions of the metal and the Rashba system, the current density across the junction, and the formula for the conductance are also obtained in this chapter. Also, the effect of the band structure and the in-

terface barrier potential are shown through the plots of conductance spectra and spin polarization of conductance spectra. The conclusion of this thesis is given in Chapter V.



CHAPTER II

ELECTRON DESCRIPTION OF RASHBA SPIN-ORBIT COUPLING SYSTEM IN TWO MODELS

In this chapter, we describe a two-dimensional electron gas (2DEG) with Rashba spin-orbit coupling (RSOC) using two different models: a free electron model and a lattice model. In particular, we will consider the density of states and the carrier density of the system.

2.1 Free Electron Model

A free electron approximation is the simplest way to represent the electronic structure of a system. In this model, the interaction of conduction electrons with ions of the lattice and the interaction between the conduction electron are included into the electronic effective mass. That is the total energy of the system is a summation of the energy of each electron. This energy is the kinetic energy and the Rashba spin-orbit coupling interaction. In order to obtain a better understanding of the atomic contributions to spin-orbit coupling interaction at the surface, a tight-binding model will be considered.

The one-electron Hamiltonian of the 2DEG with RSOC in a free electron model can be written as (Rashba, 1960a; Rashba, 1960b; Bychhov and Rashba,

1984a),

$$H = \frac{p^2}{2m^*} + \frac{\lambda}{\hbar}(\vec{\sigma} \times \vec{p}) \cdot \hat{z} \quad (2.1)$$

where the electrons are confined to move in the xy plane. The first term of Eq.(A.2) is the kinetic energy of an electron with the effective mass m^* . The second term is the Rashba spin-orbit coupling interaction, where λ is the parameter describing a strength of the spin-orbit coupling, $\vec{\sigma}$ denote the Pauli matrix vector, \vec{p} is the momentum operator, and \hat{z} is a unit vector perpendicular to the 2DEG plane.

The dispersion relation obtained from the Hamiltonian is more detailed in an Appendix A. The eigenvalues are

$$E_{RS}^{\pm} = \frac{\hbar^2 k^2}{2m^*} \pm \lambda k = \frac{\hbar^2}{2m^*} ((k \pm k_0)^2 - k_0^2), \quad (2.2)$$

where $k_0 = \frac{\lambda m^*}{\hbar^2}$, the \pm sign correspond to the $+$ and $-$ branches in Figure 2.1(a), respectively. The free electron energy dispersion is split into two branches due to the RSOC. In the figure, the dotted line is shifted by $+\lambda k$, while the solid line shifted by $-\lambda k$. The two branches meet at $k = 0$. The energy at this point is called "crossing point". Notice that the bottom of the $-$ branch is lower in energy than the crossing point by the Rashba energy: $E_{\lambda} = \frac{\hbar^2 k_0^2}{2m^*}$. The two concentric circles in Figure 2.1(b) and Figure 2.1(c) represent the energy contour lines above and below the crossing point, respectively. The arrows shown in the figure indicated the spin orientations that are always perpendicular to the electron momentum.

The eigenfunction of the electron in the Rashba system with the momentum $\vec{k} = k_x \hat{x} + k_y \hat{y}$ for each branch is written as

$$\psi_{RS}^{\vec{k}, \pm} = \frac{1}{\sqrt{2}} \begin{bmatrix} 1 \\ \pm \frac{\sqrt{k_x^2 + k_y^2}}{ik_x + k_y} \end{bmatrix} e^{i\vec{k} \cdot \vec{r}} \quad (2.3)$$

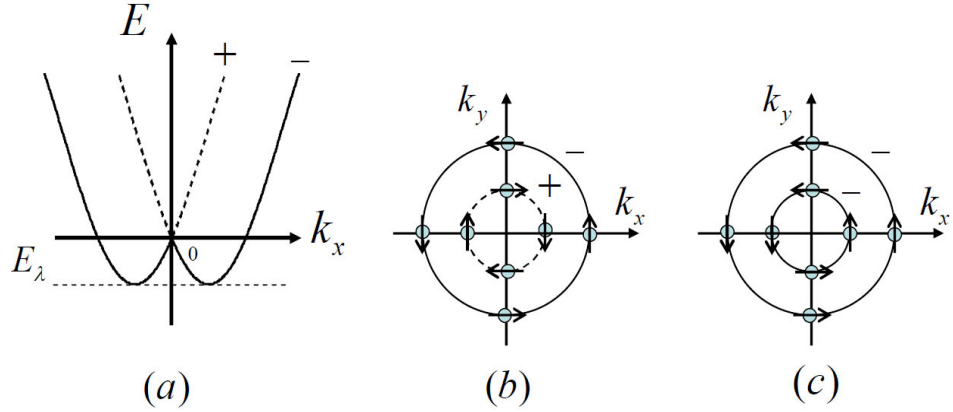


Figure 2.1 Schematic illustration of the energy-momentum dispersion of Rashba system (a). The energy contours in the momentum space, (b) above the crossing point, (c) below the crossing point. The arrows represent the direction of electron spin at the corresponding momentum on the contours.

2.1.1 Density of States (DOS)

The total density of states of the system is defined as:

$$D(E) = \frac{2}{\mathbf{A}} \sum_{\vec{k}} \delta(E - E_{\vec{k}}), \quad (2.4)$$

where \mathbf{A} is the area, \vec{k} is the wave vector, the sum runs over all possible values of \vec{k} . For the 2DEG in the polar coordinate system form an integral:

$$D(E) = \frac{1}{\pi} \int_0^{\infty} k dk \cdot \delta(E - E_{\vec{k}}). \quad (2.5)$$

By changing the integral variable, we have

$$D(E) = \frac{m^*}{\pi \hbar^2} \int_{E_b}^E \left(\frac{k}{k \pm k_0} \right) dE \cdot \delta(E - E_{\vec{k}}). \quad (2.6)$$

Where E_b is the lowest energy. When the zero energy is set to be at the crossing point, as shown in Figure 2.1(a), the DOS of each branch can be calculated and

obtained as follows. For $E \geq 0$,

$$D^\pm(E) = \frac{m^*}{\pi\hbar^2} \left(1 \mp \frac{k_0}{\sqrt{\frac{2m^*E}{\hbar^2} + k_0^2}} \right), \quad (2.7)$$

where $D^+(E)$ and $D^-(E)$ are the DOS for the + and - branches, respectively. Thus, the total DOS for $E \geq 0$ is the sum of $D^+(E)$ and $D^-(E)$ and equal to

$$D^>(E) = \frac{2m^*}{\pi\hbar^2}, \quad (2.8)$$

which is a constant similar to the DOS of the two-dimensional free electron gas. For $E < 0$, the DOS is deviated from the 2D free electron system. Below the crossing point, there is only one branch, the DOS is

$$D^-(E) = \frac{m^*}{\pi\hbar^2} \left(\frac{k_0}{\sqrt{\frac{2m^*E}{\hbar^2} + k_0^2}} \mp 1 \right), \quad (2.9)$$

where the \mp are for the states with $|k| < k_0$ and $|k| > k_0$, respectively. This leads to the total DOS below the crossing point to be

$$D^<(E) = \frac{2m^*}{\pi\hbar^2} \left(\frac{k_0}{\sqrt{\frac{2m^*E}{\hbar^2} + k_0^2}} \right), \quad (2.10)$$

diverging at $E_\lambda = -\frac{\hbar^2 k_0^2}{2m^*}$, as a van Hove singularity (see Figure 2.2 (a)).

2.1.2 Carrier Density at Zero Temperature

One can obtain the carrier density (n) at zero temperature as a function of energy by integrating the DOS over the energy range from the bottom to top of the band:

$$n(E) = \int_{E_b}^E D(E') dE', \quad (2.11)$$

where E_b is the energy level at bottom of the band, and E is the energy corresponding to the filling level. The expression of the carrier density for the energy

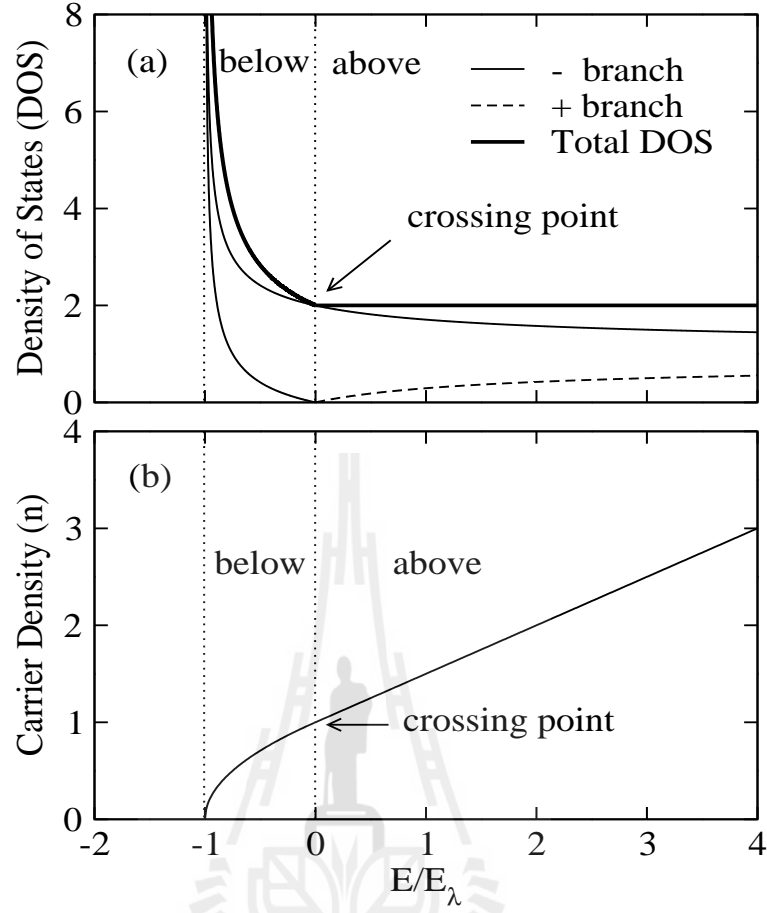


Figure 2.2 (a) Plots of $-$ branch (solid curves), $+$ branch (dashed curve), and total (thick-solid curve) density of states in unit of $m^*/\pi\hbar^2$ (b) and the total electron density in unit of k_0^2/π .

below crossing point ($E < 0$) is obtained as

$$n^<(E) = \frac{k_0}{\pi} \sqrt{k_0^2 + \frac{2m^*E}{\hbar^2}}, \quad (2.12)$$

and the carrier density for the energy above the crossing point ($E \geq 0$) is

$$n^>(E) = \frac{m^*E}{\pi\hbar^2} + \frac{k_0^2}{\pi}. \quad (2.13)$$

The plot of the carrier density is shown in Figure 2.2(b).

2.2 Lattice Model

The simplest tight binding Hamiltonian that includes the influence of Rashba spin-orbit coupling in a square lattice was given by Mireles and Kirczenow (Mireles and Kirczenow, 2001). This Hamiltonian is obtained by discretizing the free electron Hamiltonian: $p^2/2m^* + \lambda(\sigma_y p_x - \sigma_x p_y)$, m^* is the electron effective mass and p is the electron momentum, λ is the Rashba parameter, σ_x, σ_y are the Pauli's matrices. It can be written as

$$H_{RS} = \sum_{nm\sigma} (\epsilon_{nm\sigma} - \mu) C_{nm\sigma}^\dagger C_{nm\sigma} - t_R \sum_{nm\sigma} (C_{n+1,m\sigma}^\dagger C_{nm\sigma} + C_{n,m+1,\sigma}^\dagger C_{nm\sigma} + H.C.) - t_{so} \sum_{nm\sigma\sigma'} \{C_{n+1,m\sigma'}^\dagger (i\sigma_y)_{\sigma\sigma'} C_{nm\sigma} - C_{n,m+1,\sigma'}^\dagger (i\sigma_x)_{\sigma\sigma'} C_{nm\sigma} + H.C.\}. \quad (2.14)$$

Where we assume only nearest-neighbor interactions, the subscripts n and m indicate the column and row indices of the square lattice. $\epsilon_{nm\sigma}$ is the on-site energy, μ is the chemical potential, $C_{nm\sigma}^\dagger$ ($C_{nm\sigma}$) is the creation (annihilation) operator of an electron at site (nm) at lattice site with spin σ , $t_R = \hbar^2/2m^*a$ is the hopping energy for a lattice constant a (see Figure 2.3), $t_{so} = \lambda/2a$ denotes the RSOC strength in the lattice representation.

The calculations of an eigenvalue and eigenstates of Rashba Hamiltonian are described in more details in an Appendix B. There, we write down the energy dispersion relation of electron in the Rashba system as

$$E(\mathbf{k}) = E_0(\mathbf{k}) \pm 2t_{so} \sqrt{\sin^2(k_x a) + \sin^2(k_y a)}, \quad (2.15)$$

where $E_0(\mathbf{k}) = (\epsilon_R - \mu) - 2t_R (\cos(k_x a) + \cos(k_y a))$ is the eigenenergy for a 2DEG without spin-orbit coupling. The plus and minus signs are for the plus and minus branch. k_x, k_y are the wave vector in x and y direction, respectively.

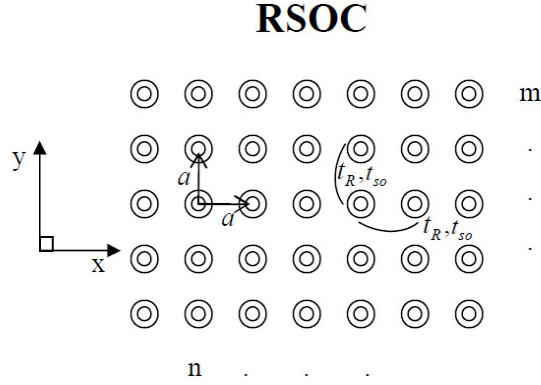


Figure 2.3 Schematic illustration of the square lattice of the 2DEG with RSOC, $t_R(t_{\sigma\sigma'(\sigma'\sigma')\rightarrow\sigma'\sigma'(\sigma\sigma)})$ and $t_{so}(t_{\sigma\sigma'(\sigma'\sigma')\rightarrow\sigma'\sigma'(\sigma\sigma')})$ are the normal hopping energy and the ROSC strength.

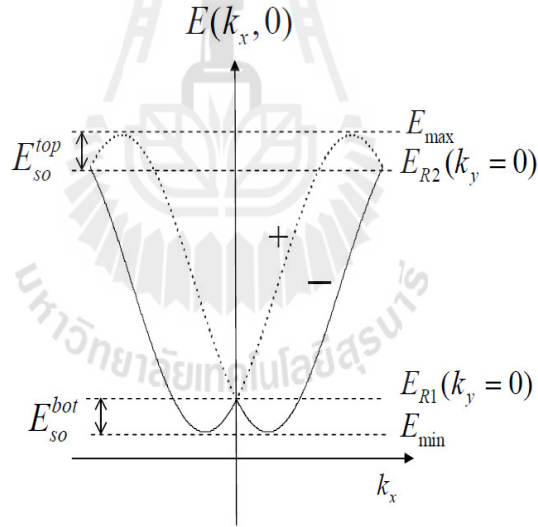


Figure 2.4 The energy-momentum dispersion of RSOC in a lattice model, when $k_y = 0$. $E_{so}^{bot,top} \equiv \frac{t_{so}^2 a}{t_R}$, $E_{R1}(k_y)$, and $E_{R2}(k_y)$ are defined in the text.

The eigenstates can be obtain as

$$U_R^{k_y, \pm}(n, m) = \left[e^{ik_x^{\pm} an} \frac{1}{\sqrt{2}} \begin{pmatrix} \pm \frac{i \sin k_x^{\pm} a + \sin k_y a}{\sqrt{\sin^2 k_x^{\pm} a + \sin^2 k_y a}} \\ 1 \end{pmatrix} \right] e^{ik_y ma}. \quad (2.16)$$

The illustration of energy dispersion is shown in Figure 2.4. It is split by the effect of Rashba spin-orbit coupling. The plus and minus branch meet when $k_x = k_y = 0$ and $k_x = 0, k_y = \pm\pi/a$. The $E(k_x = 0, k_y = 0)$ is $\frac{t_{so}^2 a}{t_R}$ above the bottom of the band, whereas $E(k_x = 0, k_y = \pm\pi/a)$ is $\frac{t_{so}^2 a}{t_R}$ below the top of the band. These two levels are called the 1st and the 2nd crossing point of two branches, respectively. Note that $E_{R1}(k_y) = (\epsilon_R - \mu) - 2t_R(1 + \cos(k_y a)) - 2t_{so} \sin(k_y a)$ and $E_{R2}(k_y) = (\epsilon_R - \mu) - 2t_R(-1 + \cos(k_y a)) + 2t_{so} \sin(k_y a)$. The energy below and above two crossing points is the Rashba energy; $E_{so}^{bot,top} = \frac{t_{so}^2 a}{t_R}$. The contour energy for different energy of the plus and minus branch was showed in Figure 2.5.

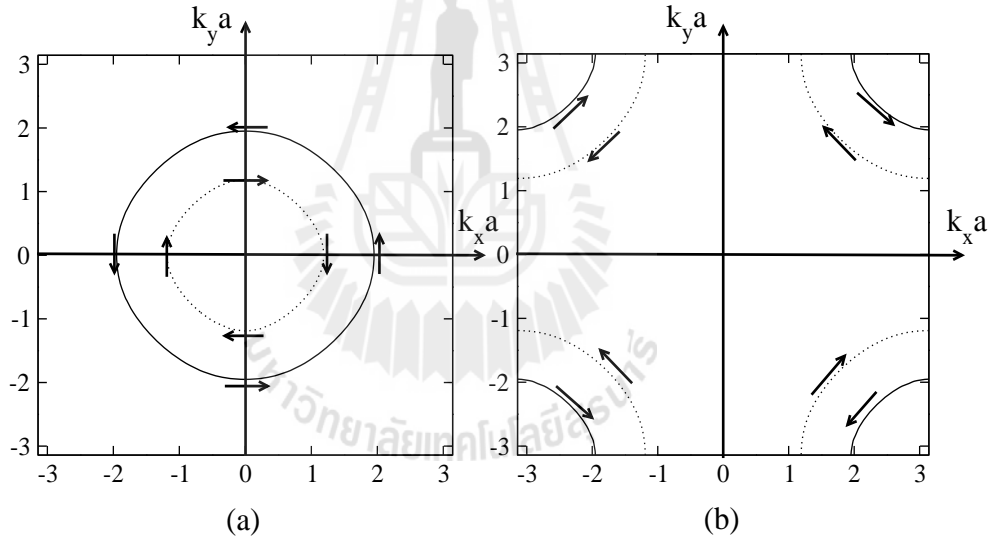


Figure 2.5 Plots of the energy contour of Rashba system, (a) the energy slightly above the 1st crossing point, (b) the energy slightly below the 2nd crossing point. The solid line and dotted line are for the minus and plus branch, respectively.

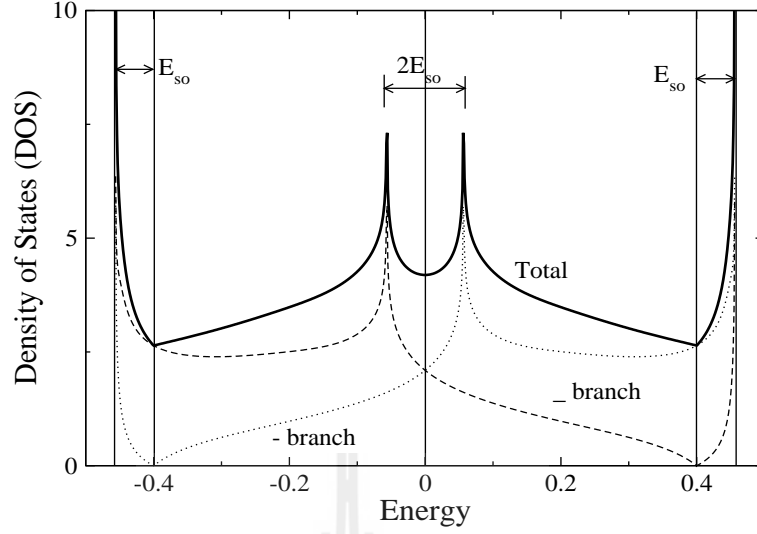


Figure 2.6 Density of states of Rashba system is in a unit of $\mathcal{A}/8\pi^2 t_R$, where \mathcal{A} is the area of the system.

2.2.1 Density of States (DOS)

According to the total density of states for 2DEG in Eq.(2.4), the summations between a double integral:

$$D(E) = \frac{1}{2\pi^2} \int dk_x a \int dk_y a \cdot \delta(E - E_{\vec{k}}). \quad (2.17)$$

By changing the integral variable, we have

$$dk_x a = \frac{dE \sqrt{\sin^2(k_x a) + \sin^2(k_y a)}}{2t_R \sin(k_x a) [\sqrt{\sin^2(k_x a) + \sin^2(k_y a)} \pm 2t_{so} \cos(k_x a)]}. \quad (2.18)$$

Substitute Eq.(2.18) into Eq.(2.17), we obtain

$$D(E) = \frac{1}{4\pi^2 t_R} \int_0^{\kappa^{\pm} a} dk_y a \frac{\sqrt{\sin^2(k_x a) + \sin^2(k_y a)}}{\sin(k_x a) [\sqrt{\sin^2(k_x a) + \sin^2(k_y a)} \pm (t_{so}/t_R) \cos(k_x a)]}, \quad (2.19)$$

where

$$\cos(\kappa^{\pm} a) = \frac{1}{2} \left(\frac{t_R(2t_R - E)}{t_R^2 + t_{so}^2} \pm \sqrt{\frac{t_{so}^2(4t_{so}^2 + 4Et_{so}^2 - E^2)}{(t_R^2 + t_{so}^2)^2}} \right), \quad (2.20)$$

and

$$\begin{aligned} \cos(k_x a) = & \frac{1}{2} \left(\frac{t_R(E + 2t_R \cos(k_y a))}{t_R^2 + t_{so}^2} \right) \\ & \pm \frac{1}{2} \sqrt{\frac{t_{so}^2 (4t_R^2 + 6t_{so}^2 - E^2 - 4t_R E \cos(k_y a)) - 2(2t_R^2 + t_{so}^2) \cos(2k_y a)}{(t_R^2 + t_{so}^2)^2}}. \end{aligned} \quad (2.21)$$

The plus and minus signs in Eq.(2.18) - Eq.(2.21) are for plus and minus branch. The numerical solution of the DOS of RSOC system as shown in Figure 2.6.

The numerical solution of the DOS in Eq.(2.19), it seen that the DOS of Rashba system in this model shows strong energy dependence. There are four van Hove singularities in the DOS, the top and the bottom of the band, and the two points near the half-filled level (see Figure 2.6). Each of the two later points is E_{so} below and above the half-filled level. Figure 2.7 is the DOS when $t_{so} = 0$. Notice that in this case there is only one van Hove singularity at the half-filled level only.

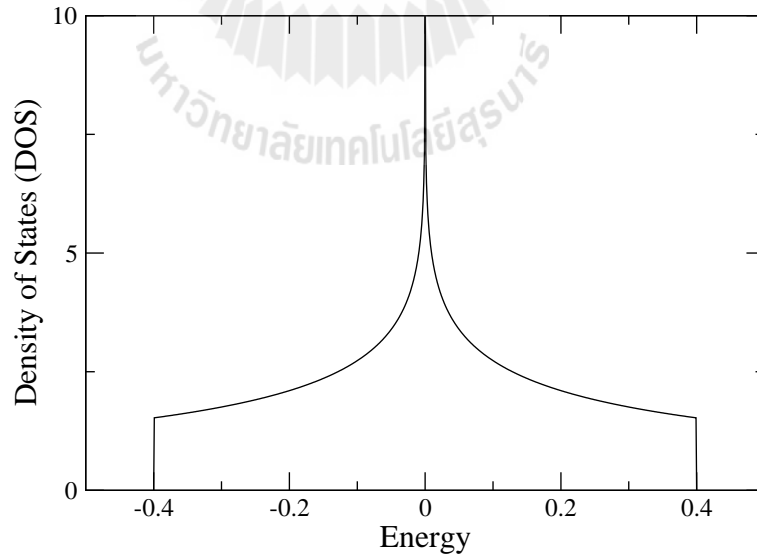


Figure 2.7 Density of states of 2DEG without RSOC is in a unit of $\mathcal{A}/8\pi^2 t_N$.

2.2.2 Carrier Density at Zero Temperature

The carrier density of the 2DEG with RSOC system is plotted in Figure 2.8. In the Rashba energy, the carrier density is similar with obtained by the continuous model. Beyond the crossing the carrier density change its slope at the energy equivalent to around the half-filled level. While the carrier density investigated by a continuous model is linearly.

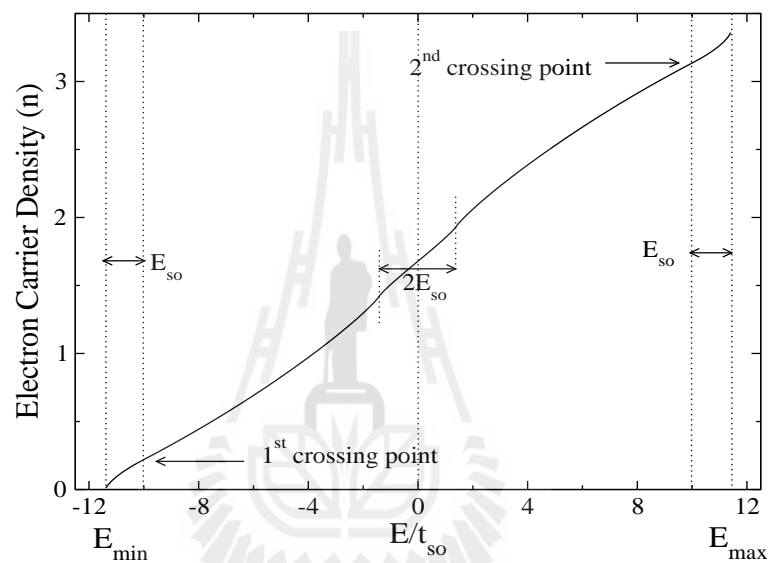


Figure 2.8 The plot of carrier density of particle of the 2DEG with RSOC system in a lattice model.

CHAPTER III

A METAL/RASHBA SYSTEM JUNCTION IN A CONTINUOUS MODEL

We now consider the particle transport across the junction between a metal and a 2DEG with the RSOC. In particular, we will calculate the conductance spectrum of the junction and look into how the conductance depends on the physical properties of the junction, such as the insulating barrier at the interface, the RSOC strength, and the density of the carriers in the Rashba system. In this work we analyze the conductance in the continuous model and in the next chapter the lattice model.

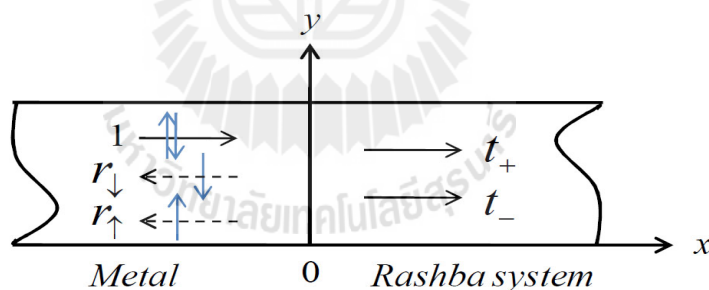


Figure 3.1 Example of a metal/Rashba system junction in a 2-dimensional system.

3.1 Model and Assumptions

We model our junction as a 2D system, which lies on an xy plane. This junction consists of a 2DEG with the RSOC and a metal as show in Fig 3.1.

We assume that the interface is smooth, and the barrier at each interface can be represented by a Dirac-delta function potential (Blonder et al., 1982) at $x = 0$. We use the free electron model to describe the electronic properties of each side of the junction.

We describe our system in the continuous model using the following Hamiltonian:

$$\vec{H} = \left\{ \hat{p} \frac{1}{2m(x)} \hat{p} + V(x, y) \right\} \hat{I} + \vec{H}_{RS}(x). \quad (3.1)$$

\hat{I} is a 2×2 unity matrix. $\hat{p} = -i\hbar(\hat{x}\frac{\partial}{\partial x} + \hat{y}\frac{\partial}{\partial y})$. The effective mass $m(x)$ is position dependent: $[m(x)]^{-1} = m^{-1}\Theta(-x) + (m^*)^{-1}\Theta(x)$, where m and m^* are the effective electron mass in the metal and the Rashba system, respectively, and $\Theta(x)$ is the Heaviside step function. $V(x, y)$ is also a position dependent function and is modelled by the expression

$$V(x, y) = H\delta(x) - E_F(\Theta(-x)) + U_0(\Theta(x)), \quad (3.2)$$

where H represents the scattering potential matrix of the barrier. The diagonal elements of H , $H^{\uparrow\uparrow}$ and $H^{\downarrow\downarrow}$, correspond to the spin-conserving scattering potential, whereas the off-diagonal elements, $H^{\uparrow\downarrow}$ and $H^{\downarrow\uparrow}$, correspond to the spin-flip scattering potentials. U_0 is the offset energy which is assumed to be much smaller than the Fermi energy $E_F = \frac{\hbar^2 q_F^2}{2m}$ of the metal. $\vec{H}_{RS}(x)$ is the RSOC term that is expressed as (Rashba, 1960a; Rashba, 1960b; Bychkhov and Rashba, 1984a; Bychkhov and Rashba, 1984b)

$$\vec{H}_{RS} = \frac{1}{2} \left(\frac{\lambda(x)}{\hbar} [\vec{\sigma} \times \vec{p}] \cdot \hat{z} + [\vec{\sigma} \times \vec{p}] \cdot \hat{z} \frac{\lambda(x)}{\hbar} \right), \quad (3.3)$$

where $\lambda(x) = \lambda\Theta(x)$ is the spin-orbit coupling parameter, which can be tuned by applying an external electric field perpendicular to the 2D plane (Nitta et al., 1997; Koga et al., 2002; Heida et al., 1998; Engels et al., 1997; Sato et al., 2001; Hu et al.,

1999), \hat{z} is the direction perpendicular to the plane of motion, $\vec{\sigma} = (\sigma_x, \sigma_y, \sigma_z)$ is the Pauli spin matrix vector, and \vec{k} is the wave vector of electron.

The electron energy on the metallic side ($x > 0$) is therefore

$$E(q) = \frac{\hbar^2 q^2}{2m} - E_F, \quad (3.4)$$

where $q = \sqrt{q_x^2 + q_y^2}$ is the magnitude of the electron wave vector.

The electron energy dispersion relation on the Rashba side ($x > 0$) is

$$E_{\pm}(k) = \frac{\hbar^2}{2m^*} [k^2 \pm 2k_0 k] + U_o, \quad (3.5)$$

where $k = \sqrt{k_x^2 + k_y^2}$ is the magnitude of the electron wave vector and $k_0 = m^* \lambda / \hbar$ is related to the strength of the RSOC. Figure 3.2 shows the electronic energy dispersion relation of each side of the junction and the corresponding energy contour.

The goal is to find the current density as a function of applied voltage across the junction by using the scattering method. In this method, we first consider an incoming electron from one side of the junction, and calculate the reflection and transmission probabilities, which are later used to obtain the current density of the junction. Thanks to the principle of microscopic reversibility (Datta, 1995; Askerov, 1994; Thomas, 2004), we can freely choose which side of the incoming electron comes from, and in our case we consider it coming from the metal in region $x < 0$.

The wave function of the electron on the metal side with energy E is therefore written as a linear combination of incident momentum state and reflected states of the same energy and the momentum along the surface $\hbar k_y$. Because there are equal number of electrons with opposite spin directions, there are two possibilities of the wave function. That is, in general, the two possibilities of the spin part of an incoming electron are: $|\delta\rangle = \cos\delta |\uparrow\rangle + \sin\delta |\downarrow\rangle$ and $|\delta\rangle = -\sin\delta |\uparrow\rangle + \cos\delta |\downarrow\rangle$,

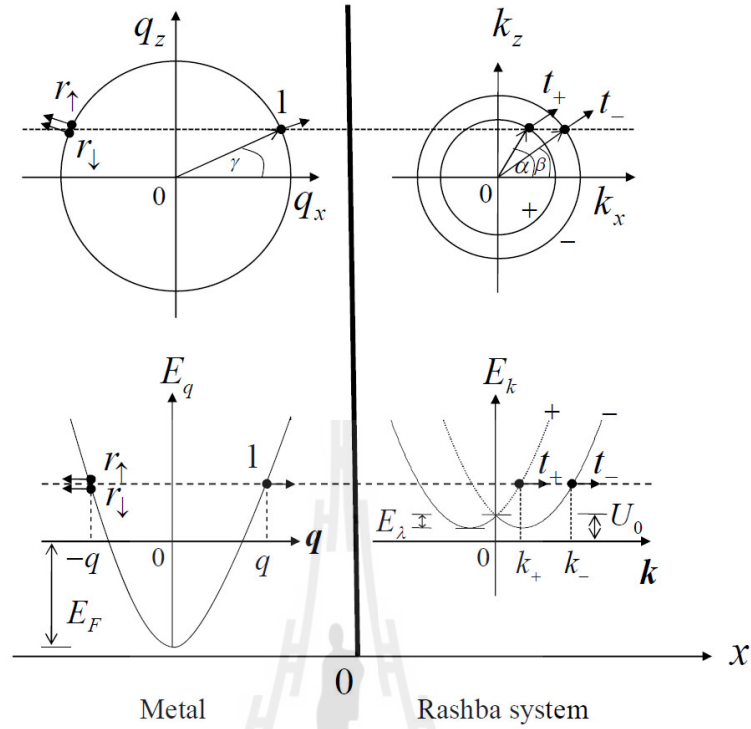


Figure 3.2 The sketches of the energy spectra of the metal (on the left) and the Rashba system (on the right). E_F , U_0 , and $E_\lambda = \hbar^2 k_0^2 / 2m^*$ are the Fermi energy, the Rashba offset energy and the Rashba energy, respectively.

where δ is the angle of the spin direction with respect to the x axis. Because we only consider the system in zero applied magnetic field, we can freely choose the direction of the electron spin in the metal to be in the $+y$ and $-y$ direction, i.e., by setting $\delta = 0$. The wave function of the electron in the metal side can be written in two cases, depending on the spin orientation of the incident electron, as:

$$\psi_M^{(1)} = \left(\begin{bmatrix} \cos \delta \\ \sin \delta \end{bmatrix} e^{iq_x x} + \begin{bmatrix} r_{1\uparrow} \\ r_{1\downarrow} \end{bmatrix} e^{-iq_x x} \right) e^{iq_y y} \quad (3.6)$$

$$\psi_M^{(2)} = \left(\begin{bmatrix} -\sin \delta \\ \cos \delta \end{bmatrix} e^{iq_x x} + \begin{bmatrix} r_{2\uparrow} \\ r_{2\downarrow} \end{bmatrix} e^{-iq_x x} \right) e^{iq_y y}, \quad (3.7)$$

where $q_x = q \cos \gamma$ and $q_y = q \sin \gamma$, where γ is the angle between \vec{q} and x axis and

$q = \sqrt{2m(E_F - E)/\hbar^2}$, $r_{j\sigma}$ is the reflection coefficient for the reflected electron with spin σ in case j of the incident electron.

In the RSOC region ($x \geq 0$), the wave function is obtained as a linear combination of two outgoing states of the same energy and k_y . Because of the different nature of the states with energy above and below the crossing point, we have two forms of the electronic wave functions for the Rashba system, dependent on the energy of the electron. For $E > U_0$,

$$\begin{aligned} \psi_{RS}^{(j)}(E \geq U_0) = & \frac{1}{\sqrt{2}} \left(\begin{bmatrix} 1 \\ \frac{|k^+|}{ik_x^+ + k_y} \end{bmatrix} t_{j+} e^{ik_x^+ x} \right. \\ & \left. + \begin{bmatrix} 1 \\ -\frac{|k^-|}{ik_x^- + k_y} \end{bmatrix} t_{j-} e^{ik_x^- x} \right) e^{ik_y y}, \end{aligned} \quad (3.8)$$

for $E < U_0$,

$$\begin{aligned} \psi_{RS}^{(j)}(E < U_0) = & \frac{1}{\sqrt{2}} \left(\begin{bmatrix} 1 \\ -\frac{|k^+|}{-ik_x^+ + k_y} \end{bmatrix} t_{j+} e^{-ik_x^+ x} \right. \\ & \left. + \begin{bmatrix} 1 \\ -\frac{|k^-|}{ik_x^- + k_y} \end{bmatrix} t_{j-} e^{ik_x^- x} \right) e^{ik_y y}. \end{aligned} \quad (3.9)$$

In both equations above, The k_y is parallel momentum of the electron and $k_y = q_y$ due to the conservation of the momentum along the interface. t_{j+} and t_{j-} are the transmission amplitudes for plus (minus) branch of RSOC for the incident electron case j from the metal side, and $k_x^+ = k^+ \cos \alpha$ and $k_x^- = k^- \cos \beta$, where α and β are the angle k^+ and k^- with respect to the x axis (see Figure 3.2 for function of α and β). k^\pm depends on energy as

$$k^-(E) = k_0 + \sqrt{k_0^2 + \frac{2m^*}{\hbar^2}(E - U_0)}, \quad (3.10)$$

and

$$k^+(E) = \pm \left(k_0 - \sqrt{k_0^2 + \frac{2m^*}{\hbar^2}(E - U_0)} \right). \quad (3.11)$$

The + and - signs in Eq.(3.11) are for $E < U_0$ and $E \geq U_0$, respectively.

Notice that k^\pm can also be written as a function of electron density. That is, for $E \geq U_0$, it can be obtained as

$$k^\pm(E) = \sqrt{k_0^2 + 2\pi(n(E) - n_u)} \mp k_0, \quad (3.12)$$

where $n_u = 0.5n_F$, n_F is the carrier density at Fermi energy. The corresponding group velocities are $v_{RS}^\pm = \frac{\hbar}{m^*} \sqrt{2n(E)\pi + k_0^2}$. The + and - signs in the equation are for the plus and minus branches, respectively.

For $E < U_0$, the wave vector is obtained as

$$k(E) = k_0 \mp \frac{(n(E) - n_u)\pi}{k_0}. \quad (3.13)$$

The corresponding group velocities are $v_{RS}^\mp = \frac{\hbar}{m^*} \frac{n(E)\pi}{k_0}$. The - and + signs in the two previous equations are for $k_0 \leq |k| < 2k_0$ and $-k_0 \leq |k| < 0$, respectively.

We now apply the matching conditions to the wave functions on both sides to obtain the transmission and reflections amplitude: the continuity of the wave function and the discontinuity in the slope of the wave function ($\partial\psi/dx$), due to the delta-function like barrier at the interface. That is,

$$\psi_M^{(j)}(x = 0^+, y) = \psi_{RS}^{(j)}(x = 0^-, y) = \psi^{(j)}(0), \quad (3.14)$$

$$\left(\frac{m}{m^*} \frac{\partial\psi_{RS}^{(j)}}{\partial x} - \frac{\partial\psi_M^{(j)}}{\partial x} \right) \Big|_0 = \left(2k_F Z - ik_0 \frac{m}{m^*} \sigma_y \right) \psi^{(j)}(0), \quad (3.15)$$

where $Z = \frac{mH}{\hbar^2 q_F}$ that determines the strength interfacial scattering. The diagonal components $Z_{\uparrow\uparrow} = \frac{mH_{\uparrow\uparrow}}{\hbar^2 q_F}$ and $Z_{\downarrow\downarrow} = \frac{mH_{\downarrow\downarrow}}{\hbar^2 q_F}$. We assume $Z_{\uparrow\uparrow} = Z_{\downarrow\downarrow} = Z_0$. The off-diagonal components $Z_{\uparrow\downarrow} = \frac{mH_{\uparrow\downarrow}}{\hbar^2 q_F} = Z_{\downarrow\uparrow} = \frac{mH_{\downarrow\uparrow}}{\hbar^2 q_F} \equiv Z_F$. From these matching conditions, we can calculate the reflection and transmission amplitudes ($r_{j\sigma}, t_{j\sigma}$), and their corresponding probabilities can also be obtained as follows:

$$R_{j\sigma} = |r_{j\sigma}|^2, \quad (3.16)$$

$$T_{j+} = \frac{m}{m^*} |t_{j+}|^2 \left(\frac{\mp k^+ + k_0 \cos \alpha}{q} \right), \quad (3.17)$$

$$T_{j-} = \frac{m}{m^*} |t_{j-}|^2 \left(\frac{k^- - k_0 \cos \beta}{q} \right), \quad (3.18)$$

where $j = 1, 2$ correspond to the spin orientation of the incident electron. $R_{j\sigma}$ are the reflection probabilities of spin- σ states and T_{j+} and T_{j-} are the corresponding transmission probabilities for the two branches. Also, the upper and lower signs in $T_{i\pm}$ are for $E < U_0$ and $E \geq U_0$, respectively. The matching conditions ensure that $R_{i\uparrow} + R_{i\downarrow} + T_{i+} + T_{i-} = 1$.

Because the current density is the same for all planes parallel to the interface, we can consider only the current density in a metal. That is, the current density of electron in the x direction is given by

$$j_x^e = \sum_k n_k v_x e, \quad (3.19)$$

where n_k is the density of electrons, i.e., $n_k = \sum_{i=1}^2 (1 - R_{i\uparrow} - R_{i\downarrow}) f(E)$, where $f(E)$ is the Fermi Dirac distribution function, v_x is the x component of the group velocities, and e is the electron charge.

As a function of applied voltage V as follows, we can write the current density as

$$j_x^e(eV) = \sum_{q_x > 0, q_z} e v_x \sum_{i=1}^2 (1 - R_{i\uparrow} - R_{i\downarrow}) f(E) \times (f[E(q) - eV] - f[E(q)]). \quad (3.20)$$

By transforming the summation into the integration and considering at the zero temperature, we can obtain the expression for the electric current density as

$$j_x^e(eV) = \frac{e}{h} \frac{A q_F}{2\pi} \int_0^{eV} dE \int_{-\gamma_m}^{\gamma_m} d\gamma \cos \gamma \sqrt{1 + \frac{E}{E_F}} \sum_{i=1}^2 (1 - R_{i\uparrow} - R_{i\downarrow}), \quad (3.21)$$

where \mathcal{A} is the area of the metal and $\gamma_m = \sin^{-1}[k^-(E)/q(E)]$ is the maximum angle incident electron from the metal.

The differential conductance, $G(V) \equiv dj_x^e/dV$, can be found to be

$$G(V) = \frac{e^2}{h} \frac{\mathcal{A}q_F}{2\pi} \int_{-\gamma_m}^{\gamma_m} d\gamma \cos\gamma \sqrt{1 + \frac{eV}{E_F}} \sum_{i=1}^2 (1 - R_{i\uparrow} - R_{i\downarrow}). \quad (3.22)$$

In the next section, we show and discuss the results from these equations.

3.2 Results and Discussion

In this section, we consider the effect of the following physical properties on the conductance: the spin-conserving and non-conserving interfacial scattering strength, the RSOC strength, and the carrier density of the Rashba system. All numerical solutions of conductance are plotted in a unit of $e^2\mathcal{A}^2q_F/\pi h$. We set the offset energy; $U_0 = 0.5E_F$. Unless we state otherwise, we set $m/m^* = 20$ and $k_0 = 0.05q_F$, which are the values similar to those obtained in experiments in RSOC systems (Hirahara et al., 2006; Ast et al., 2007; Ast et al., 2008). Also, in all plots of the conductance spectra (G vs eV), we assume the Rashba band is empty; so that, the spectra occur in the positive applied voltage region.

The conductance spectra G as a function of applied voltage for different Z_0 , when $Z_F = 0$ are shown in Figure 3.3. One can see that the conductance is zero until the applied voltage equal to the bottom of the Rashba band, where $eV = E_\lambda$. For $eV > E_\lambda$, the conductance rapidly increases with large slope and then slowly increases until $eV = 2E_\lambda$, the crossing point of the two branches. After that the conductance linearly increases. The two features of energy different between the onset and the discontinuity in the slope of the conductance spectra can be used to determine the Rashba energy; E_λ (Srisongmuang et al., 2008). Also, in the absence of spin-flip scattering, the presence of the spin-conserving

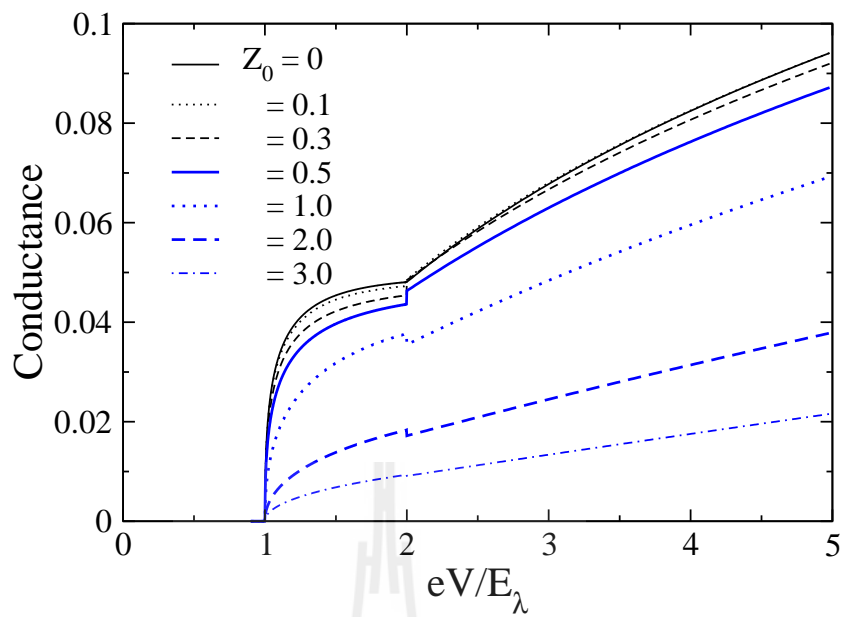


Figure 3.3 Differential conductance spectra G as a function of applied voltage for different Z_0 in case of $Z_F = 0$.

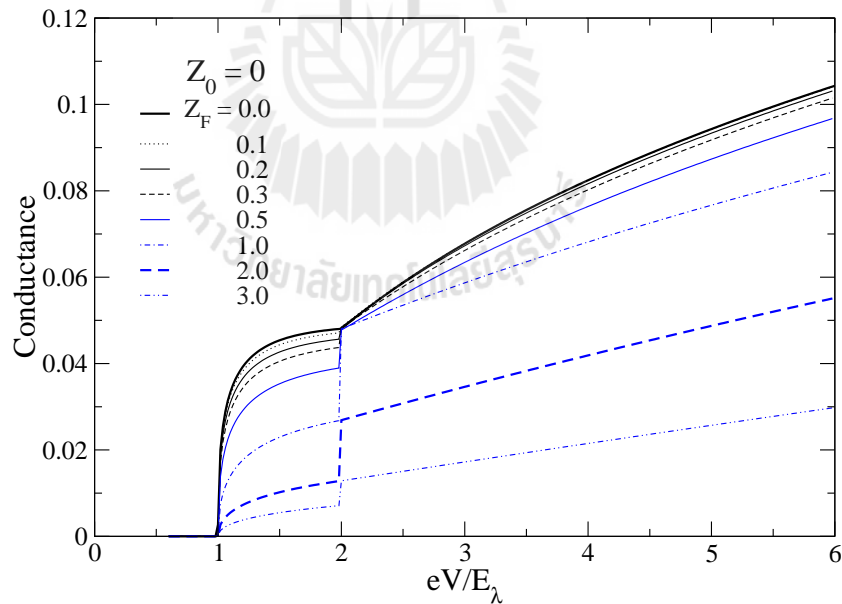


Figure 3.4 Differential conductance spectra G as a function of applied voltage for different Z_F in case of $Z_0 = 0$.

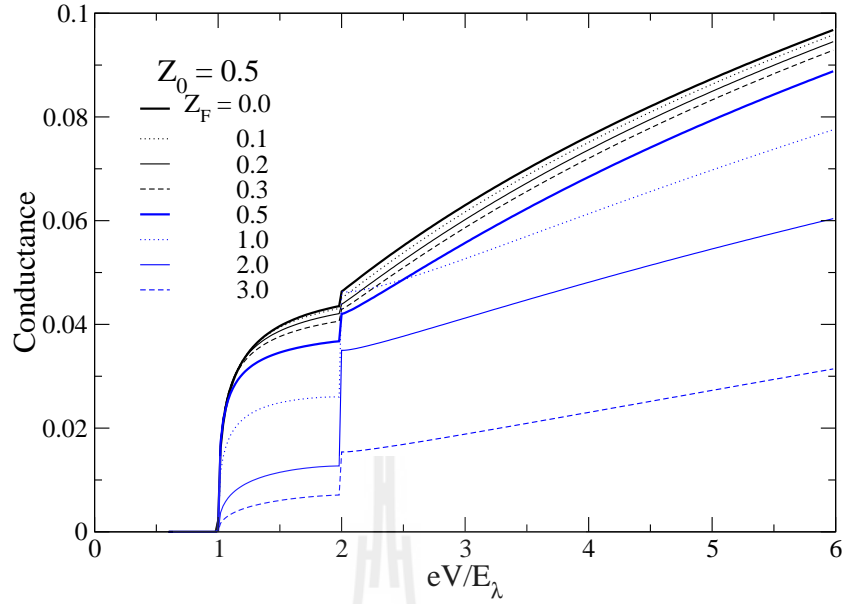


Figure 3.5 Differential conductance spectra G as a function of applied voltage for different Z_F in case of $Z_0 = 0.5$.

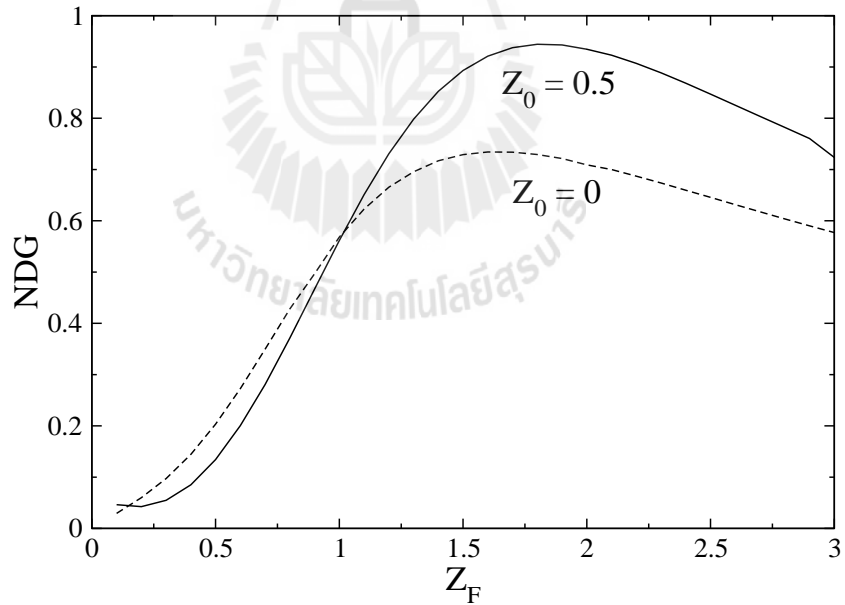


Figure 3.6 Plots of normalization of discontinuity of conductance at the crossing point (NDG) of Figure 3.4 (dashed line) and of Figure 3.5 (solid line), depends on the spin-flip scattering Z_F .

scattering at the interface suppresses the conductance spectrum. It should be noted that the slope of the conductance spectra, when the voltage is higher than the corresponding energy at crossing point, is decreased with the increase in Z_0 .

In Figure 3.4 and Figure 3.5, the plots of tunneling conductance spectrum as a function of applied voltage for different spin-flip scattering strength Z_F , when $Z_0 = 0$ (high transparency) and $Z_0 = 0.5$ (intermediate transparency) are shown, respectively. In these two cases, the conductance spectra are suppressed with an increase in Z_F . Notice that the discontinuity of the conductance spectrum at the crossing point (NDG) can be prominently seen for large value of Z_F . In Figure 3.6, we plot $(G(eV = 2E_\lambda^+) - (eV = 2E_\lambda^-))/(G(eV = 2E_\lambda^+) + (eV = 2E_\lambda^-))$, the normalized discontinuity of the conductance at the crossing point as a function of Z_F .

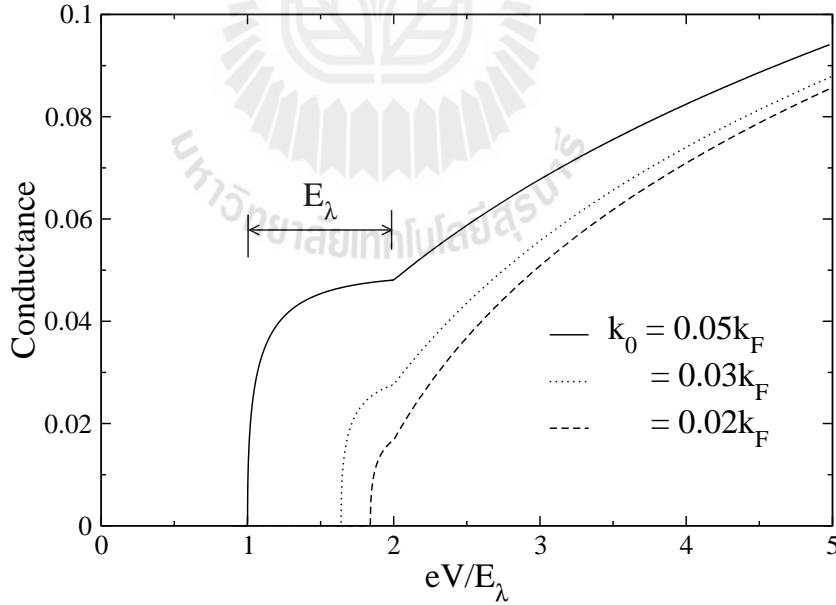


Figure 3.7 Plots of conductance spectrum as a function of applied voltage for different values of k_0 . In these plots, we set $Z_0 = 0$, $Z_F = 0$.

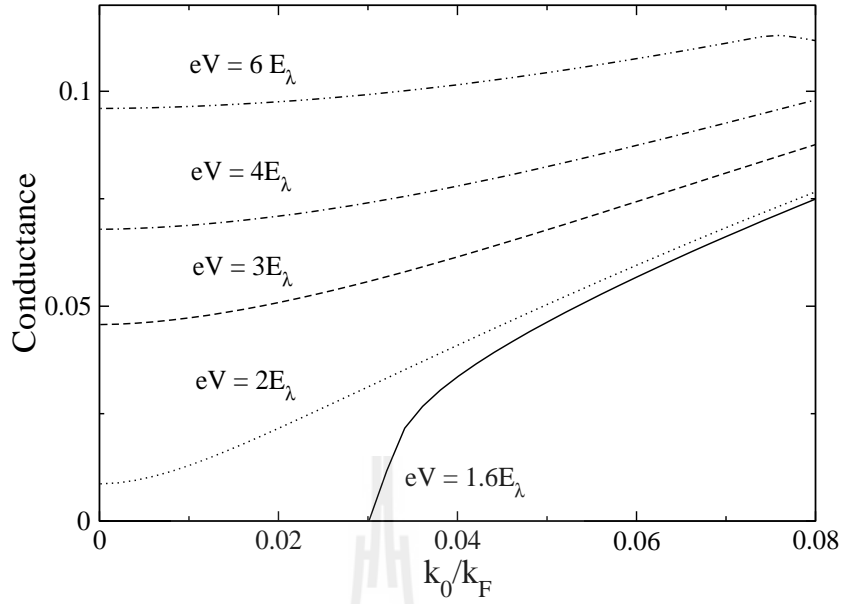


Figure 3.8 Conductance G at different apply voltages as a function of k_0 . We set $Z_0 = 0, Z_F = 0$.

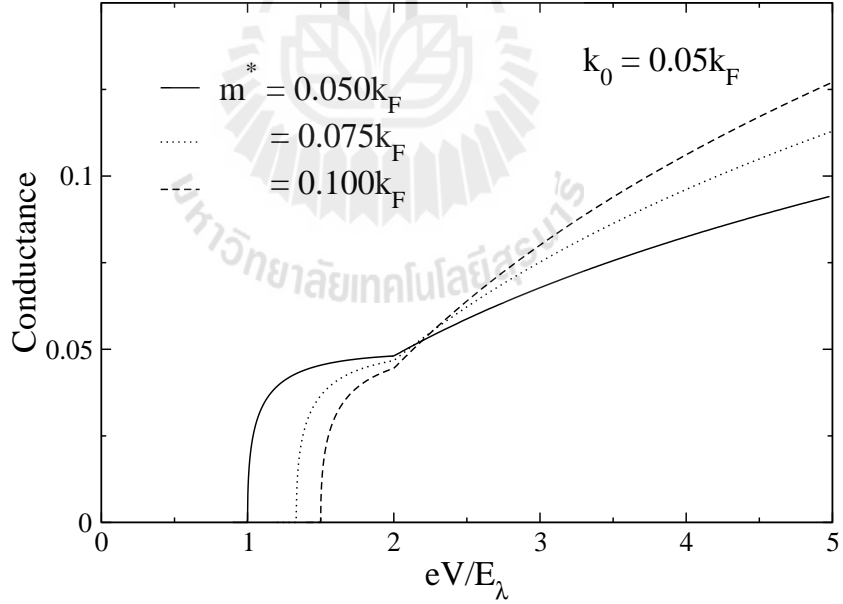


Figure 3.9 Plots of conductance spectrum as a function of applied voltage for different values of m^* . In these plots, we set $Z_0 = 0, Z_F = 0$.

The plots of conductance spectra as a function of applied voltage for different values of k_0 are shown in Figure 3.7. Changing k_0 means changing the Rashba energy and increasing k_0 can enhance the conductance. Figure 3.8 shows the plot of conductance as a function of k_0 for different applied voltages when $Z_0 = Z_F = 0$, for low applied voltage the conductance increases with a larger slope than the high applied voltage. When Z_0, Z_F are non zero the conductance also increases but its magnitude is smaller.

In Figure 3.9, we plot the conductance spectra for different values of m^* (in these plots, $Z_0 = 0, Z_F = 0$). As can be seen, the variation of m^* does two things to the conductance spectrum. First, it changes the Rashba energy, as appeared in the plots via the different voltage separation of the two distinguished features. Second, the effective-mass variation causes the similar effect to that of the spin-conserving interface scattering, i.e., we can see this effect via the change in the slope of the conductance spectrum after the crossing point.

We now plot the conductance at the Fermi level (or zero applied voltage) of the Rashba system as a function of the carrier density in Figure 3.10. Experimentally, one can control the density by applying the gate voltage. As can be seen, the conductance depends quite strongly on the carrier density. There is a kink in the spectra occurring at a critical value n^* corresponding to the filling of the energy band up to the crossing point of the band. This kink was not found in the report on the ferromagnet/Rashba system junction in 1D (Grundler, 2001) and 2D (Matsuyama et al., 2002) system. Previous works did not see this kink because they ignored the change in sign of one of the wave vectors of the minus branch below the crossing point. Fig 3.11 shows the dependence of n^* on k_0 .

Figure 3.12 shows the dependence on the strength of the Rashba spin-orbit coupling of the conductance at zero voltage for various values of the carrier

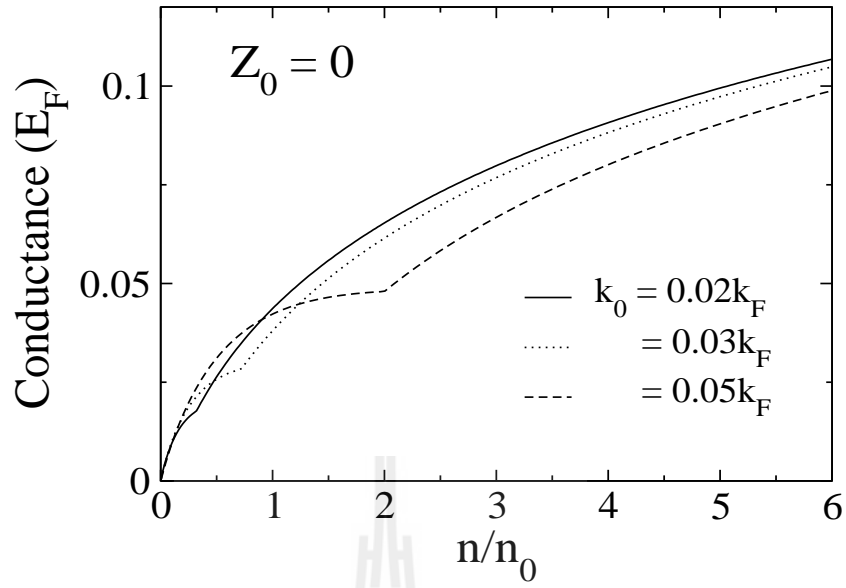


Figure 3.10 Differential conductance at zero voltage G as a function of carrier density of electron for different k_0 in case of $Z_0 = 0$ and $Z_F = 0$. where $n_0 = m^* E_\lambda / \pi \hbar^2$ is the Rasha carrier density.

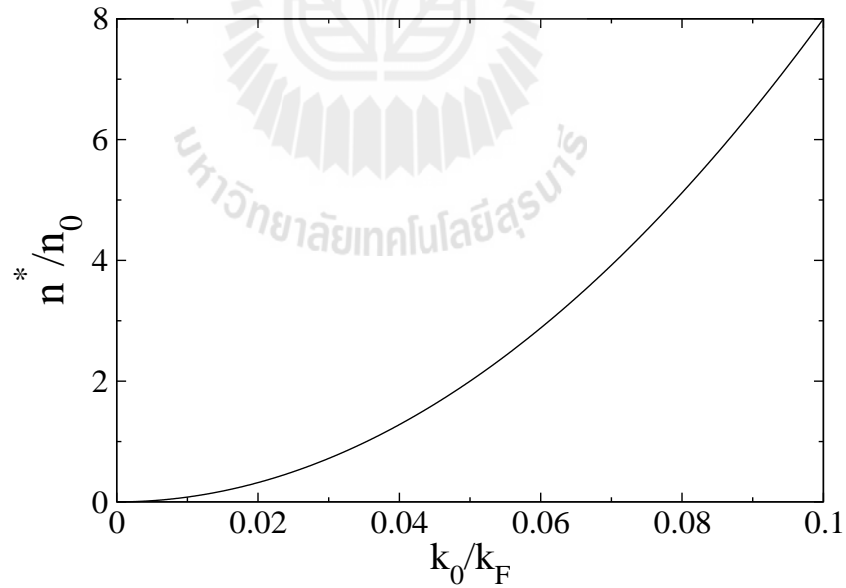


Figure 3.11 Plots of critical value of electron carrier density and k_0 in case of $Z_0 = 0$ and $Z_F = 0$.

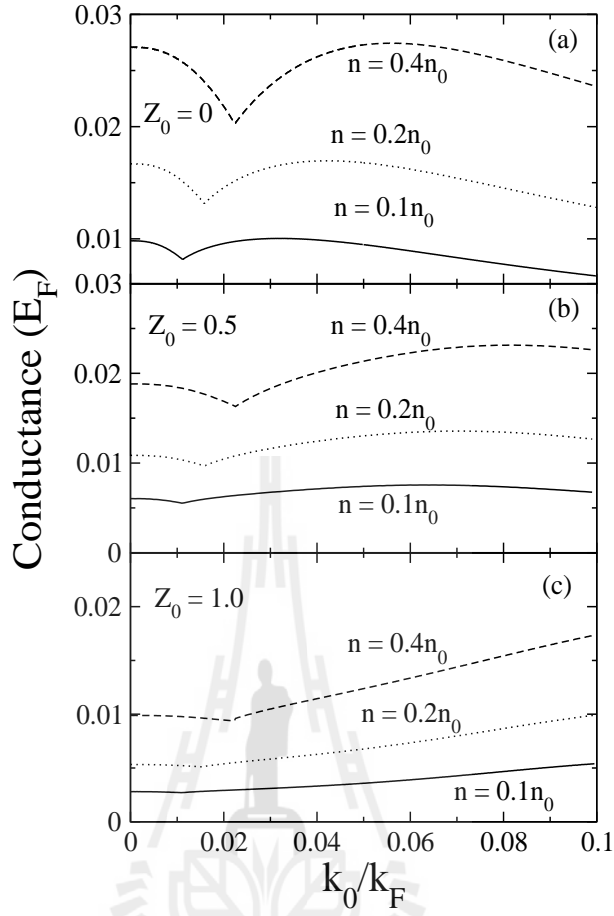


Figure 3.12 Differential conductance at zero voltage G as a function of strength of Rashba spin-orbit coupling k_0 for different n in case of $Z_0 = 0$ (a), $Z_0 = 0.5$ (b), and $Z_0 = 1.0$ (c). All plots set $Z_F = 0$.

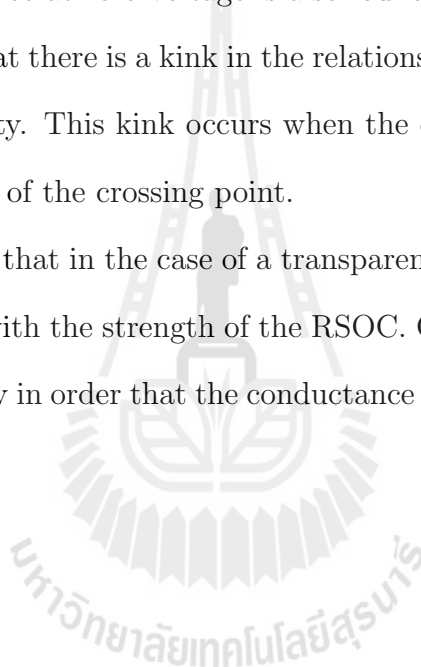
density and the interface barrier strength. In the absence of the interface spin-flip scattering and for $Z_0 \leq 0.5$ (high and intermediate transparency), one can see that the conductance is decreased with k_0 , until k_0 reaches a critical value after which the conductance can be increased with k_0 . After the conductance reaches a maximum value, it is again decreased with k_0 . For junctions with low transparency, i.e. $Z_1 = 1$, one can increase the conductance with the RSOC strength.

3.3 Conclusions

In this chapter, we used the continuous model and the scattering method to calculate the conductance across a metal/Rashba system junction. The conductance spectra provide us the method to determine the Rashba energy. Both spin-conserved and spin-flip interfacial scatterings strongly affect the conductance spectra.

The conductance at zero voltage is also found to be affected by the carrier density. We found that there is a kink in the relationship between the conductance and the carrier density. This kink occurs when the carrier density of the Rashba system is at the level of the crossing point.

We also found that in the case of a transparent junction the conductance is generally decreased with the strength of the RSOC. One needs to make a junction with low transparency in order that the conductance is increased with the strength of the RSOC.



CHAPTER IV

A METAL/RASHBA SYSTEM JUNCTION IN A LATTICE MODEL

In this chapter, we look into the transport properties of carriers in a heterostructure consisting of a metal and a 2DEG with the RSOC by using the tight binding approximation. Similar to the continuous model, we need to find appropriate matching conditions between the electronic wave functions of both sides, in order to obtain the reflection and transmission probabilities and hence the conductance across the junction. We then show and discuss the results for those probabilities and the conductance. We will also look into the spin polarization of conductance in the metal side, to see how the interface scattering can affect the imbalance of spins in the supposedly spin-balanced system.

4.1 Model and Assumptions

In a lattice model, we represent both the normal metal and the RSOC with an infinite 2D square lattice in an xy plane (see Figure 4.1). The system has a translational symmetry along the interface (the y direction), meaning the momentum $\hbar k_y$ is conserved within the reciprocal lattice vector.

As in the continuous model, we use the scattering method to calculate the conductance spectrum in this system. That is, we assume an incoming electron from the normal metal side, write down suitable electronic wave functions for both sides of the junction, and obtain appropriate matching conditions for them

to calculate the reflection and transmission probabilities.

Following the above-mentioned procedure, the electronic wave function of electron with the energy E in the metal is written as a linear combination of incident momentum state and reflected states of the same energy and k_y . Based on the spin part of the wave function, we again have two equally likely incident states. In the absence of the applied magnetic field, we write the two cases of the wave function in the metal side as

$$U_{M,1}^{k_y}(n, m) = \left[e^{iq_x an} \begin{pmatrix} 1 \\ 0 \end{pmatrix} + e^{-iq_x an} \begin{pmatrix} r_{1\downarrow} \\ r_{1\uparrow} \end{pmatrix} \right] e^{ik_y ma} \quad (4.1)$$

$$U_{M,2}^{k_y}(n, m) = \left[e^{iq_x an} \begin{pmatrix} 0 \\ 1 \end{pmatrix} + e^{-iq_x an} \begin{pmatrix} r_{2\downarrow} \\ r_{2\uparrow} \end{pmatrix} \right] e^{ik_y ma}, \quad (4.2)$$

where n, m represent the indices of the columns and rows of the lattice points, $q_x = \frac{1}{a} \cos^{-1} [(E - \epsilon_N + \mu + 2t'_N \cos(k_y a)) / -2t_N]$ is the wave vector along the x direction with $|q_x| < \pi/a$ and $|k_y| < \pi/a$. $r_{j\sigma}$ is the reflection amplitudes of spin- σ state in case j .

In order to focus our attention on the effect of the Rashba system on the particle transport across the junction, we set the hopping energy along the surface in the metal to be smaller than that along the direction perpendicular to the surface, i.e., $t'_N = 0.1t_N$. This choice of the parameter results in the energy contours as shown in Figure 4.3. The parameter $F_N = (\epsilon_N - \mu) / 2(t_N + t'_N)$ is called the filling parameter. In this work, we use the half-filling Fermi surface ($F_N = 0$) represented as the thickest energy contour in the figure. Also, in most cases the energy band width of a metal is about an order of magnitude larger than that of a Rashba system, we therefore set our energy parameters accordingly. That is, we set the hopping energy in the Rashba system to be $t_R = 0.1t_N$. The spin-orbit coupling energy that causes the spin-splitting states is t_{so} , which is set

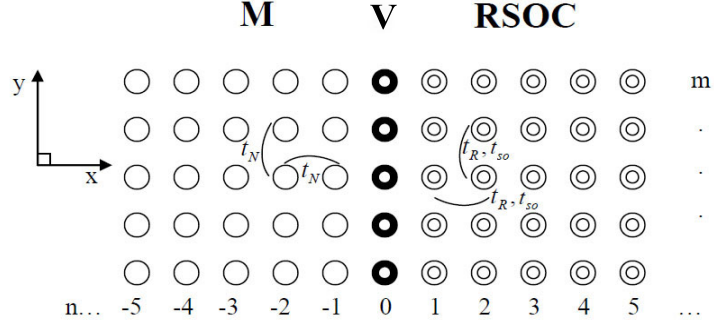


Figure 4.1 Schematic illustration of the square lattice representing the metal/Rashba system junction. This system is the same lattice constant a , and n, m indicate the column and row indices of the lattice, respectively. The energy at on-site ϵ_M is for metal and ϵ_{RS} is for RSOC system.

to be $t_{so} = 0.4t_R = 0.04t_N$, unless we state otherwise. Similarly, we define the filling parameter for the Rashba system as $F_{RS} \equiv (\mu - \epsilon_R)/4t_{so}$. Each filling level is shown in Figure 4.4, where the left panel is for the plus branch and the right panel is for the minus branch.

There are three forms of the electronic wave function, depending on the energy. For $E < E_{R1}(k_y)$,

$$\begin{aligned}
 U_R^{k_y}(n, m) = & \left[t_{j+} e^{i(-k_x^+)an} \frac{1}{\sqrt{2}} \begin{pmatrix} -\frac{i \sin(-k_x^+ a) + \sin k_y a}{\sqrt{\sin^2(-k_x^+ a) + \sin^2 k_y a}} \\ 1 \end{pmatrix} \right. \\
 & \left. + t_{j-} e^{ik_x^- an} \frac{1}{\sqrt{2}} \begin{pmatrix} -\frac{i \sin(k_x^- a) + \sin k_y a}{\sqrt{\sin^2(k_x^- a) + \sin^2 k_y a}} \\ 1 \end{pmatrix} \right] e^{ik_y ma}, \quad (4.3)
 \end{aligned}$$

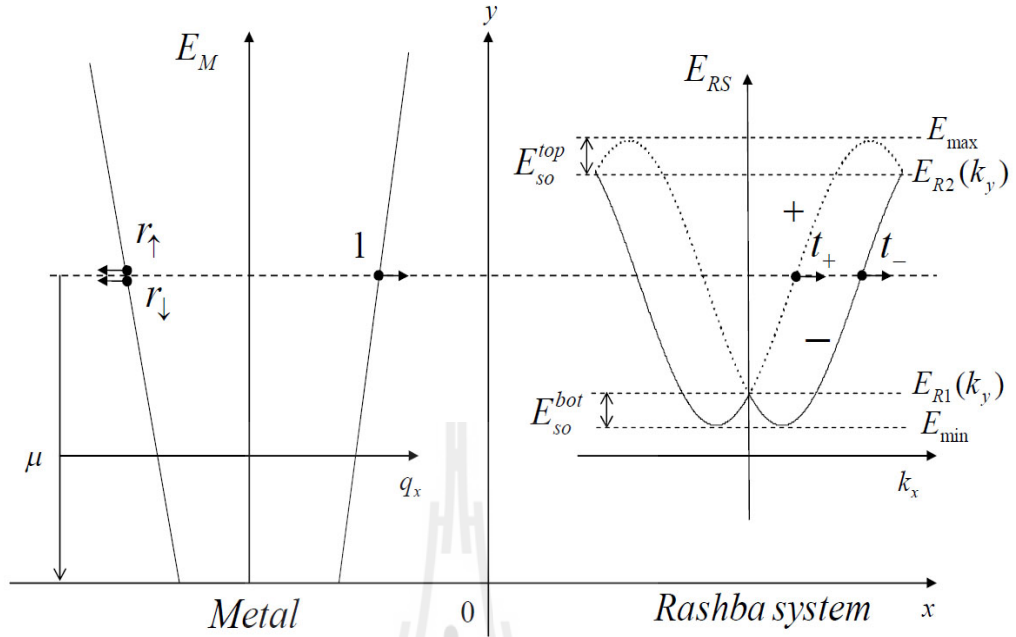


Figure 4.2 The sketches of the energy dispersion relations of an electron in the metal (left) and the Rashba system (right) for $k_y = 0$. The dashed line represents the same energy. E_{max} , E_{min} , E_{R1} , and E_{R2} are dependent on k_y and are defined in the text.

for $E_{R1}(k_y) \leq E \leq E_{R2}(k_y)$,

$$\begin{aligned}
 U_R^{k_y}(n, m) = & \left[t_{j+} e^{ik_x^+ an} \frac{1}{\sqrt{2}} \begin{pmatrix} \frac{i \sin k_x^+ a + \sin k_y a}{\sqrt{\sin^2 k_x^+ a + \sin^2 k_y a}} \\ 1 \end{pmatrix} \right. \\
 & \left. + t_{j-} e^{ik_x^- an} \frac{1}{\sqrt{2}} \begin{pmatrix} -\frac{i \sin(k_x^- a) + \sin k_y a}{\sqrt{\sin^2(k_x^- a) + \sin^2 k_y a}} \\ 1 \end{pmatrix} \right] e^{ik_y ma}, \quad (4.4)
 \end{aligned}$$

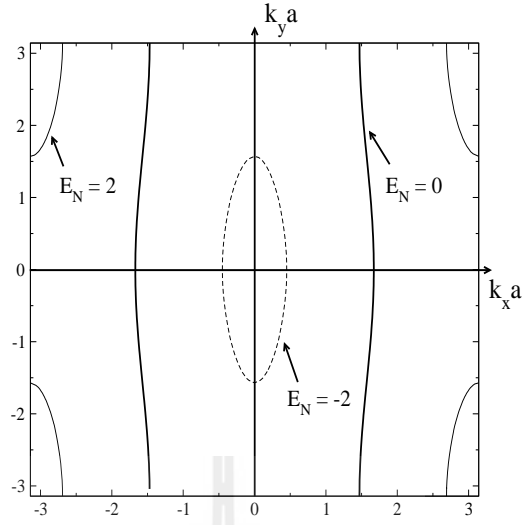


Figure 4.3 Energy contours of the metal, where $t'_N = 0.1t_N$.

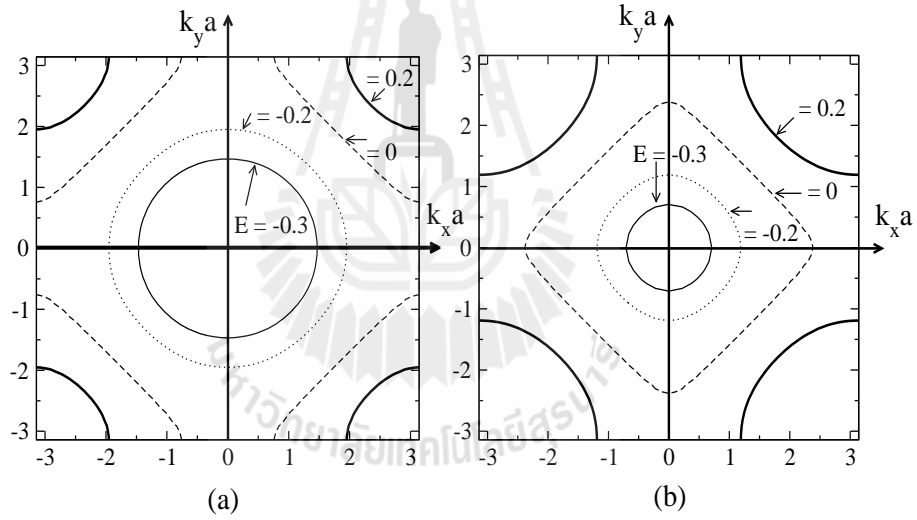


Figure 4.4 Plots of energy contours of the Rashba system. On the left is for the plus branch and on the right is for the minus branch.

for $E > E_{R2}(k_y)$,

$$\begin{aligned}
 U_R^{k_y}(n, m) = & \left[t_{j+} e^{ik_x^+ an} \frac{1}{\sqrt{2}} \begin{pmatrix} \frac{i \sin k_x^+ a + \sin k_y a}{\sqrt{\sin^2 k_x^+ a + \sin^2 k_y a}} \\ 1 \end{pmatrix} \right. \\
 & \left. + t_{j-} e^{i(-k_x^-)an} \frac{1}{\sqrt{2}} \begin{pmatrix} \frac{i \sin(-k_x^- a) + \sin k_y a}{\sqrt{\sin^2(-k_x^- a) + \sin^2 k_y a}} \\ 1 \end{pmatrix} \right] e^{ik_y ma}, \quad (4.5)
 \end{aligned}$$

where $E_{R1}(k_y) = \epsilon_R - 2t_R(1 + \cos k_y a) - 2t_{so} \sin k_y a$ and $E_{R2}(k_y) = \epsilon_R - 2t_R(1 + \cos k_y a) + 2t_{so} \sin k_y a$, $j = 1, 2$ refer to the two cases of different incoming states in the metal, and k_x^\pm are defined as

$$\begin{aligned} \cos(k_x a) &= \frac{1}{2} \left(\frac{t_R(E + 2t_R \cos(k_y a))}{t_R^2 + t_{so}^2} \right) \\ &\pm \frac{1}{2} \sqrt{\frac{t_{so}^2 (4t_R^2 + 6t_{so}^2 - E^2 - 4t_R E \cos(k_y a)) - 2(2t_R^2 + t_{so}^2) \cos(2k_y a)}{(t_R^2 + t_{so}^2)^2}}. \end{aligned} \quad (4.6)$$

The \pm signs are for the plus and minus branch, and $t_{j\pm}$ correspond the transmission amplitudes of plus and minus branch in case j , respectively.

Now to obtain the matching conditions for the wave functions, we follow the procedure used to obtain the conditions for a metal/superconductor junction in a lattice model by Pairor and Walker (Pairor and Walker, 2002).

4.2 Boundary Conditions

Here, we describe how we obtain the matching conditions for electron in at the interface of a metal and a Rashba system in our lattice model. These conditions are obtained by considering the Hamiltonian, which described the junction. We use the lattice network to present our junction as shown in Figure 4.1. On each side and at the interface, we have the following set of the equations

$$EU_M(n \leq -2, m) = \epsilon_M U_M(n, m) - t_N [U_M(n \pm 1, m) + U_M(n, m \pm 1)], \quad (4.7)$$

$$EU_M(n = -1, m) = \epsilon_M U_M(n, m) - t_N [U_M(-2, m) + U_R(0, m)] - t_N U_M(-1, m \pm 1), \quad (4.8)$$

$$\begin{aligned}
EU_R(n = 0, m) &= (\epsilon_{RS} - V)U_R(0, m) - t_N U_M(-1, m) - t_R U_R(1, m) \\
&\quad - t_R U_R(0, m \pm 1) \pm \sigma_x t_{so} U_R(1, m) \\
&\quad + i\sigma_x t_{so} [U_R(0, m + 1) - U_R(0, m - 1)], \tag{4.9}
\end{aligned}$$

$$\begin{aligned}
EU_R(n \geq 1, m) &= \epsilon_{RS} U_R(n, m) - t_R [U_R(n \pm 1, m) + U_R(n, m \pm 1)] \\
&\quad \pm \sigma_x t_{so} [U_R(n + 1, m) - U_R(n - 1, m)] \\
&\quad + i\sigma_x t_{so} [U_R(n, m + 1) - U_R(n, m - 1)], \tag{4.10}
\end{aligned}$$

where n and m are the column and low indices as shown in the Figure 4.1, σ_x is the spin Pauli matrix. $U_{M(R)}$ is the eigenstate of a metal in the left side (the RSOC in the right hand side), t_N and t_R are the hopping energy in nearest-neighbor of metal and non spin splitting in Rashba system, respectively and t_{so} is the hopping energy for Rashba spin orbit coupling. ϵ_1, ϵ_2 are the energy at on-site for metal and Rashba system, respectively. $V = \begin{pmatrix} V_0 & V_F \\ V_F & V_0 \end{pmatrix}$ is the scattering potential at the interface. The diagonal elements of V , $V_0 = V_{\uparrow\uparrow} = V_{\downarrow\downarrow}$ are non-spin-flip scattering potentials, and the off-diagonal elements are denoted by $V_F = V_{\uparrow\downarrow} = V_{\downarrow\uparrow}$, which are the spin-flip scattering potentials.

With the translational symmetry along the interface, the wave functions of both side can be written in the following form.

$$U(n, m) = e^{imk_y a} U^{k_y}(n), \tag{4.11}$$

where $-\pi/a \leq k_y \leq \pi/a$. So, the 2D equations above are reduced to the following 1D equations.

$$EU_M^{k_y}(n \leq -2) = \epsilon_M U_M^{k_y}(n) - t_N U_M^{k_y}(n \pm 1) - 2t_N \cos(k_y a) U_M^{k_y}(n), \tag{4.12}$$

$$\begin{aligned}
EU_M^{k_y}(n = -1) &= \epsilon_M U_M^{k_y}(-1) - t_N [U_M^{k_y}(-2) + U_R^{k_y}(0)] - 2t_N \cos(k_y a) U_M^{k_y}(-1), \\
\end{aligned} \tag{4.13}$$

$$\begin{aligned}
EU_R^{k_y}(n=0) &= (\epsilon_{RS} - V)U_R^{k_y}(0) - t_N[U_M^{k_y}(-1) - t_R U_R^{k_y}(1)] \\
&\quad - 2t_R \cos(k_y a)U_R^{k_y}(0) \pm \sigma_x t_{so} U_R^{k_y}(1) - \sigma_x 2t_{so} \sin(k_y a)U_R^{k_y}(0), \quad (4.14)
\end{aligned}$$

$$\begin{aligned}
EU_R^{k_y}(n \geq 1) &= \epsilon_{RS}U_R^{k_y}(n) - t_R U_R^{k_y}(n \pm 1) - 2t_R \cos(k_z a)U_R^{k_z}(n) \\
&\quad \pm \sigma_x t_{so}[U_R^{k_y}(n+1) - U_R^{k_y}(n-1)] - \sigma_x 2t_{so} \sin(k_y a)U_R^{k_y}(n). \quad (4.15)
\end{aligned}$$

Eq.(4.12) and Eq.(4.15) describe the bulk states of the metal and the Rashba system respectively. Eq.(4.13) and Eq.(4.14) provide us with the matching conditions between $U_M^{k_y}(n)$ and $U_R^{k_y}(n)$. First Eq.(4.13) gives:

$$\begin{aligned}
EU_M^{k_y}(-1) &= \epsilon_M U_M^{k_y}(-1) - t_N[U_M^{k_y}(-2) + U_R^{k_y}(0)] - 2t_N \cos(k_y a)U_M^{k_y}(-1) \\
&= \underline{\epsilon_M U_M^{k_y}(-1)} - \underline{t_N U_M^{k_y}(-2)} - t_N U_R^{k_y}(0) - \underline{t_N U_M^{k_y}(0)} \\
&\quad + t_N U_M^{k_y}(0) - \underline{2t_N \cos(k_y a)U_M^{k_y}(-1)}. \quad (4.16)
\end{aligned}$$

The sum of the underline terms is equal to $EU_M^{k_y}(-1)$. Therefore,

$$U_R^{k_y}(0) - U_M^{k_y}(0) = 0, \quad (4.17)$$

Eq.(4.14) gives:

$$\begin{aligned}
EU_R^{k_y}(0) &= \underline{\epsilon_{RS}U_R^{k_y}(0)} - \underline{t_N U_M^{k_y}(-1)} + t_N U_M^{k_y}(-1) - t_R U_R^{k_y}(-1) \\
&\quad - \underline{V U_R^{k_y}(0)} + V U_R^{k_y}(0) - \underline{2t_R \cos(k_y a)U_R^{k_y}(0)} \pm \underline{\sigma_x t_{so}[U_R^{k_y}(1) - U_R^{k_y}(-1)]} \\
&\quad - \underline{\sigma_x 2t_{so} \sin(k_y a)U_R^{k_y}(0)}. \quad (4.18)
\end{aligned}$$

The sum of the underline terms is equal to $EU_R^{k_y}(0)$. Therefore,

$$t_N U_M^{k_y}(-1) - t_R U_R^{k_y}(-1) + V_0 U_R^{k_y}(0) \mp \sigma_x t_{so} U_R^{k_y}(-1) = 0, \quad (4.19)$$

which can be written as

$$t_N U_M^{k_y}(-1) - T_{so} U_R^{k_y}(-1) + V U_R^{k_y}(0) = 0, \quad (4.20)$$

where $T_{so} = \begin{pmatrix} t_R & -t_{so} \\ t_{so} & t_R \end{pmatrix}$.

After substituting the electronic wave functions of both sides by using the boundary conditions Eq.(4.17) and Eq.(4.20), we obtain the transmission (T) and reflection (R) probabilities for $E < E_{R1}(k_y)$ as

$$R_{j\uparrow} = |r_{j\uparrow}|^2, \quad (4.21)$$

$$R_{j\downarrow} = |r_{j\downarrow}|^2, \quad (4.22)$$

$$T_{j+} = |t_{j+}|^2 \times \left(\frac{t_R \sin(-k_x^+ a)}{\sin(q_x a)} - \frac{t_{so} \sin(-k_x^+ a) \cos(-k_x^+ a)}{\sin(q_x a) \sqrt{\sin^2(-k_x^+ a) + \sin^2(k_y a)}} \right), \quad (4.23)$$

$$T_{j-} = |t_{j+}|^2 \times \left(\frac{t_R \sin(k_x^- a)}{\sin(q_x a)} - \frac{t_{so} \sin(k_x^+ a) \cos(k_x^- a)}{\sin(q_x a) \sqrt{\sin^2(k_x^- a) + \sin^2(k_y a)}} \right), \quad (4.24)$$

for $E_{R1}(k_y) \leq E \leq E_{R1}(k_y)$,

$$R_{j\uparrow} = |r_{j\uparrow}|^2, \quad (4.25)$$

$$R_{j\downarrow} = |r_{j\downarrow}|^2, \quad (4.26)$$

$$T_{j+} = |t_{j+}|^2 \times \left(\frac{t_R \sin(k_x^+ a)}{\sin(q_x a)} + \frac{t_{so} \sin(k_x^+ a) \cos(k_x^+ a)}{\sin(q_x a) \sqrt{\sin^2(k_x^+ a) + \sin^2(k_y a)}} \right), \quad (4.27)$$

$$T_{j-} = |t_{j+}|^2 \times \left(\frac{t_R \sin(k_x^- a)}{\sin(q_x a)} - \frac{t_{so} \sin(k_x^+ a) \cos(k_x^- a)}{\sin(q_x a) \sqrt{\sin^2(k_x^- a) + \sin^2(k_y a)}} \right), \quad (4.28)$$

and for $E > E_{R2}(k_y)$,

$$R_{j\uparrow} = |r_{j\uparrow}|^2, \quad (4.29)$$

$$R_{j\downarrow} = |r_{j\downarrow}|^2, \quad (4.30)$$

$$T_{j+} = |t_{j+}|^2 \times \left(\frac{t_R \sin(k_x^+ a)}{\sin(q_x a)} + \frac{t_{so} \sin(k_x^+ a) \cos(k_x^+ a)}{\sin(q_x a) \sqrt{\sin^2(k_x^+ a) + \sin^2(k_y a)}} \right), \quad (4.31)$$

$$T_{j-} = |t_{j+}|^2 \times \left(\frac{t_R \sin(-k_x^- a)}{\sin(q_x a)} + \frac{t_{so} \sin(-k_x^+ a) \cos(-k_x^- a)}{\sin(q_x a) \sqrt{\sin^2(-k_x^- a) + \sin^2(k_y a)}} \right), \quad (4.32)$$

where $R_{j\sigma}$ are the reflection probabilities of spin- σ states in case j , and $T_{j\pm}$ are

the transmission probabilities for the plus and minus branch in case j respectively.

The matching conditions ensure that $R_{j\uparrow} + R_{j\downarrow} + T_{j+} + T_{j-} = 1$.

4.3 Electric Current Density and Conductance Formula

The current density flowing across the junction is given by

$$j = \sum_{\vec{k}} en_e v_x, \quad (4.33)$$

where e is the charge on an electron, n_e is the carrier density, and v_x is the x component of the group velocity. Changing the summation to an integration, we have

$$\begin{aligned} j &= \frac{eL_x L_y}{(2\pi)^2} \int dk_x \int dk_y \vec{v}_k \cdot T(E) (f(E_k - eV) - f(E_k)) \\ &= \frac{eL_x L_y}{(2\pi)^2} \int dk_{\parallel} \int dk_{\perp} \vec{v}_k \cdot T(E) (f(E_k - eV) - f(E_k)), \end{aligned} \quad (4.34)$$

where $f(E)$ is the Fermi distribution function,

$$dk_{\parallel} = dk_y \sqrt{1 + \left(\frac{dk_x}{dk_y}\right)^2}, \quad (4.35)$$

and

$$\begin{aligned} dk_{\perp} &= \frac{dE}{(dE/dk_{\parallel})} \\ &= \frac{dE}{|\vec{\nabla} E|}. \end{aligned} \quad (4.36)$$

Substitute Eq.(4.35) and Eq.(4.36) into Eq.(4.34) to obtain

$$j = \frac{eL_x L_y}{(2\pi)^2} \int dk_y \sqrt{1 + \left(\frac{dk_x}{dk_y}\right)^2} \int \frac{dE}{|\vec{\nabla} E|} \vec{v}_k \cdot T(E) (f(E - eV) - f(E)). \quad (4.37)$$

The energy dispersion of normal metal is given by

$$E(\mathbf{k}) = \epsilon_N - 2t_N \cos(k_x a) - 2t'_N \cos(k_y a). \quad (4.38)$$

Consider

$$\begin{aligned} |\vec{\nabla}_k E| &= \frac{1}{\hbar} \sqrt{v_x^2 + v_y^2} \\ &= \frac{2t_N \sin(k_x a)}{a\hbar} \sqrt{1 + \left(\frac{t'_N \sin(k_y a)}{t_N \sin(k_x a)} \right)^2}, \end{aligned} \quad (4.39)$$

thus

$$\left(\frac{dk_x}{dk_y} \right)^2 = \left(\frac{t'_N \sin(k_y a)}{t_N \sin(k_x a)} \right)^2. \quad (4.40)$$

The group velocity along x direction can be obtained

$$\begin{aligned} v_x &= \frac{1}{a\hbar} \frac{\partial E}{\partial k_x} \\ &= \frac{t_N \sin(k_x a)}{a\hbar}. \end{aligned} \quad (4.41)$$

Substitute Eq.(4.39), Eq.(4.40) and Eq.(4.41) into Eq.(4.37) and obtain

$$j(V) = \frac{eL_x L_y}{(2\pi)^2} \int dk_y \int dE \cdot T(E) (f(E - eV) - f(E)). \quad (4.42)$$

At zero temperature, thus the conductance is

$$\begin{aligned} G(eV) &= \frac{dj}{dV} \\ &= \frac{e^2 L_x L_y}{(2\pi)^2} \int dk_y T(E). \end{aligned} \quad (4.43)$$

We also consider the spin polarization of conductance (Srisongmuang et al., 2008) to investigate the spin imbalance that occurs during the current flow on the metal side. The spin polarization of the conductance $P(E)$ is defined as the difference in the number of spin carriers crossing a plane normal to x in unit time, normalized to the total particle current at energy E ,

$$P(E) = \frac{\sum'_{q_x > 0, q_y} (j_{x,\uparrow} - j_{x,\downarrow})}{\sum'_{q_x > 0, q_y} (j_{x,\uparrow} + j_{x,\downarrow})}, \quad (4.44)$$

where $j_{x,\sigma}$ is the particle current density with spin σ . The \sum' indicates that the summations are over q_x, q_y with a specific value of energy E . In metal, this

spin polarization of the conductance can be written in terms of the reflection probabilities as

$$P_M(E) = \frac{\int_{-\pi/a}^{\pi/a} dk_y \sum_{j=1}^2 (-R_{j\uparrow} + R_{j\downarrow})}{\int_{-\pi/a}^{\pi/a} dk_y \sum_{j=1}^2 (R_{j\uparrow} + R_{j\downarrow})}, \quad (4.45)$$

One can see that $P(E)$ depends on the relative difference in the net number of the carriers with spin up and spin down.

4.4 Results and Discussions

In this section, we show and discuss the result of the transmission probabilities, the conductance spectrum $G(E)$, and the spin polarization of conductance $P(E)$. We emphasize on the effect of the potential barrier height, both non-spin-flip part and spin-flip part.

The main features of the total transmission probability and the conductance spectrum at the bottom of the band are not much different to those investigated by the continuous model. However, because of the nature of the lattice model, we now too have features around the top of the band to consider.

4.4.1 Transmission Probability

We plot the total transmission probability as a function of energy $T(E, k_y)$ for different values of k_y in Figure 4.5. For each value of k_y , $T(E, k_y)$ was zero until the energy reach the lowest energy for that k_y . Beyond this point, it increases with decreasing until it reaches a maximum value at the middle point of the band for that k_y . After that, it decreases and reaches zero at highest energy for that k_y . For $k_y \neq 0$, $T(E, k_y)$ reveals two kinks near a lowest and highest energy as can be seen in Figure 4.5(b)-4.5(d). We show the magnified pictures of the two kinks for

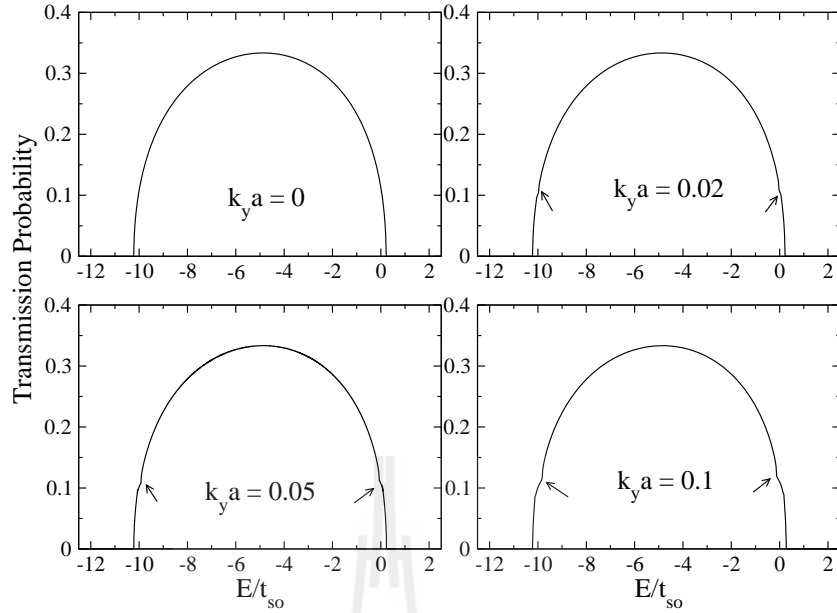


Figure 4.5 Plots of total transmission probability as a function of energy for different $k_y a$.

$k_y = 0.02/a$ and $k_y = 0.05/a$ in the insets of Figure 4.6 and Figure 4.7 respectively. The energy width (ΔE) of the kink depends on k_y as $\Delta E = 4t_{so} \sin k_y a$.

Now we break down the transmission probability into two terms $T^+(E, k_y)$ and $T^-(E, k_y)$ as shown in Figure 4.8 and Figure 4.9. It can be seen that for $k_y = 0$ both of transmission probabilities of plus and minus branch are always equal. However, when k_y is non-zero, the $T^+(E, k_y)$ and $T^-(E, k_y)$ are different in two particular ranges of the width ΔE near the bottom and top of the energy band. One can see in Figure 4.8 and Figure 4.9 that in the range near the bottom $T^+(E, k_y) > T^-(E, k_y)$, but near the top of one $T^+(E, k_y) < T^-(E, k_y)$. The energy range ΔE corresponds to the energy gap at $k_x = 0$ between the two branches near the bottom and the top of the Rashba energy band (see in Figure 4.10). This splitting, caused by the two dimensionality, is similar to the splitting due to magnetic field in the previous work by Středa and Šeba's on the 1D junction of two

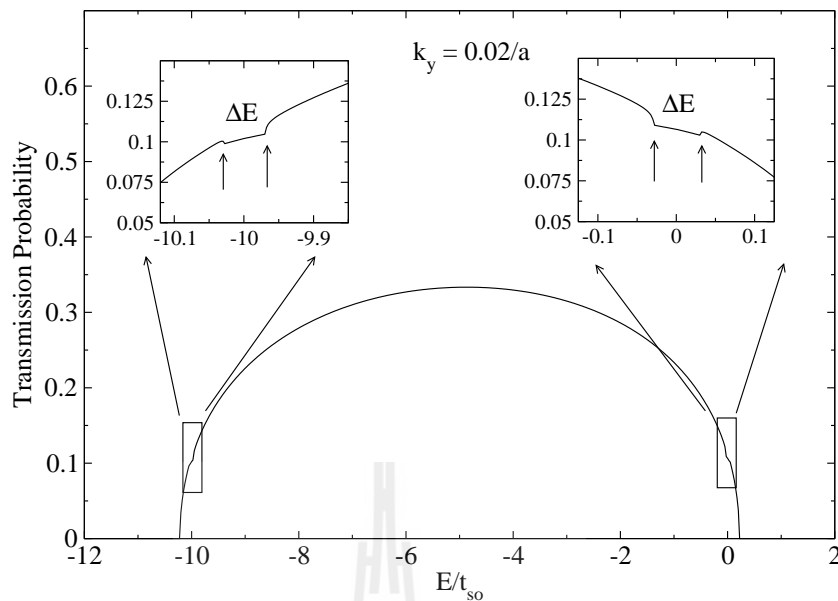


Figure 4.6 Plots of transmission probability as a function of energy for $k_y = 0.02/a$.

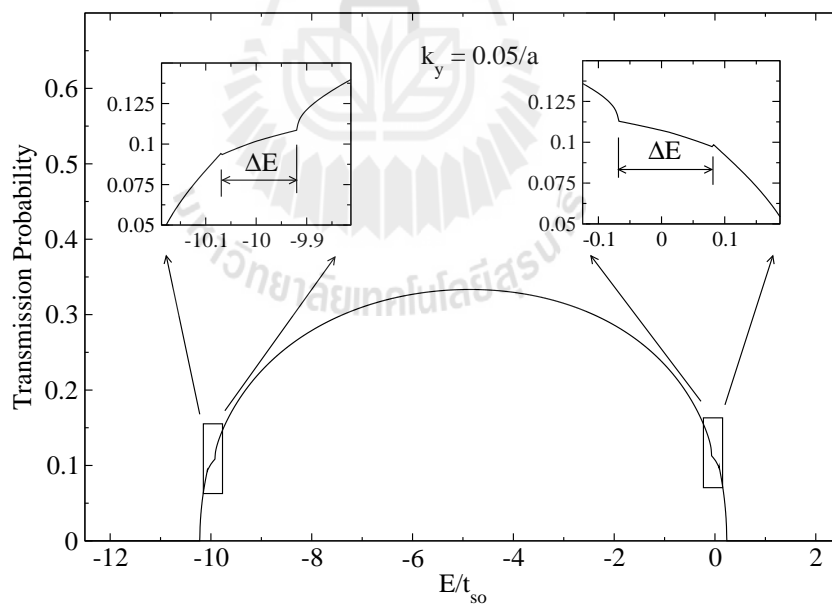


Figure 4.7 Plots of transmission probability as a function of energy for $k_y = 0.05/a$.

2DEG with RSOC (Středa and Šeba, 2003).

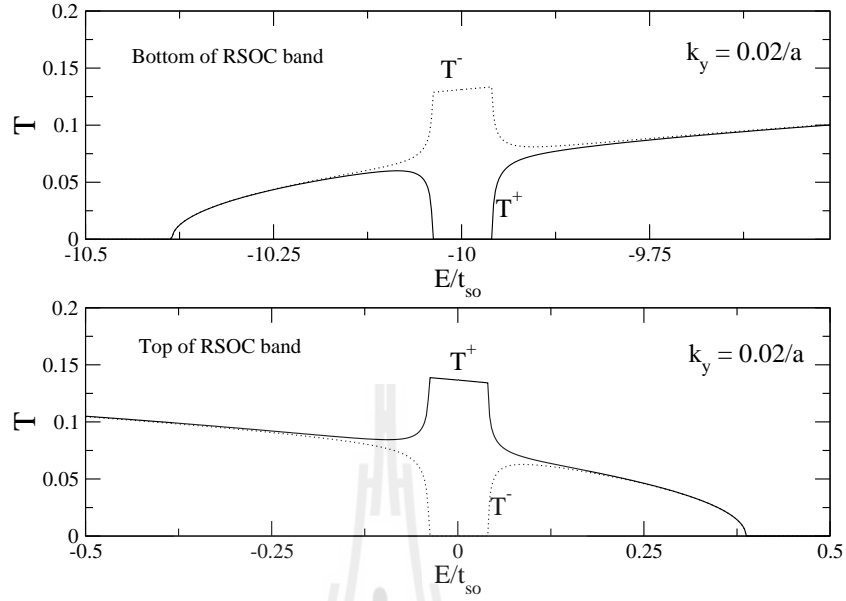


Figure 4.8 Plots of $T^+(E, k_y)$ and $T^-(E, k_y)$ as a function of energy for $k_y = 0.02/a$ near bottom of the Rashba band.

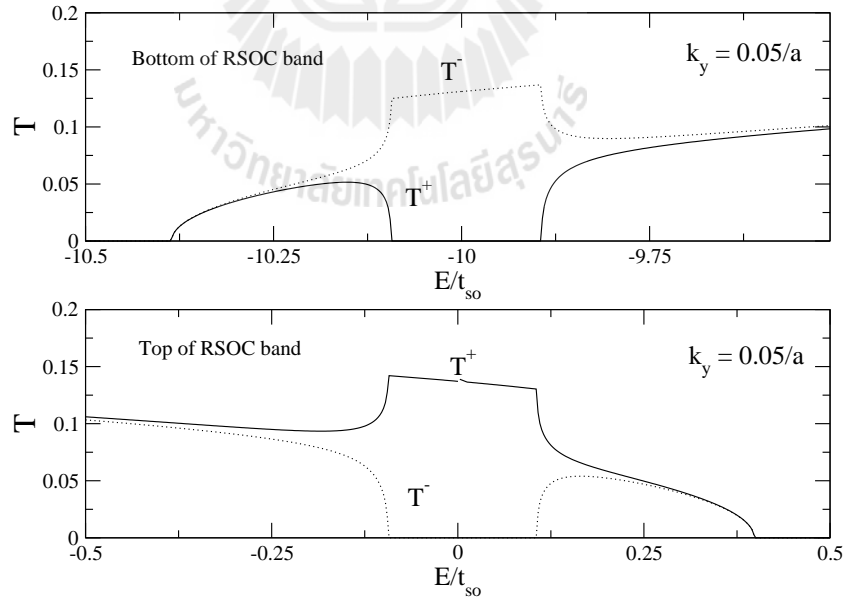


Figure 4.9 Plots of $T^+(E, k_y)$ and $T^-(E, k_y)$ as a function of energy for $k_y = 0.05/a$ near top of Rashba band.

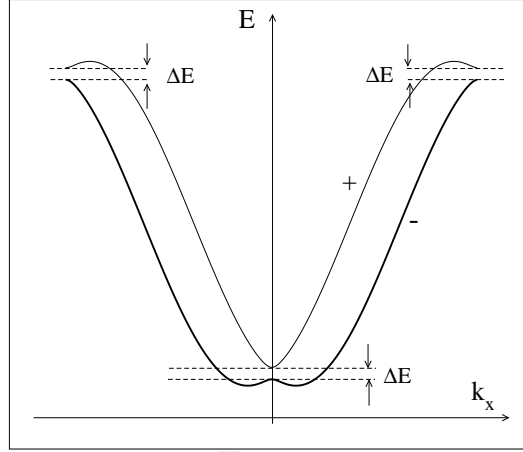


Figure 4.10 Sketch of RSOC energy dispersion is split by k_y , the range of energy splitting is $4t_{so} \sin k_y a$.

4.4.2 Differential Conductance

By assuming the energy band of the Rashba system is empty, we use Eq. (4.43) to calculate the conductance for different values of interfacial scattering potential at column $n = 0$. We consider two kinds of scattering: V_0 which is the spin-conserving scattering potential, and V_F is the spin-flip scattering potential. All conductance spectra are plotted as a function of energy in the unit of $e^2 a^2 / (2\pi)^2$.

Figure 4.11 shows the conductance spectra for the voltage range equivalent to the whole band width of RSOC system, when $V_0 = 0$, $V_0 = 0.5t_N$, $V_0 = 1.0t_N$ and $V_0 = 2.0t_N$. The conductance is zero until the applied voltage reach the bottom of the Rashba band. It is increased and reached the maximum near the middle of the band, which appears as two double peaks symmetric in voltage positions around the middle of the band, and then decreased to zero at the top of the band. We also zoom the conductance spectra in three regions, i.e., the voltage near the 1st crossing point, the middle of the band, and near the 2nd

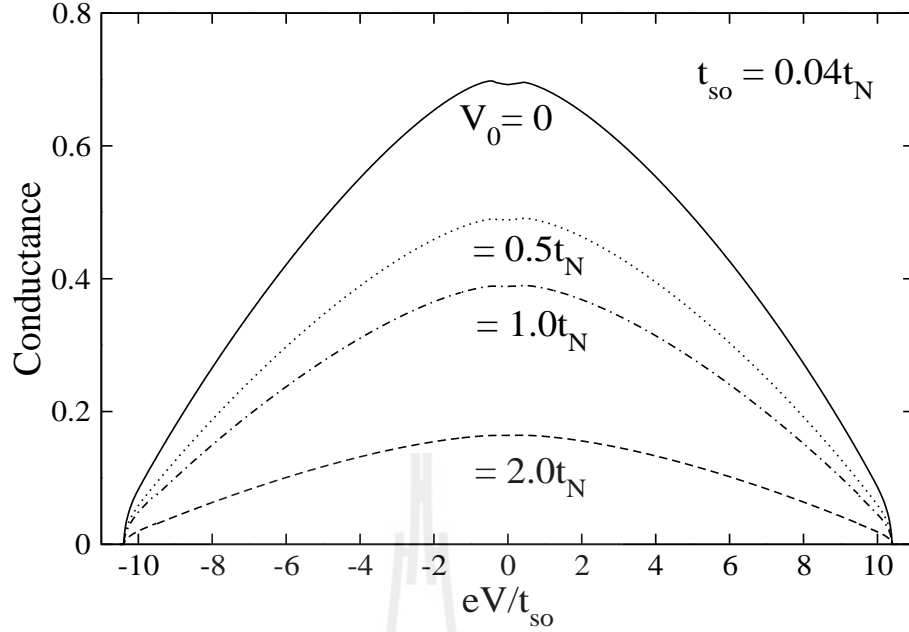


Figure 4.11 Plots of conductance spectra as a function of energy for $V_0 = 0$ and $V_0 = 0.5t_N$. V_F is zero in these plots.

crossing point. The conductance spectrum was suppressed with increased either spin-conserved scattering or spin-flip scattering potential as can clearly be seen in Figure 4.12. Unlike in the continuous model, one can see that there is no kink in the spectrum at the crossing points when either V_F or V_0 is zero (see Figure 4.12 and Figure 4.13).

For a small value of V_0 ($V_0 = 0.5t_N$), the increase in V_F , suppresses the conductance spectrum. The kinks also appear at the energies corresponding to the crossing points. The higher the value of V_0 , the more prominent the kinks. It should also be noted that the kink near the voltage close to the bottom of the band is dip-like or pointing down, similar to the kink in the conductance spectrum in the continuous model, whereas the kink near the top of the band is sharp and pointing upward. The different natures of the kinks reflect the difference in nature of the electron-like (close to the bottom) and hole-like (close to the top) energy

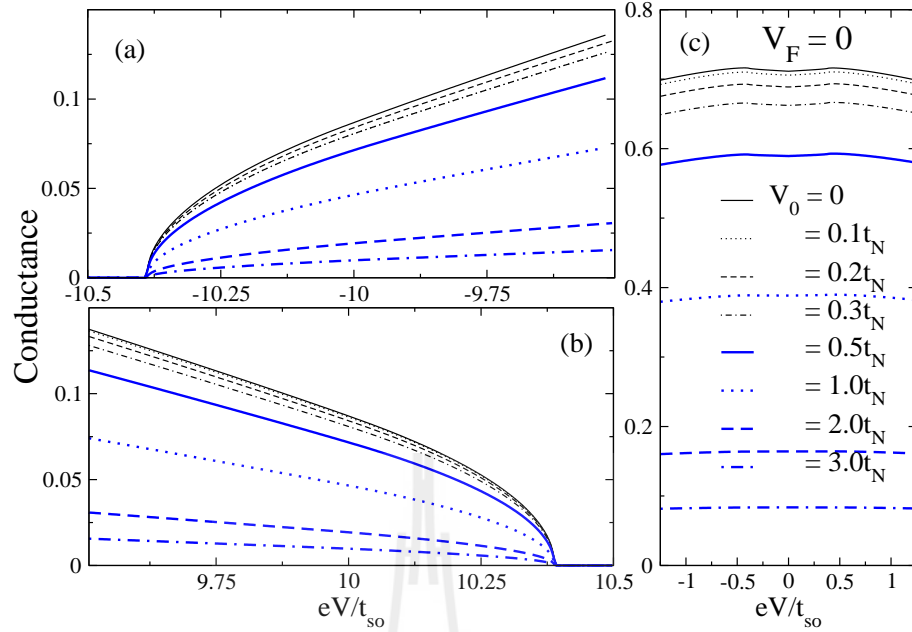


Figure 4.12 Magnified plots of conductance spectra as a function of energy for several values of V_0 near the bottom, middle, and top of the band. V_F is zero in these plots.

contours of the energy band.

The effect of the presence of both V_F and V_0 can also be seen around the energy corresponding to the middle of the band, i.e., the double peaks of conductance spectrum near the maximum point are shifted towards the bottom of the band. They are no longer symmetric around the middle of the band (see Figure 4.14). When $V_F > 1.0t_N$, the double peaks are invisible. For high barrier strength, i.e., $V_0 = 1.0t_N$ (see Figure 4.15) and $V_0 = 2.0t_N$ (see Figure 4.16), the conductance reaches maximum value when of $V_F \simeq V_0$.

We also plot of conductance at the five different voltages as a function of V_0 (see Figure 4.18 and Figure 4.17): $eV = -10.125t_{so}$ (just below the 1st crossing point), $eV = -9.5t_{so}$ (just above the 1st crossing point), $eV = 0$ (the middle of the band), $eV = 9.5t_{so}$ (just below the 2nd crossing point), and $eV = 10.125t_{so}$

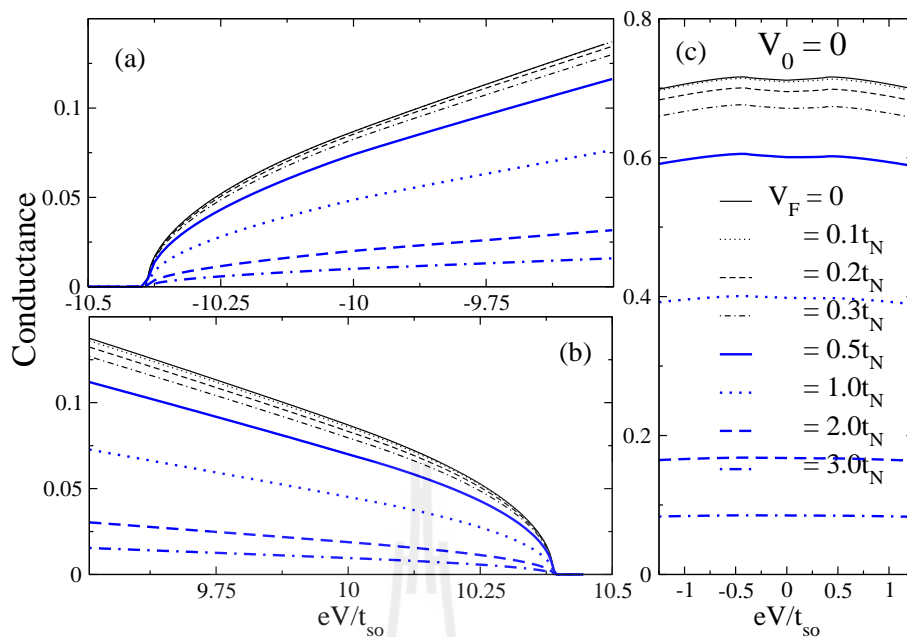


Figure 4.13 Plots of conductance spectra as a function of energy for several values of V_F and V_0 is taken to be zero.

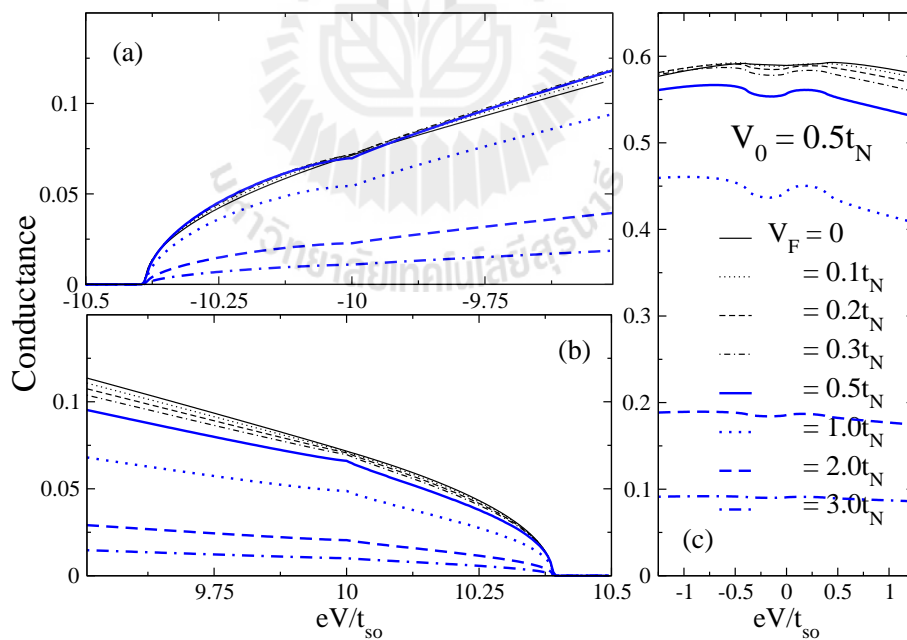


Figure 4.14 Plots of conductance spectra as a function of energy for several values of V_F in case of $V_0 = 0.5t_N$.

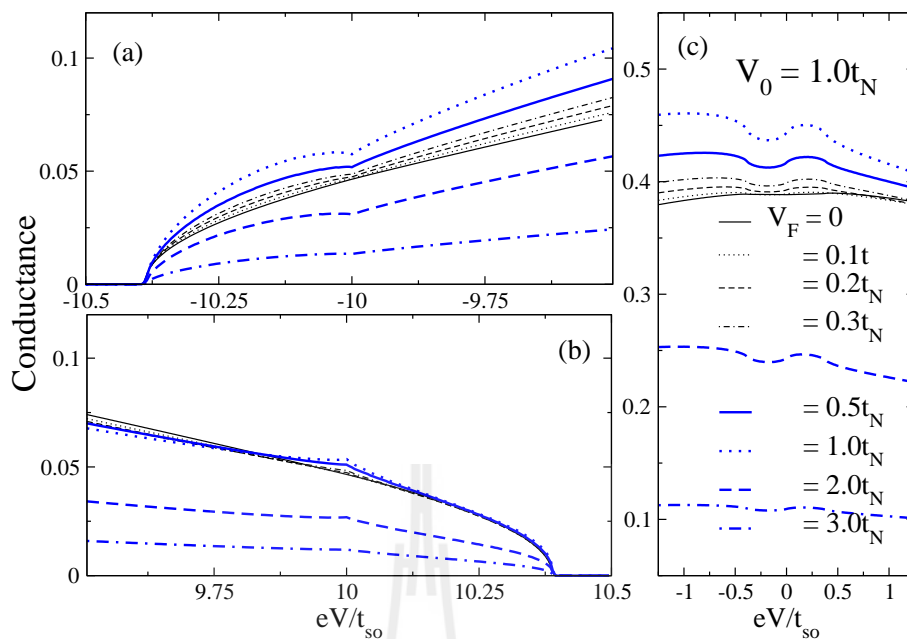


Figure 4.15 Plots of conductance spectra as a function of energy for several values of V_F in case of $V_0 = 1.0t_N$.

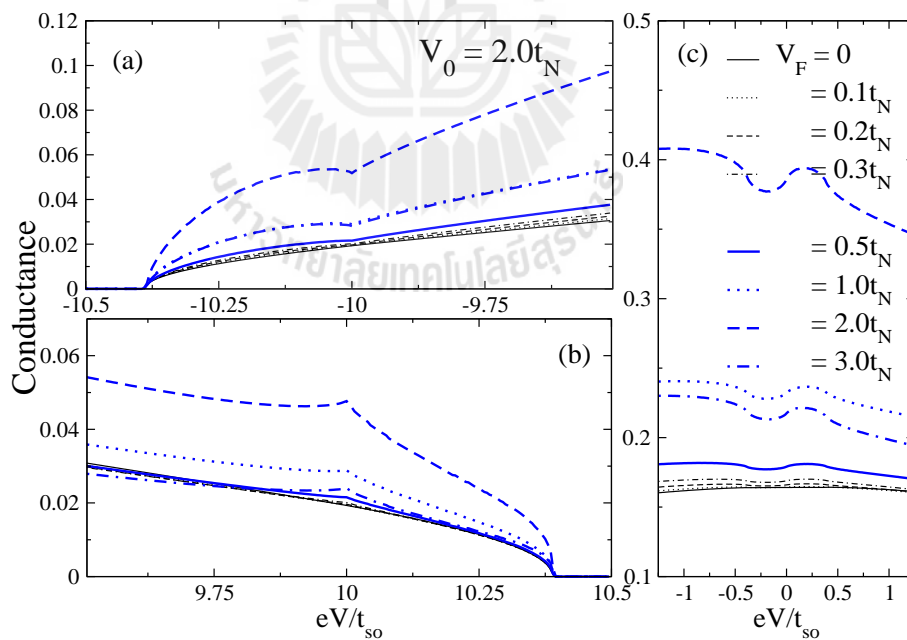


Figure 4.16 Plots of conductance spectra as a function of energy for several values of V_F in case of $V_0 = 2.0t_N$.

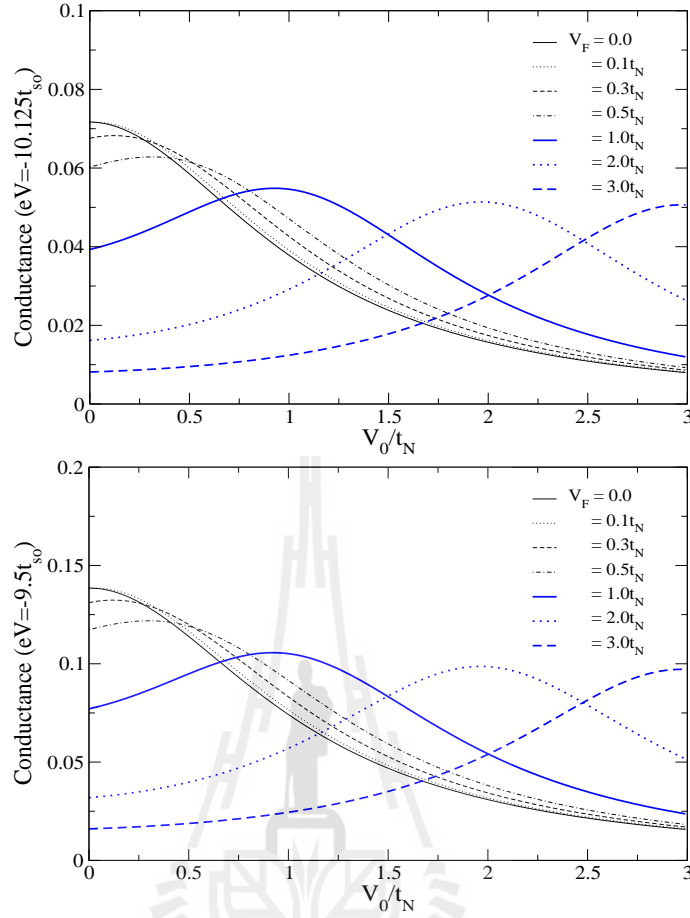


Figure 4.17 Differential conductance at applied voltage $eV = -10.125t_{so}$ (top panel) and $eV = -9.5t_{so}$ (bottom panel) plotted as a function of the barrier strength V_0 for different V_F , the maximum conductance is occurred at the value of $V_0 \simeq V_F$.

(just above the 2nd crossing point). One can see that for the small value of V_F the conductance is decreased with V_0 as expected. But for V_F is higher than around $0.3t_N$, the conductance is surprisingly increased with V_0 , until it reaches its maximum at $V_0 \simeq V_F$. When V_0 is more than V_F , the conductance is suppressed. The increasing of V_F and V_0 values lead to the maximum tunneling conductance as show in Figure 4.19. It seen that resulting of the slope, the V_0 is slightly larger than the V_F value.

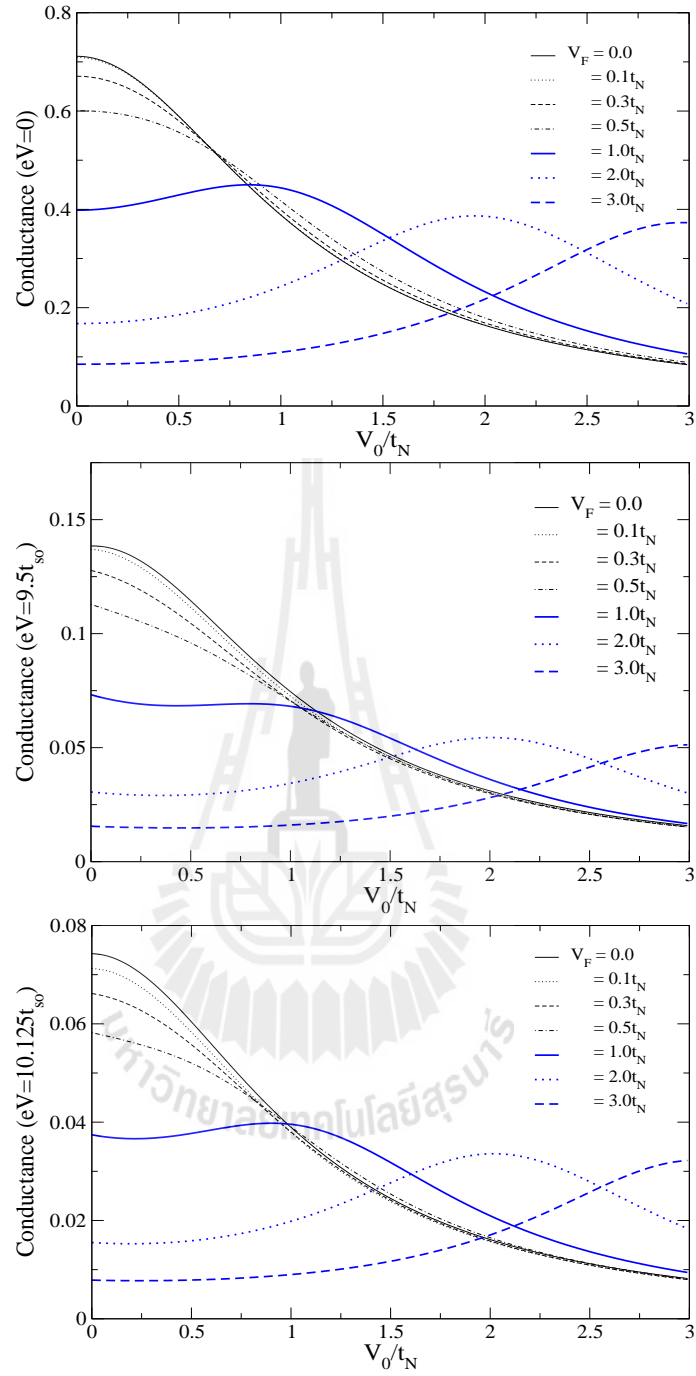


Figure 4.18 Differential conductance at applied voltage $eV = 0$ (top panel), $eV = 9.5t_{so}$ (middle panel), and $eV = 10.125t_{so}$ (bottom panel) plotted as a function of the barrier strength V_0 for different V_F , the maximum conductance is occurred at the value of $V_0 \simeq V_F$.

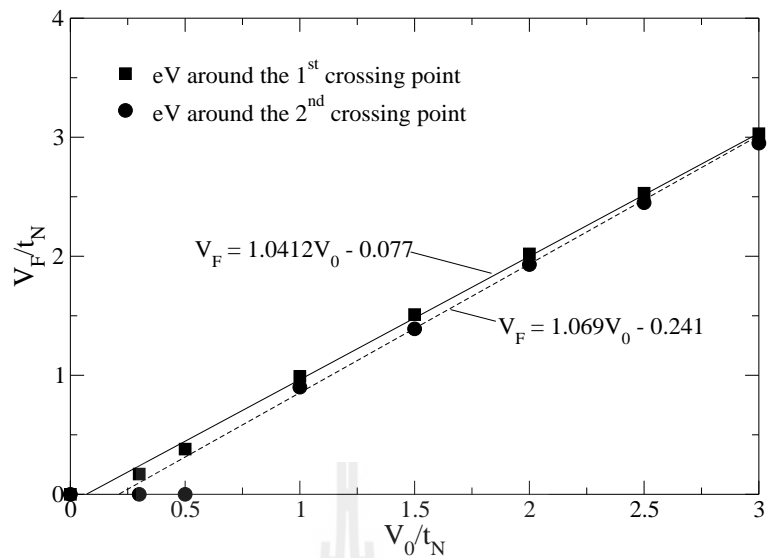


Figure 4.19 Plots of the spin-flip V_F and the spin-conserving V_0 scattering values lead to the maximum tunneling conductance. The square is for the apply voltage equivalent to the energy around the 1st crossing point and the circle is for the energy around the 2nd crossing point.

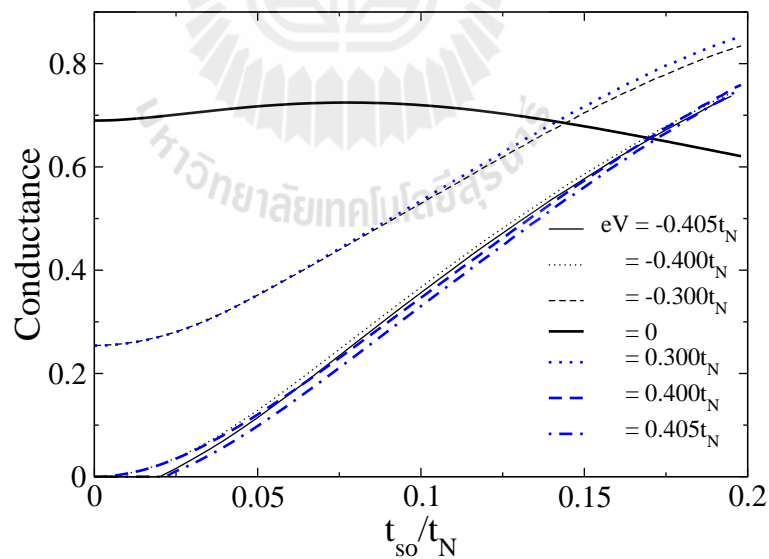


Figure 4.20 Differential conductance plotted as a function of t_{so} for different values of applied voltages.

The conductance at different values of the applied voltages as a function of t_{so} is shown in Figure 4.20. One can see that the conductance is increased with t_{so} for most values of the voltages except those equivalent to the middle of the band.

The different results between the lattice model and the continuous model can be seen by comparing in the second boundary condition in Eq.(4.20) and the discontinuity of the slope of the wave function at the interface in the continuous model. The second term of the right hand side of Eq.(4.46) for the lattice model is included effect of the nearest-neighbor in the metal side. The corresponding reduce the potential barrier effects.

$$T(U_R^{k_y}(0) - U_R^{k_y}(-1)) - t_N(U_M^{k_y}(0) - U_M^{k_y}(-1)) = (V - t_N - T)U_M^{k_y}(0) - 2t_N U_M^{k_y}(-1) \quad (4.46)$$

$$\left(\frac{1}{m^*} \frac{\partial \psi_{RS}}{\partial x} - \frac{1}{m} \frac{\partial \psi_M}{\partial x} \right) \Big|_0 = \left(\frac{2k_F}{m} Z - ik_0 \frac{1}{m^*} \sigma_y \right) \psi(0) \quad (4.47)$$

4.4.3 Spin Polarization of Conductance

We now investigate the dependence of spin polarization of conductance on the interface scattering potentials. In Figure 4.21, we plot the spin polarization of conductance as a function of applied voltage for different values of V_0 and set $V_F = 0$. When the voltage is equivalent to the energy around the 1st crossing point of the Rashba energy band, the spin polarization of conductance is negative, meaning there are more carriers with spin down than spin up. The maximum magnitude occurs at the crossing point. When the voltage is equivalent to the energy around the 2nd crossing point, the spin polarization of conductance is also negative, and the maximum magnitude occurs at the crossing point. For eV around the half-filled level, the spin polarization of conductance is a small value. The spin polarization of conductance does not depend on V_0 .

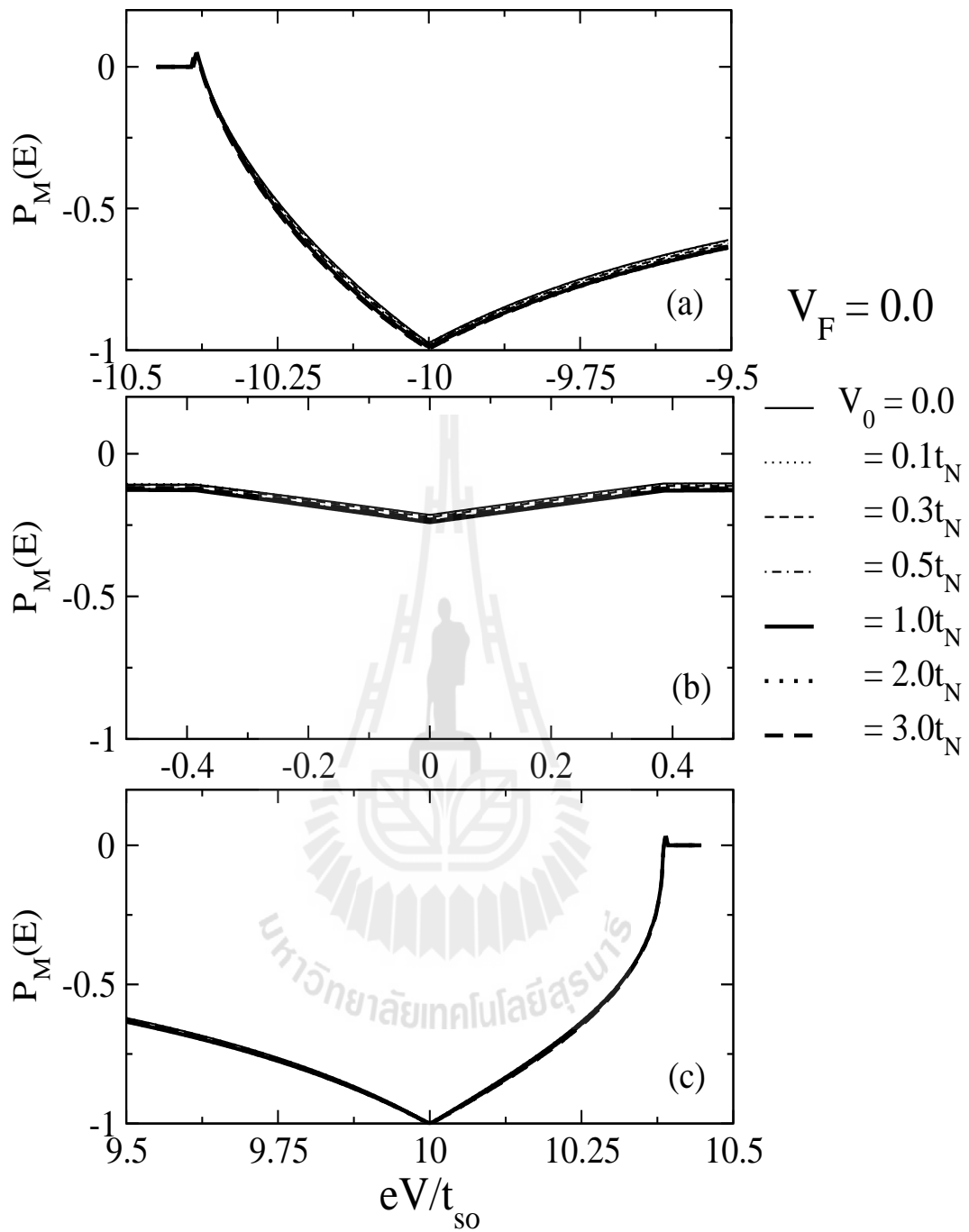


Figure 4.21 Spin polarization of conductance in the metal side plotted as a function of eV for different values of V_0 in case of $V_F = 0$. The upper panel is for eV equivalent to the energy around the lower crossing point and lower panel is for eV equivalent to the energy around the higher crossing point.

When V_F is non-zero, things are more interesting. The spin polarization of conductance shows strong dependence on V_F . As can be seen in Figure 4.22, Figure 4.23, and Figure 4.24, the change in sign of the spin polarization can occur, when V_F is bigger. However, the spin polarization of conductance near the half-filled band still show weak depend on both V_F and V_0 .

The spin polarization of conductance as a function of spin-conserving scattering V_0 (see Figure 4.25) and a function of spin-flip scattering (see Figure 4.26) for three apply voltages. At the eV is lower the 1st crossing point and eV is higher the 2nd crossing point, the small increase V_F does not much affect on the spin polarization of conductance. For eV at the half-filled level, the spin polarization of conductance is weakly dependent on V_0 and V_F .

4.5 Conclusions

In this chapter, we investigated the particle and spin transport across metal/Rashba system junction in the lattice model, using a scattering method. We obtained appropriate matching conditions to calculate the reflection and transmission probabilities, which were used to obtain the conductance and spin polarization of conductance of the junction.

The results of these calculation showed us that the conductance spectrum depends on the barrier potential. Increase in either spin-conserving or spin-flip scattering generally suppressed the conductance. However, one can enhance it by increasing the spin-conserving barrier potential in the presence of spin-flip scattering potential.

The conductance also depends on the Rashba coupling strength. The coupling strength enhances the conductance at the voltages equivalent to the energy around the two crossing points in the Rashba energy band, but slightly suppresses

the conductance at the voltages equivalent to the energy around the middle of the band.

As for spin polarization of conductance in the absence of spin-flip scattering potential, the maximum magnitude occurs at the voltages equivalent to the two crossing points in the Rashba energy band. The spin polarization of conductance does not strongly depend on the spin-conserving interface scattering potential, but strongly depend on the spin-flip one. In the voltage region, where the spin polarization is negative in the absence of spin-conserving interface scattering potential, the increase in the spin-flip interface scattering potential can flip the polarization of conductance to positive sign.



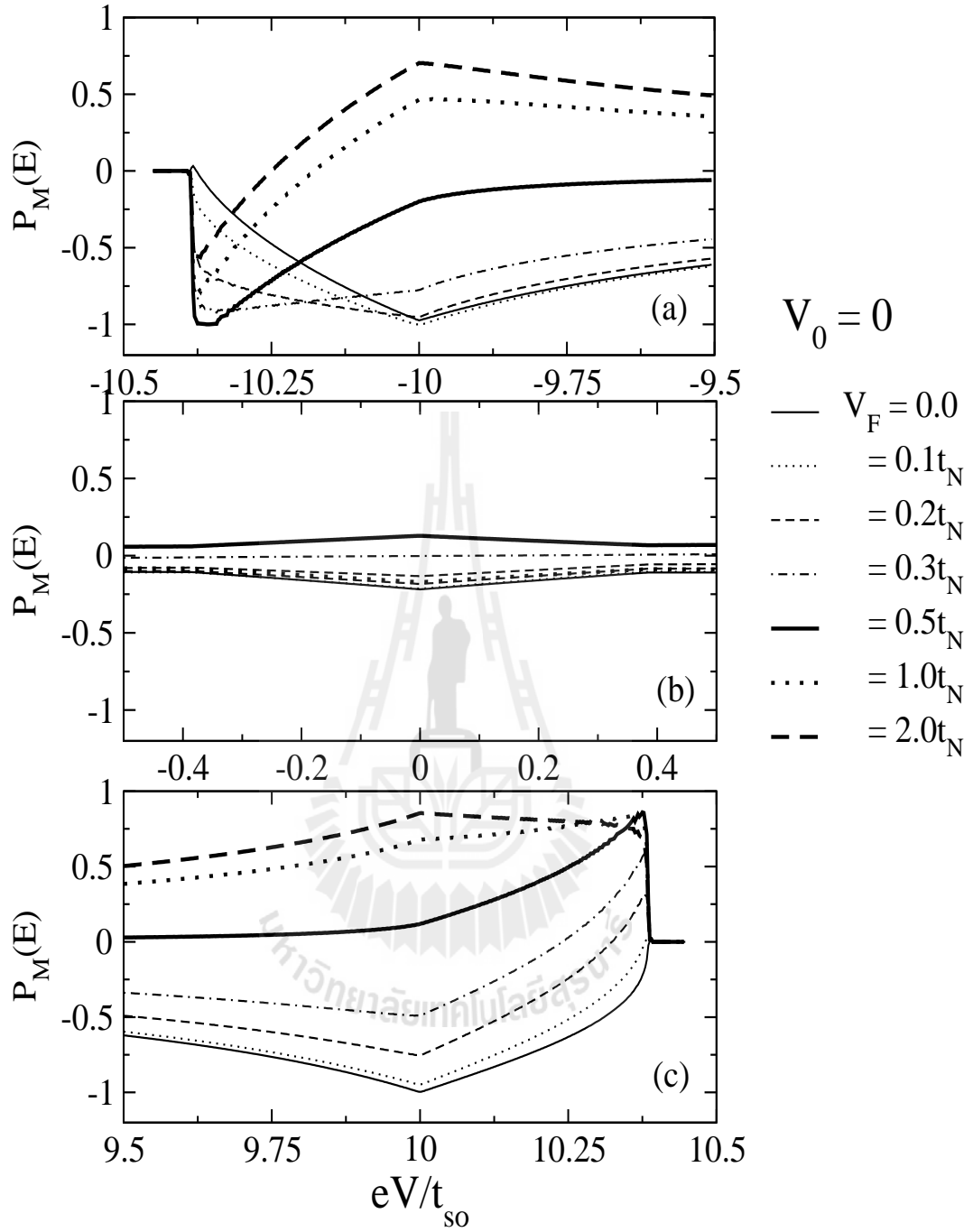


Figure 4.22 Spin polarization of conductance in the metal side plotted as a function of eV for different values of V_F in case of $V_0 = 0$. (a) is for eV equivalent to the energy around the 1st crossing point, (b) is for eV equivalent to the energy around half-filled level, and (c) is for eV equivalent to the energy around the 2nd crossing point.

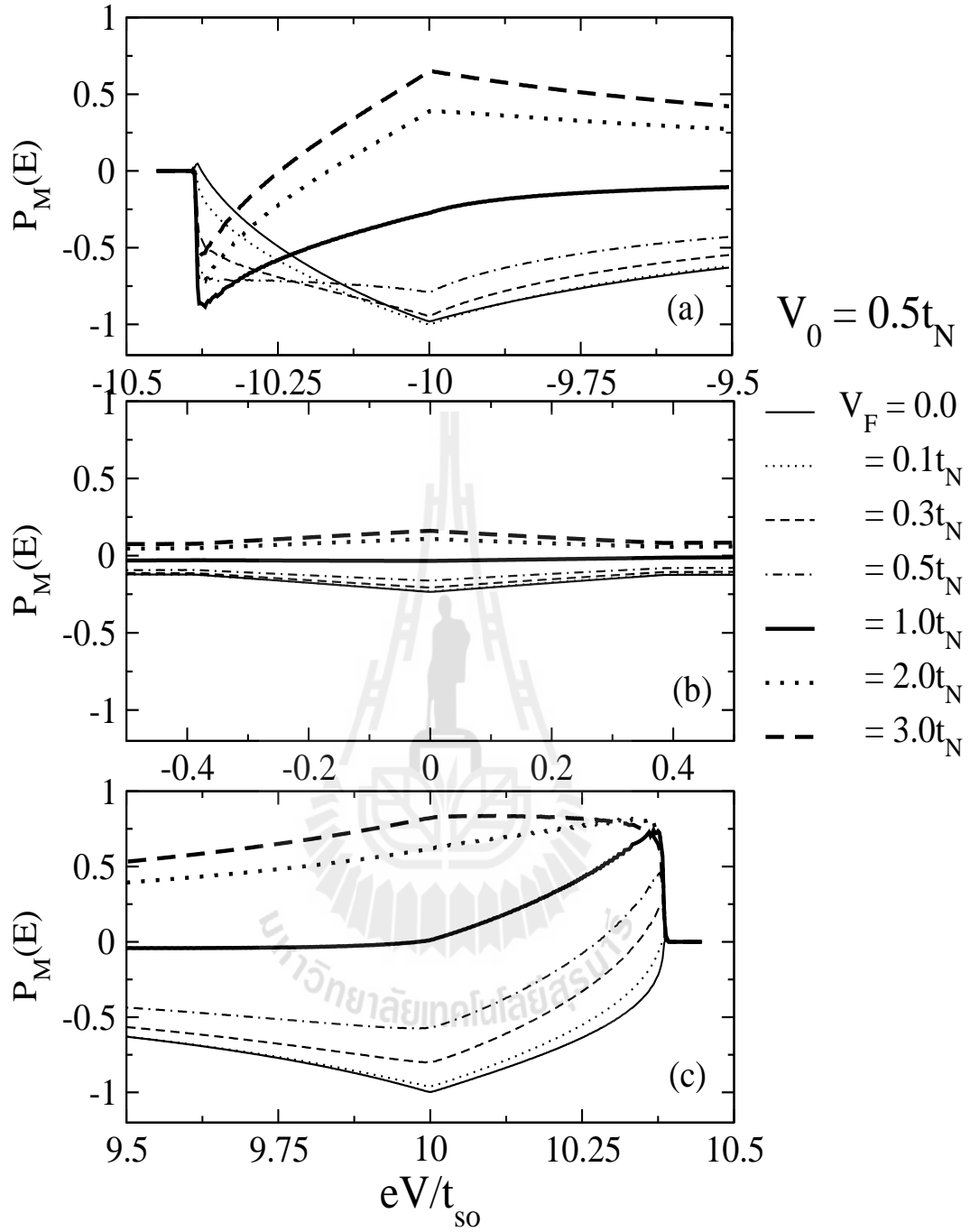


Figure 4.23 Spin polarization of conductance in the metal side plotted as a function of eV for different values of V_F in case of $V_0 = 0.5t_N$. (a) is for eV equivalent to the energy around the 1st crossing point, (b) is for eV equivalent to the energy around half-filled level, and (c) is for eV equivalent to the energy around the 2nd crossing point.

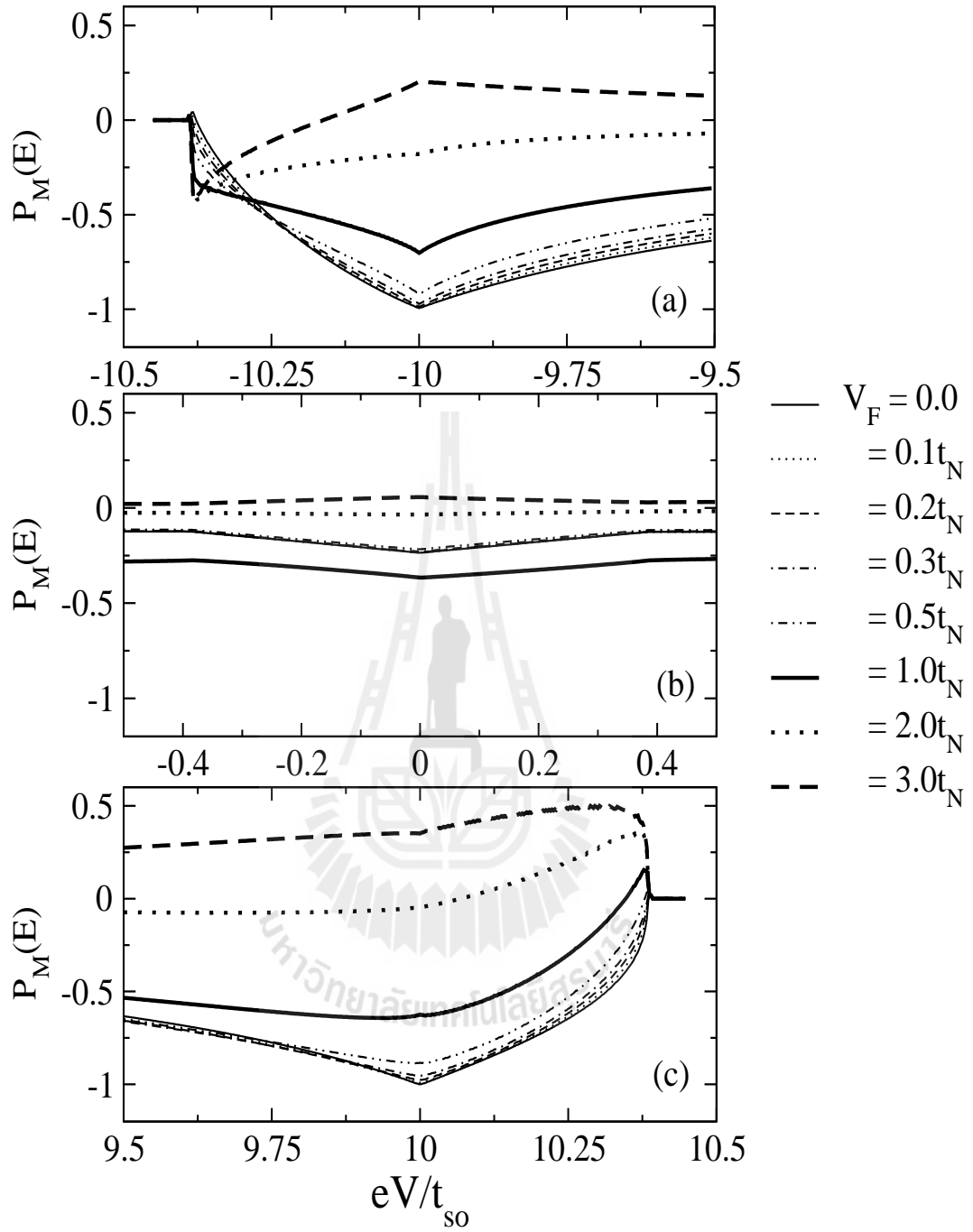


Figure 4.24 Spin polarization of conductance in the metal side plotted as a function of eV for different values of V_F in case of $V_0 = 2.0t_N$. (a) is for eV equivalent to the energy around the 1st crossing point, (b) is for eV equivalent to the energy around half-filled level, and (c) is for eV equivalent to the energy around the 2nd crossing point.

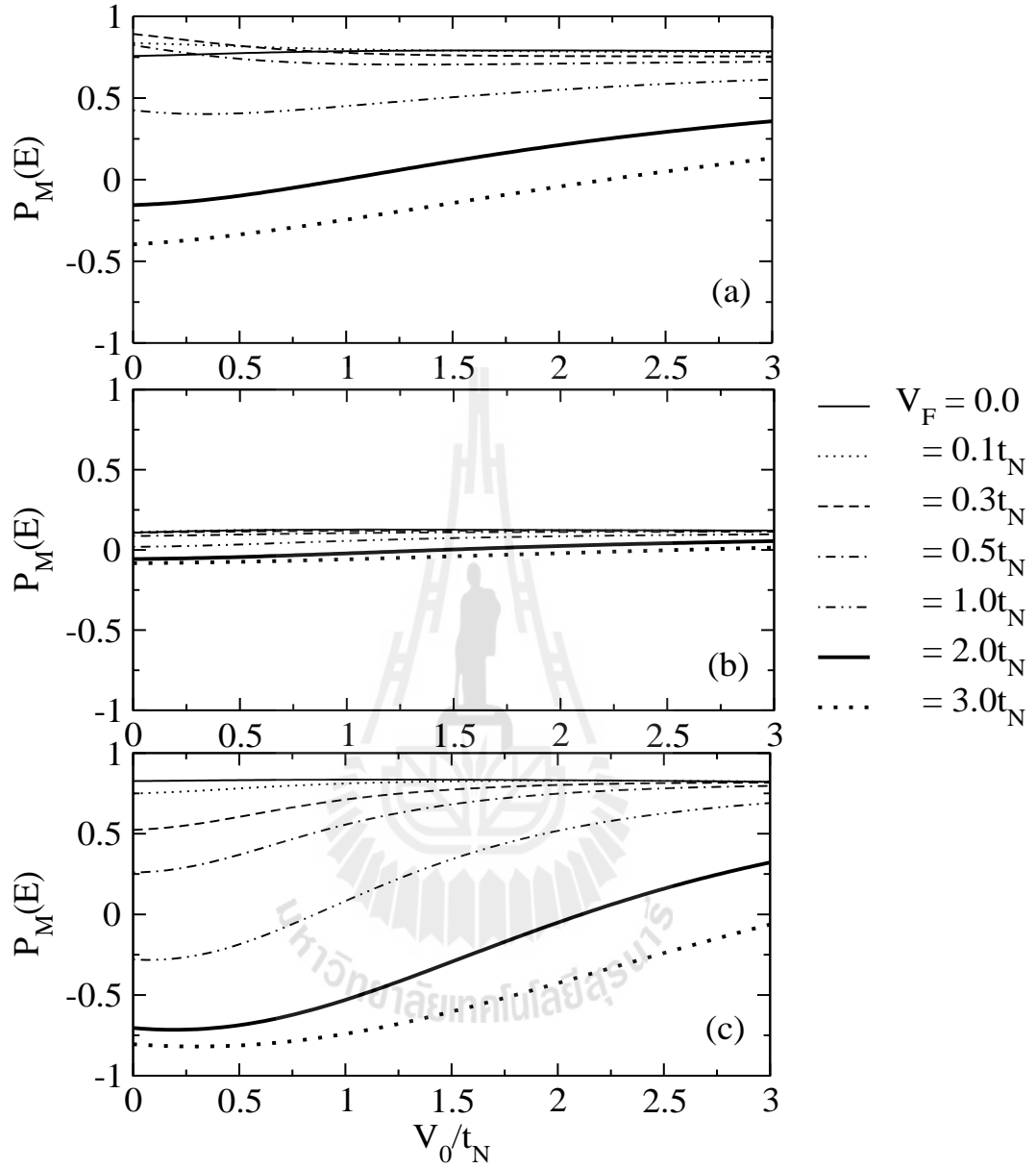


Figure 4.25 Spin polarization of conductance in the metal side plotted as a function of spin-conserving scattering V_0 for different values of V_F . (a) is for eV equivalent to the energy below the 1st crossing point, (b) is for eV equivalent to the energy at half-filled level, and (c) is for eV equivalent to the energy above the 2nd crossing point.

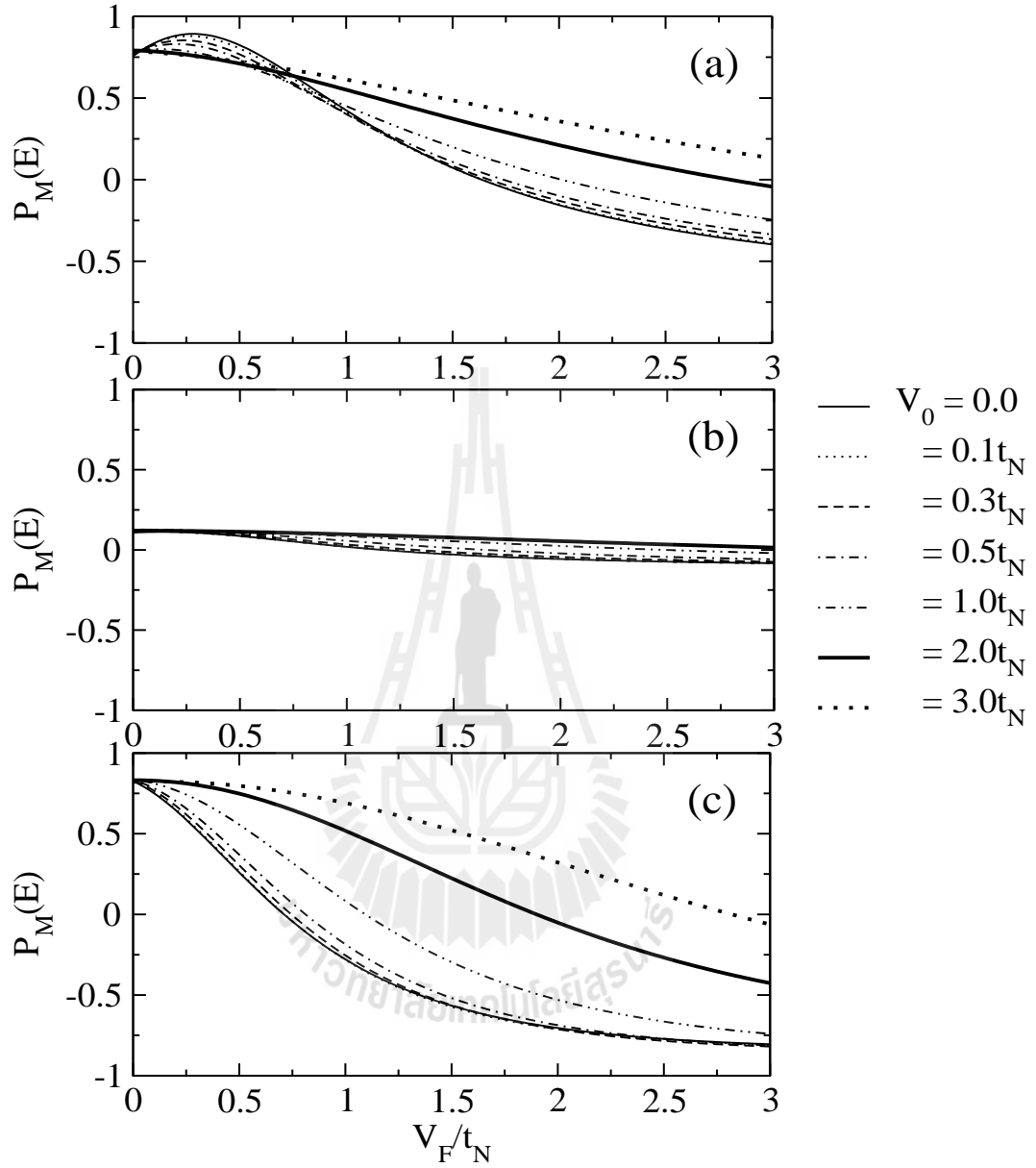


Figure 4.26 Spin polarization of conductance in the metal side plotted as a function of spin-flip scattering V_F for different values of V_0 . (a) is for eV equivalent to the energy below the 1st crossing point, (b) is for eV equivalent to the energy at half-filled level, and (c) is for eV equivalent to the energy above the 2nd crossing point.

CHAPTER V

CONCLUSIONS

This thesis is a theoretical investigation of particle and spin transport across a 2D heterostructure consisting of a metal and a 2DEG with Rashba spin-orbit coupling. By employing a scattering method in a continuous model and a lattice model, we calculate the conductance and spin polarization of conductance, and consider the influence of the scattering barrier potential and the spin-orbit coupling strength on such physical properties of the junction. In the lattice model, the appropriate matching conditions, used in the scattering method to calculate the transmission and reflection probabilities and hence the conductance, are developed.

In both models, it is shown that the conductance spectrum of the junction provides us the method to determine the Rashba energy, and both spin-conserved and spin-flip interfacial scattering strongly affect the conductance spectra. An increase in either spin-conserving or spin-flip scattering generally suppressed the conductance. However, one can enhance it by increasing the spin-conserving barrier potential in the presence of spin-flip scattering potential. It also is found that the conductance at zero voltage is affected by the carrier density. There is a kink in the relationship between the conductance and the carrier density, where the carrier density of the Rashba system is at the level of the crossing point. The conductance also depends on the Rashba coupling strength. The coupling strength enhances the conductance at the voltages equivalent to the energy around the crossing points in the Rashba energy band.

The attachment to a Rashba system affects the spin balance in the metal. In the absence of spin-flip scattering potential, the maximum magnitude occurs at the voltages equivalent to the crossing points in the Rashba energy band. The spin polarization of conductance does not strongly depend on the spin-conserving interface scattering potential, but strongly depend on the spin-flip one. In the voltage region where the spin polarization is negative in the absence of spin-conserving interface scattering potential, the increase in the spin-flip interface scattering potential can flip the polarization of conductance to positive sign.

It should be emphasized that the results in this thesis obtained by setting the temperature of the system to be zero. The finite temperature is expected to smooth out sharp features, however, as long as the temperature is not too high, the features should still be noticeable. The positions of the features in the conductance spectrum are not affected by finite temperature. It should also be pointed out that in the lattice model, only the nearest neighbor hopping integrals of a square lattice are considered to describe the electronic properties of the junction. Including the next nearest neighbor terms will not change the number of van Hove singularities in the DOS of the the system but may change the position in the energy spectrum. This means one will obtain the same main results as nearest neighbor approximation.

Experimentally, angle-resolved photoelectron spectroscopy can be used to measure the Rashba energy of a semiconductor-based heterostructure that includes, for example, InAs (Grundler, 2000; Matsuyama et al., 2000), InGaAs (Koga et al., 2002; Fujii et al., 2002), InSb (Khodaparast et al., 2004a; Khodaparast et al., 2004b), and in surface alloys such as Li/W(110), Pb/Ag(111), and Bi/Ag(111) (Hirahara et al., 2006; Ast et al., 2007; Ast et al., 2008; Pacilé et al., 2006). The conductance spectrum measurements of these systems are still rare.

Fundamental understanding of spin current is important to application of spintronic devices. As found in this thesis, the maximum of spin polarization of conductance of metal/Rashba system junction for an applied voltage equivalent to the energy at the crossing point can be tuned by the strength of RSOC. This may lead to an efficient method to design a spin-filter device in the absence of ferromagnetic materials or without applying external magnetic field.

In the future, we expect further calculation of the spin polarization on the RSOC system, effect of the surface orientation of RSOC system, the effect of the RSOC in graphene, and the transport properties in a double junction with the RSOC system.





REFERENCES

REFERENCES

- Andreev, A. F. (1964a). Thermal conductivity of the intermediate state of superconductors. **Zh. Eksp. Teor. Fiz.** 46: 1823.
- Andreev, A. F. (1964b). Thermal conductivity of the intermediate state of superconductors-II. **Sov. Phys. JETP** 19: 1228.
- Askerov, B. M. (1994). **Electron Transport Phenomena in Semiconductors.** World Scientific: Singapore.
- Ast, C. R., Henk, J., Ernst, A., Moreschini, L., Falub, M. C., Pacilé, D., Bruno, P., Kern, K., and Grioni, M. (2007). Giant Spin Splitting through Surface Alloying. **Phys. Rev. Lett.** 98: 186807.
- Ast, C. R., Pacilé, D., Moreschini, L., Falub, M. C., Papagno, M., Kern, K., and Grioni, M. (2008). Spin-orbit split two-dimensional electron gas with tunable Rashba and Fermi energy. **Phys. Rev. B** 77: R081407.
- Barnas, J., Fuss, A., Camley, R. R., Grunberg, P., and Zinn, W. (1990). Novel magnetoresistance effect in layered magnetic structures: Theory and experiment. **Phys. Rev. B** 42: 8110.
- Blonder, G. E., Tinkham, M., and Klapwijk, T. M. (1982). Transition from metallic to tunneling regimes in superconducting microconstrictions: Excess current, charge imbalance, and supercurrent conversion. **Phys. Rev. B** 25: 4515.
- Bychkov, Y. A. and Rashba, E. I. (1984a). Oscillatory effects and the magnetic susceptibility of carriers in inversion layers. **J. Phys. C** 17: 6039.

- Bychhov, Y. A. and Rashba, E. I. (1984b). Properties of a 2D electron gas with lifted spectral degeneracy. **JETP Lett.** 39: 78.
- Datta, S. (1995). **Electronic Transport in Mesoscopic System.** Cambridge University Press: Cambridge.
- Engels, G., Lange, J., Schäpers, T., and Lüth, H. (1997). Experimental and theoretical approach to spin splitting in modulation-doped $In_xGa_{1-x}As/InP$ quantum wells for $B- > 0$. **Phys. Rev. B** 55: R1958.
- Fujii, K., Morikamia, Y., Ohyamaa, T., Gozub, S., and Yamadab, S. (2002). Determination of Rashba spin splitting in $In_xGa_{1-x}As/In_yAl_{1-y}As$ by far-infrared magneto-optical absorption. **Physica E** 12: 432.
- Grundler, D. (2000). Large Rashba Splitting in InAs Quantum Wells due to Electron Wave Function Penetration into the Barrier Layers. **Phys. Rev. Lett.** 84: 6074–6077.
- Grundler, D. (2001). Oscillatory Spin-Filtering due to Gate Control of Spin-Dependent Interface Conductance. **Phys. Rev. Lett.** 86: 1058.
- Heida, J. P., Van Wees, B. J., Kuipers, J. J., Klapwijk, T. M., and Borghs, G. (1998). Spin-orbit interaction in a two-dimensional electron gas in a $InAs/AlSb$ quantum well with gate-controlled electron density. **Phys. Rev. B** 57: 011911.
- Hirahara, T., Nagao, T., Matsuda, I., Bihlmayer, G., Chulkov, E., Koroteev, Y. M., Echenique, P. M., Saito, M. ., and Hasegawa, S. (2006). Role of Spin-Orbit Coupling and Hybridization Effects in the Electronic Structure of Ultrathin Bi Films. **Phys. Rev. Lett.** 97: 146803.

- Hu, C.-M., Nitta, J., Akazaki, T., Takayanagi, H., Osaka, J., Pfeffer, P., and Zawadski, W. (1999). Zero-field spin splitting in an inverted $In_{0.53}Ga_{0.47}As/In_{0.52}Al_{0.48}As$ heterostructure: Band nonparabolicity influence and the subband dependence. **Phys. Rev. B** 60: 7736.
- Julliere, M. (1975). Tunneling between ferromagnetic films. **Phys. Lett. A** 54: 225.
- Khodaparast, G. A., Doezema, R. E., Chung, S. J., Goldammer, K. J., and Santos, M. B. (2004a). Spectroscopy of Rashba spin splitting in InSb quantum wells. **Phys. Rev. B** 70: 155322.
- Khodaparast, G. A., Meyer, R. C., Zhang, X. H., Kasturiarachchi, T., Doezema, R. E., Chung, S. J., Goel, N., Santos, M. B., and Wang, Y. J. (2004b). Spin effects in InSb quantum wells. **Physica E** 20: 386.
- Koga, T., Nitta, J., Akazaki, T., and Takayanagi, H. (2002). Rashba Spin-Orbit Coupling Probed by the Weak Antilocalization Analysis in $InAlAs/InGaAs/InAlAs$ Quantum Wells as a Function of Quantum Well Asymmetry. **Phys. Rev. Lett.** 89: 046801.
- Lommer, G., Malcher, F., and Rossler, U. (1988). Spin splitting in semiconductor heterostructures for $B- > 0$. **Phys. Rev. Lett.** 60: 728.
- Maekawa, S. and Gafvert, U. (1982). Electron-tunneling between ferromagnetic films. **IEEE Trans. Magn.** 18: 707.
- Matsuyama, T., Hu, C. M., Grundler, D., Meier, G., and Merkt, U. (2002). Ballistic spin transport and spin interference in ferromagnet/InAs(2DES)/ferromagnet devices. **Phys. Rev. B** 65: 155322.

- Matsuyama, T., Kürsten, R., Meiner, C., and Merkt, U. (2000). Rashba spin splitting in inversion layers on p-type bulk InAs. **Phys. Rev. B** 61: 15588–15591.
- Mireles, F. and Kirczenow, G. (2001). Ballistic spin-polarized transport and Rashba spin precession in semiconductor nanowires. **Phys. Rev. B** 64: 024426.
- Molenkamp, L. W., Schmidt, G., and Bauer, G. E. W. (2000). Fundamental obstacle for electrical spin injection from a ferromagnetic metal into a diffusive semiconductor. **Phys. Rev. B** 62: R4790.
- Moodera, J. S., Kinder, L. R., Wong, T. M., and Meservey, R. (1995). Large Magnetoresistance at Room Temperature in Ferromagnetic Thin Film Tunnel Junctions. **Phys. Rev. Lett.** 74: 3273.
- Nitta, J., Akazaki, T., Takayanagi, H., and Enoki, T. (1997). Gate Control of Spin-Orbit Interaction in an Inverted $In_{0.53}Ga_{0.47}As/In_{0.52}Al_{0.48}As$ Heterostructure. **Phys. Rev. Lett.** 78: 1335.
- Oestreich, M. (1999). Materials science: Injecting spin into electronics. **Nature (London)** 402: 735.
- Pacilé, D., Ast, C. R., Papagno, M., Da Silva, C., Moreschini, L., Falub, M., Seitsonen, A. P., and Grioni, M. (2006). Electronic structure of an ordered Pb/Ag(111) surface alloy: Theory and experiment. **Phys. Rev. B** 73: 245429.
- Pairor, P. and Walker, M. B. (2002). Tunneling conductance for d-wave superconductors: Dependence on crystallographic orientation and Fermi surface. **Phys. Rev. B** 65: 064507.

- Pareek, T. P. and Bruno, P. (2001). Magnetic scanning tunneling microscopy with a two-terminal nonmagnetic tip: Quantitative results. **Phys. Rev. B** 63: 165424.
- Rashba, E. I. (1960a). Properties of semiconductors with an extremum loop I. Cyclotron and combinational resonance in a magnetic field perpendicular to the plane of the loop. **Fiz. Tverd. Tela** 2: 1224.
- Rashba, E. I. (1960b). Properties of semiconductors with an extremum loop I. Cyclotron and combinational resonance in a magnetic field perpendicular to the plane of the loop. **Solid state Ionics** 2: 1109.
- Saibich, M. N., Broto, J. M., Fert, A., Nguyen, F., Dau, V., Petroff, F., Eitenne, P., Creuzet, G., Friederich, A., and Chazelas, J. (1988). Giant Magnetoresistance of (001)Fe/(001)Cr Magnetic Superlattices. **Phys. Rev. Lett.** 61: 2472.
- Sato, Y., Kita, T., Gozu, S., and Yamada, S. (2001). Large spontaneous spin splitting in gate-controlled two-dimensional electron gases at normal $In_{0.75}Ga_{0.25}As/In_{0.75}Al_{0.25}As$ heterojunctions. **J. Appl. Phys.** 89: 8017.
- Schapers, T., Engels, G., Lange, J., Klocke, T., Hollfelder, M., and Luth, H. (1998). Effect of the heterointerface on the spin splitting in modulation doped $In_xGa_{1-x}As/InP$ quantum wells for $B- > 0$. **J. Appl. Phys.** 83: 4324.
- Slonczewski, J. C. (1989). Conductance and exchange coupling of two ferromagnets separated by a tunneling barrier. **Phys. Rev. B** 39: 6995.
- Srisongmuang, B., Pairor, P., and Berciu, M. (2008). Tunneling conductance of

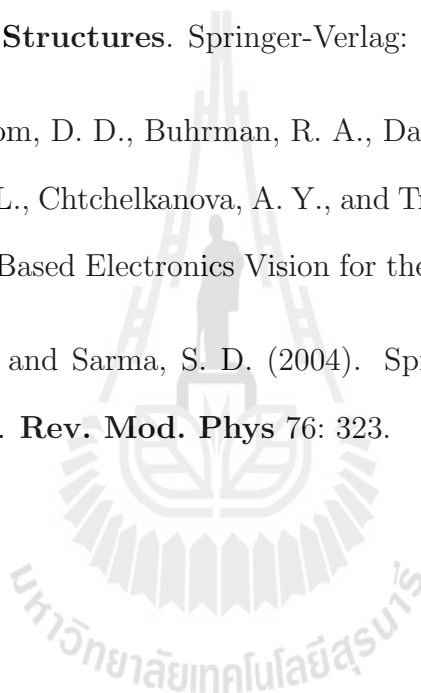
a two-dimensional electron gas with Rashba spin-orbit coupling. **Phys. Rev. B** 78: 155317.

Středa, P. and Šeba, P. (2003). Antisymmetric Spin Filtering in One-Dimensional Electron Systems with Uniform Spin-Orbit Coupling. **Phys. Rev. Lett.** 90: 256601.

Thomas, I. (2004). **Electronic Quantum Transport in Mesoscopic Semiconductor Structures**. Springer-Verlag: New York.

Wolf, S. A., Awschalom, D. D., Buhrman, R. A., Daughton, J. M., Molnar, S. V., Roukes, M. L., Chtchelkanova, A. Y., and Treger, D. M. (2001). Spintronics: A Spin-Based Electronics Vision for the Future . **Science** 294: 1488.

Zutić, I., Fabian, J., and Sarma, S. D. (2004). Spintronics: Fundamentals and applications. **Rev. Mod. Phys** 76: 323.





APPENDICES

APPENDIX A

HAMILTONIAN AND EIGENENERGY OF THE RSOC SYSTEM IN A CONTINUOUS MODEL

The one-electron Hamiltonian with RSOC is written as

$$H = \frac{p^2}{2m^*} + \frac{\lambda}{\hbar} (\vec{\sigma} \times \vec{p}) \cdot \hat{z}. \quad (\text{A.1})$$

Where the first term is the kinetic energy with the electron effective mass m^* . The second is the RSOC term, the electron propagate with momentum $\vec{p} = \hbar\vec{k}$ in an electric field (point towards the z -axis). $\vec{\sigma}$ denote the Pauli matrix vector. We rewrite the Rashba Hamiltonian in the form;

$$H_{RS} = \lambda \begin{pmatrix} 0 & 0 & \hat{z} \\ \sigma_x & \sigma_y & \sigma_z \\ k_x & k_y & k_z \end{pmatrix} \quad (\text{A.2})$$

$$= \lambda \begin{pmatrix} 0 & ik_y - k_x \\ ik_y + k_x & 0 \end{pmatrix}. \quad (\text{A.3})$$

The full wave function of an electron can be written as:

$$\psi(\vec{k}) = e^{ik_x x + ik_y y} \begin{pmatrix} a_1 \\ a_2 \end{pmatrix}. \quad (\text{A.4})$$

To determine the eigenvalues of the Hamiltonian, one has to solve the system of homogeneous equation, the determinant of the coefficient has to be zero,

$$\det(\hat{H}\psi - EI) = 0 \quad (\text{A.5})$$

or

$$\begin{vmatrix} E_0 - E_\lambda & ik_y - k_x \\ ik_y + k_x & E_0 - E_\lambda \end{vmatrix} = 0. \quad (\text{A.6})$$

Hence, the eigenenergies are

$$E^\pm = E_0 \pm \lambda \sqrt{k_x^2 + k_y^2}, \quad (\text{A.7})$$

where $E_0 = \frac{\hbar^2 k^2}{2m^*}$. We can now find the phase ratio of the spin function $\begin{pmatrix} a_1 \\ a_2 \end{pmatrix}$.

First, consider the state with $E = E_\lambda^+$ and obtain

$$\begin{bmatrix} -\sqrt{k_x^2 + k_y^2} & \lambda(ik_y - k_x) \\ -\lambda(ik_y + k_x) & -\sqrt{k_x^2 + k_y^2} \end{bmatrix} \begin{pmatrix} a_1 \\ a_2 \end{pmatrix} = 0, \quad (\text{A.8})$$

$$\frac{a_1}{a_2} = \frac{ik_y - k_x}{\sqrt{k_x^2 + k_y^2}}. \quad (\text{A.9})$$

After normalizing it, we get

$$\psi_{RS}^+(\vec{k}) = \frac{1}{\sqrt{2}} \begin{pmatrix} 1 \\ \frac{\sqrt{k_x^2 + k_y^2}}{ik_y - k_x} \end{pmatrix} e^{ik_x x + ik_y y}. \quad (\text{A.10})$$

Similarly, we obtain for the state with $E = E_-$,

$$\psi_{RS}^-(\vec{k}) = \frac{1}{\sqrt{2}} \begin{pmatrix} 1 \\ -\frac{\sqrt{k_x^2 + k_y^2}}{ik_y - k_x} \end{pmatrix} e^{ik_x x + ik_y y}. \quad (\text{A.11})$$

APPENDIX B

HAMILTONIAN AND EIGENENERGY OF THE RSOC SYSTEM IN A LATTICE MODEL

The following show details of how it obtain the energy dispersion relation and eigenstate of a Rashba system in the lattice model. Below is the Hamiltonian of a Rashba system in a square lattice with up to nearest neighbour interactions:

$$\begin{aligned}
 H_{RS} = & \sum_{nm\sigma} (\varepsilon_{nm\sigma} - \mu) C_{nm\sigma}^\dagger C_{nm\sigma} - t_R \sum_{nm\sigma} (C_{n+1,m\sigma}^\dagger C_{nm\sigma} + C_{n,m+1,\sigma}^\dagger C_{nm\sigma} + H.C.) \\
 & - t_{so} \sum_{nm\sigma\sigma'} \{ C_{n+1,m\sigma'}^\dagger (i\sigma_y)_{\sigma\sigma'} C_{nm\sigma} - C_{n,m+1,\sigma'}^\dagger (i\sigma_x)_{\sigma\sigma'} C_{nm\sigma} + H.C. \}. \quad (B.1)
 \end{aligned}$$

The subscripts n and m indicate the column and row indices of the square lattice. $C_{nm\sigma}^\dagger$ ($C_{nm\sigma}$) is the creation (annihilation) operator of an electron at indices (nm) of the lattice site with spin σ , $\varepsilon_{nm\sigma}$ is the on-site energy; $t_R = \hbar^2/2m^*a$ is the nearest neighbour hopping energy for a lattice constant a and electronic effective mass m^* , and μ is the chemical potential. α is the Rashba spin-coupling parameter. $\sigma_{x(y)}$ is the Pauli's matrix and $t_{so} = \alpha/2a$ denotes the RSOC strength in the lattice representation. To start with considering the second term of the Hamiltonian.

$$H_{t_R} = -t_R \sum_{nm\sigma} \{ (C_{nm\sigma}^\dagger C_{n,m+1,\sigma} + H.C.y) + (C_{nm\sigma}^\dagger C_{n+1,m\sigma} + H.C.x) \}. \quad (B.2)$$

We can transform into the momentum space by using the Fourier transform

$$C_{nm\sigma} = \frac{1}{\sqrt{N}} \sum_k C_{nk\sigma} e^{i\vec{k}\cdot\vec{R}}. \quad (B.3)$$

We first consider the component on the x direction and obtain

$$\begin{aligned}
H_{t_R,x} &= -\frac{t_R}{N_x} \sum_{nm\sigma k_x k'_x} (C_{k_x m \sigma}^\dagger C_{k'_x, m+1, \sigma} e^{-ik_x n} \cdot e^{ik'_x n} + H.C.y) \\
&\quad + (C_{k_x m \sigma}^\dagger C_{k'_x, m \sigma} e^{-ik_x n} \cdot e^{ik'_x (n+1)} + H.C.x) \\
&= -\frac{t_R}{N_x} \sum_{nm\sigma k_x k'_x} (C_{k_x m \sigma}^\dagger C_{k'_x, m+1, \sigma} e^{-in(k_x - k'_x)} + H.C.y) \\
&\quad + (C_{k_x m \sigma}^\dagger C_{k'_x, m \sigma} e^{-in(k_x - k'_x)} e^{ik'_x} + H.C.x). \tag{B.4}
\end{aligned}$$

Using the fact that

$$\frac{1}{N} \sum_n e^{-i2\pi n(x-x')/N} = \delta_{xx'}, \tag{B.5}$$

thus,

$$H_{t_R,x} = -t_R \sum_{mk_x \sigma} \{ (C_{k_x m \sigma}^\dagger C_{k_x, m+1, \sigma} + H.C.y) + (C_{k_x m \sigma}^\dagger C_{k_x m \sigma} e^{ik_x} + H.C.x) \}, \tag{B.6}$$

where $k_x = \frac{2\pi x_x}{a_0 N_x}$.

Similarly, we also obtain

$$\begin{aligned}
H_{t_R,y} &= -\frac{t_R}{N_y} \sum_{mk_x k_y k'_y \sigma} \{ (C_{k_x k_y \sigma}^\dagger C_{k_x k'_y \sigma} e^{-ik_y m} e^{ik'_y (m+1)} + H.C.y) \\
&\quad + (C_{k_x k_y \sigma}^\dagger C_{k_x k'_y \sigma} e^{-ik_y m} e^{ik'_y m} e^{ik_x} + H.C.x) \} \tag{B.7}
\end{aligned}$$

$$\begin{aligned}
&= -\frac{t_R}{N_y} \sum_{mk_x k_y k'_y \sigma} \{ (C_{k_x k_y \sigma}^\dagger C_{k_x k'_y \sigma} e^{-im(k_y - k'_y)} e^{ik'_y} + H.C.y) \\
&\quad + (C_{k_x k_y \sigma}^\dagger C_{k_x k'_y \sigma} e^{-im(k_y - k'_y)} e^{ik_x} + H.C.x) \}. \tag{B.8}
\end{aligned}$$

Thus,

$$\begin{aligned}
H_{t_R} &= H_{t_R,x} + H_{t_R,y} \\
&= -t_R \sum_{k_x k_y \sigma} \{C_{k_x k_y \sigma}^\dagger C_{k_x k_y \sigma} (e^{ik_y} + e^{-ik_y}) + (C_{k_x k_y \sigma}^\dagger C_{k_x k_y \sigma} (e^{ik_x} + e^{-ik_x}))\} \\
&= -2t_R \sum_{k_x k_y \sigma} \{C_{k_x k_y \sigma}^\dagger C_{k_x k_y \sigma} (\cos(k_x a_0) + \cos(k_y a_0))\} \\
&= \sum_{k_x k_y \sigma} \{C_{k_x k_y \sigma}^\dagger \epsilon_k C_{k_x k_y \sigma}\}, \tag{B.9}
\end{aligned}$$

where $\epsilon_k = -2t_R(\cos(k_x a_0) + \cos(k_y a_0))$ and $k_y = \frac{2\pi x y}{a_0 N_y}$.

Now consider the second term of the Hamiltonian. We can rewrite it by using the relation $\sigma_x = \begin{pmatrix} 0 & 1 \\ 1 & 0 \end{pmatrix}$ and $\sigma_y = \begin{pmatrix} 0 & -i \\ i & 0 \end{pmatrix}$. Thus,

$$\begin{aligned}
H_{s_0} &= -t_{s_0} \sum_{nm\sigma\bar{\sigma}} \{(-C_{n+1,m\sigma}^\dagger C_{nm\bar{\sigma}} + C_{n+1,m\bar{\sigma}}^\dagger C_{nm\sigma} + H.C.x) \\
&\quad - i(C_{n,m+1,\sigma}^\dagger C_{nm\bar{\sigma}} + C_{n,m+1,\bar{\sigma}}^\dagger C_{nm\sigma} + H.C.y)\}, \tag{B.10}
\end{aligned}$$

where $\bar{\sigma}$ is the opposite spin direction. After repeating the similar procedure used for the first term of the Hamiltonian, we obtain

$$\begin{aligned}
H_{s_0} &= -t_{s_0} \sum_{\sigma\bar{\sigma} k_x k_y} \{C_{k_x k_y \sigma}^\dagger C_{k_x k_y \bar{\sigma}} ((e^{ik_x} - e^{-ik_x}) + i(e^{ik_y} - e^{-ik_y})) \\
&\quad + C_{k_x k_y \bar{\sigma}}^\dagger C_{k_x k_y \sigma} (i(e^{ik_y} - e^{-ik_y}) - (e^{ik_x} - e^{-ik_x}))\} \\
&= -2t_{s_0} \sum_{\sigma\bar{\sigma} k_x k_y} C_{k_x k_y \sigma\bar{\sigma}}^\dagger C_{k_x k_y \sigma\bar{\sigma}} (\pm i \sin(k_x a_0) - \sin(k_y a_0)) \tag{B.11}
\end{aligned}$$

$$= \sum_{\sigma\bar{\sigma} k_x k_y} C_{k_x k_y \sigma\bar{\sigma}}^\dagger E_{s_0}^{\sigma\bar{\sigma}} C_{k_x k_y \sigma\bar{\sigma}}, \tag{B.12}$$

where $E_{s_0}^{\sigma\bar{\sigma}} = E_{s_0}^{\uparrow\downarrow, \downarrow\uparrow} \mp 2t_{s_0}(i \sin(k_x a_0) \mp \sin(k_y a_0))$.

The Hamiltonian in momentum space is therefore

$$H_{RS} = \sum_{k_x k_y \sigma} C_{k_x k_y \sigma}^\dagger E_{t_R} C_{k_x k_y \sigma} + \sum_{k_x k_y \sigma\bar{\sigma}} C_{k_x k_y \sigma\bar{\sigma}}^\dagger E_{s_0}^{\sigma\bar{\sigma}} C_{k_x k_y \sigma\bar{\sigma}}, \tag{B.13}$$

where $E_{t_R} = \varepsilon_0 + \epsilon_k = \varepsilon_0 - 2t(\cos(k_x a_0) + \cos(k_y a_0))$.

To find the eigenstates with eigenenergies E at lattice index (n, m) , we write

$$\psi(n, m) = e^{ik_x an + ik_y am} \begin{pmatrix} a_1 \\ a_2 \end{pmatrix}, \quad (\text{B.14})$$

and solve the eigen equation $H_{RS}\psi = E\psi$. This equation gives

$$\det(\hat{H}_{RS}\psi - EI) = 0 \quad (\text{B.15})$$

or

$$\begin{vmatrix} E_{t_R} - E & -2t_{so}(i \sin k_x a - \sin k_y a) \\ 2t_{so}(i \sin k_x a + \sin k_y a) & E_{t_R} - E \end{vmatrix} = 0. \quad (\text{B.16})$$

Hence, the eigenenergies are

$$E^\pm = E_{t_R} \pm 2t_{so}\sqrt{\sin^2 k_x a + \sin^2 k_y a}. \quad (\text{B.17})$$

We can now obtain the corresponding spin part $\begin{pmatrix} a_1 \\ a_2 \end{pmatrix}$. First, consider the state

with $E = E^+$ and obtain

$$\begin{bmatrix} -2t_{so}\sqrt{\sin^2 k_x a + \sin^2 k_y a} & 2t_{so}(i \sin k_x a + \sin k_y a) \\ -2t_{so}(i \sin k_x a - \sin k_y a) & -2t_{so}\sqrt{\sin^2 k_x a + \sin^2 k_y a} \end{bmatrix} \begin{pmatrix} a_1 \\ a_2 \end{pmatrix} = 0, \quad (\text{B.18})$$

$$\frac{a_1}{a_2} = \frac{(i \sin k_x a + \sin k_y a)}{\sqrt{\sin^2 k_x a + \sin^2 k_y a}}. \quad (\text{B.19})$$

After normalizing it, we get

$$\psi_{RS}^+(n, m) = \frac{1}{\sqrt{2}} \begin{pmatrix} \frac{(i \sin k_x a + \sin k_y a)}{\sqrt{\sin^2 k_x a + \sin^2 k_y a}} \\ 1 \end{pmatrix} e^{ik_x an + ik_y am}. \quad (\text{B.20})$$

Similarly, we obtain for the state with $E = E_-$,

$$\psi_{RS}^-(n, m) = \frac{1}{\sqrt{2}} \begin{pmatrix} -\frac{(i \sin k_x a + \sin k_y a)}{\sqrt{\sin^2 k_x a + \sin^2 k_y a}} \\ 1 \end{pmatrix} e^{ik_x an + ik_y am}. \quad (\text{B.21})$$

CURRICULUM VITAE

NAME Mr. Aek Jantayod
DATE OF BIRTH August 19, 1983
PLACE OF BIRTH Nan, Thailand
PERSONAL ADDRESS 72 M.6, Thumbol Santong Thawangpha District,
Nan 55140, Thailand
Mobile. 66-89-4605075
E-MAIL kachai1902@yahoo.com

EDUCATIONS

PhD candidate (2006 - present)

School of Physics, Suranaree University of Technology, Nakhon Ratchasima,
Thailand

Title of Thesis: Particle and spin transport of Rashba spin-orbit coupling in
a lattice and a continuous model

Supervisors: Assoc. Prof. Dr. Puangratana Pairor

Diploma of Teaching (2005 - 2006)

Faculty of Education, Naresuan University, Phitsanulok, Thailand

Bachelor of Science (2002 - 2005)

Department of Physics, Faculty of Science, Naresuan University, Phitsanu-
lok, Thailand

Advisor: Asst. Prof. Dr. Thiranee Khumlumlert